An *in vitro* biomechanical comparison between intramedullary pinning and the use of plates in the dachshund tibia

by

Freddie Malan

Submitted in partial fulfillment of the requirements for the degree of

MSc(Veterinary Science)(Small Animal Surgery)

in the Department of Companion Animal Clinical Studies
in the Faculty of Veterinary Science
at the University of Pretoria

Pretoria, January 2012

DEDICATED TO:

- **Professor Louis Coetzee, friend and mentor, who, by his example, skill and enthusiasm, kindled my interest in small animal surgery**

- **My wife, Nadia, and sons, Jacques and Francois, who faithfully tolerated me through my years of work and study**

- **Most of all, our heavenly Father, for opening the right doors for me, and closing some others**

An *in vitro* biomechanical comparison between intramedullary pinning and the use of plates in the dachshund tibia.

By : **Dr F Malan**
Department of Companion Animal Clinical Studies
Faculty of Veterinary Science
University of Pretoria

Supervisor : **Prof A Carstens**
Department of Companion Animal Clinical Studies
Faculty of Veterinary Science
University of Pretoria

Co-supervisors : **Prof G L Coetzee**
Department of Companion Animal Clinical Studies
Faculty of Veterinary Science
University of Pretoria

Dr N D L Burger
CMTI Consulting (Pty) Ltd
Pretoria

I, Freddie Malan, hereby declare that the work on which this dissertation is based, is original (except where acknowledgements indicate otherwise) and that neither the whole work nor any part of it has been, is being or is to be submitted for another degree at this or any other University, Tertiary Education Institution, or Examining Body.

31 January 2012

CONTENTS

SUMMARY

The dachshund, a chondrodystrophic dog breed, presents a unique challenge in the treatment of tibial fractures by having short and curvaceous tibiae, leading to high implant failure risk. In this study, intramedullary pins with full cerclage wires as an option in the treatment of oblique diaphyseal tibial fractures was studied *in vitro*. This fixation technique was biomechanically compared with the current gold standard in internal stabilization, namely bone plates and screws.

Twenty tibiae recovered from adult dachshund cadavers were randomly allocated into two groups of ten bones each. Oblique fractures running in a proximo-cranial-disto-caudal direction in the middle third of the tibial diaphysis were simulated by osteotomy and each bone repaired by using one of the following methods**:**

- Pre-bent intramedullary pin, filling 40% to 60% of the medullary cavity at its narrowest point, inserted normograde and combined with a set of three full cerclage wires (group 1).
- Lag screw at the osteotomy site, combined with a six hole 2.7 mm contoured dynamic compression plate and cortical screws in neutral mode (group 2).

Each test specimen was subjected to a two point single cycle axial compression test by applying a standardized, increasing compression load to the point of fixation failure or bone collapse. A stress-strain graph for each test specimen was drawn from the raw data. Radiographs and digital photographs were made pre-osteotomy, post-osteotomy, post-repair and post-test, and modes of failure noted for each test specimen.

Stress (applied load) and strain (deformation) at yield, ultimate strength, and at failure were determined for each test specimen from the stress-strain graphs and the mean values statistically compared between the groups using the ANCOVA method. Significance levels of $p < 0.05$ were used, while $p < 0.1$ and $p < 0.01$ were also indicated.

In group 1, 50% specimens failed due to unraveling or slippage with displacement of the cerclage wires, 30% due to bone fracture at a cerclage wire, and 20% due to bone fracture elsewhere. In group 2, 80% specimens failed due to bone fracture at one or more of the screw holes, whereas 20% failed due to bone fracture not directly associated with implants. No bone plate or screw underwent plastic (permanent) deformation, whereas 80% of the intramedullary pins and 30% of the cerclage wires underwent plastic deformation. Mean stress at the yield point in groups 1 and 2 were 0.323 MPa and 0.403 MPa respectively, at the point of ultimate strength 0.383 MPa and 0.431 MPa respectively, and at the failure point 0.345 MPa and 0.403 MPa respectively. Mean strain at the yield point in groups 1 and 2 were 0.296% and 0.362% respectively, at the point of ultimate strength 0.412% and 0.472% respectively, and at the failure point 0.713% and 0.838% respectively.

Clinically, there was an indication that plates and screws were more resistant to deformation by the loads applied than intramedullary pins and cerclage wires. However, statistically, there were no significant differences in stress at yield ($p = 0.299$), ultimate strength ($p = 0.275$), or failure ($p = 0.137$) between the two groups. Similarly, there were no significant differences in strain at yield ($p = 0.684$), ultimate strength ($p = 0.778$), or failure ($p = 0.505$) between the two groups. Main limitations of the study were the relatively small number of specimens tested, the smoothness of the osteotomy cuts which limited interdigitation between the fragments, and that only three of the five recognized loads acting on bones *in vivo*, were tested *in vitro*.

In conclusion, this study did not show enough evidence to prove a significant difference between the two methods of fixation. Therefore, it is suggested that intramedullary pins and full cerclage wires be used as an acceptable alternative to bone plates and screws in the treatment of oblique mid-diaphyseal tibial fractures in chondrodystrophic dog breeds.

OPSOMMING

Die dachshund, ‘n chondrodistrofiese honderas, bied ‘n unieke uitdaging in die behandeling van frakture van die tibia, deurdat hulle tibias kort en krom is, wat lei tot ‘n hoë risiko van inplantaat mislukking. In hierdie studie is intramedullêre penne met vol sirkeldrade as ‘n keuse in die behandeling van skuins frakture van die tibiale skag *in vitro* bestudeer. Hierdie tegniek van herstel is vergelyk met die huidige goue standaard in interne stabilisering, naamlik beenplate en skroewe.

Twintig tibias wat van volwasse dachshund kadawers herwin is, is lukraak aan twee groepe van tien bene elk toegewys. Skuins frakture in ‘n proksimo-kranio-disto-koudale rigting in die middelste derde van die tibiale skag is nageboots deur ‘n osteotomie, waarna elke been herstel is deur die gebruik van een van die volgende metodes:

- Vooraf gebuigde intramedullêre pen, wat 40% tot 60% van die murgholte by die dunste punt vul, normograad geplaas en gekombineer met ‘n stel van drie vol sirkeldrade (groep 1).
- Trekskroef by die osteotomie area, gekombineer met ‘n ses-gat 2.7 mm gekontoerde dinamiese drukplaat en kortikale skroewe geplaas op neutrale wyse (groep 2).

Elke toetsmonster is onderwerp aan ‘n twee-punt enkel siklus aksiale druktoets deur die toepassing van ‘n gestandardiseerde, verhogende druklading tot by die punt van fiksasie breuk of kollaps van die been. ‘n Druk-spanning grafiek vir elke toetsmonster is vanaf die rou data saamgestel. X-straalfoto’s en digitale foto’s van elke been is pre-osteotomie, post-osteotomie, post-herstel and post-toets geneem en die maniere van faal vir elke toetsmonster aangeteken.

Druk (toegepaste lading) en spanning (vervorming) by meegee (“yield”), treksterkte (“ultimate strength”) en faal (“failure”) is vir elke toetsmonster bepaal vanaf die druk-spanning grafieke en die gemiddelde waardes statisties vergelyk tussen die groepe deur gebruik te maak van die ANCOVA metode. Beduidenis vlakke van $p < 0.05$ is gebruik, terwyl $p < 0.1$ en $p < 0.01$ ook aangedui is.

In groep 1 het 50% toetsmonsters gefaal as gevolg van losgaan of gly van die sirkeldrade met verplasing, 30% as gevolg van beenfrakture by ‘n sirkeldraad, en 20% as gevolg van beenfrakture elders. In groep 2 het 80% toetsmonsters gefaal as gevolg van beenfrakture by een of meer skroefgate, terwyl 20% gefaal het as gevolg van beenfrakture wat nie direk met die inplantate geassosieer is nie. Geen beenplaat of skroef het plastiese (permanente) vervorming ondergaan nie, terwyl 80% van die IM penne en 30% van die sirkeldrade plastiese vervorming ondergaan het. Gemiddelde druk by die meegeepunt in groepe 1 en 2 was 0.323 MPa en 0.403 MPa onderskeidelik, by die punt van treksterkte 0.383 MPa en 0.431 MPa onderskeidelik, en by die faalpunt 0.345 MPa en 0.403 MPa onderskeidelik. Gemiddelde spanning by die meegeepunt in groepe 1 en 2 was 0.296% en 0.362% onderskeidelik, by die punt van treksterkte 0.412% en 0.472% onderskeidelik, en by die faalpunt 0.713% en 0.838% onderskeidelik.

Klinies was daar ‘n indikasie dat plate en skroewe meer weerstandbiedend was teen vervorming deur die toegepaste ladings as intramedullêre penne en sirkeldrade. Statisties was die druk wat die toetsmonster laat meegee ($p = 0.299$), en die druk by die treksterkte- ($p = 0.275$) en faalpunte ($p = 0.137$) egter nie beduidend verskillend tussen die twee groepe nie. Net so was die spanning by die meegee- ($p = 0.684$), treksterkte- ($p = 0.778$) en faalpunte ($p = 0.505$) nie beduidend verskillend tussen die twee groepe nie. Hoof beperkings van die studie was die relatief klein getal monsters wat getoets is, die gladheid van die osteotomie-snitte wat interdigitasie tussen die fragmente beperk het, en dat slegs drie van die vyf erkende ladings wat op bene *in vivo* inwerk, *in vitro* getoets kon word.

Laastens het hierdie studie nie genoeg getuienis opgelewer om ‘n beduidende verskil te bewys trussen die twee metodes van herstel nie. Derhalwe word voorgestel dat IM-penne en vol sirkeldrade gebruik word as aanvarbare alternatief tot beenplate en skroewe in die behandeling van skuins midskag tibia frakture in chondrodistrofiese honderasse.

ACKNOWLEDGEMENTS

Without the help of the following people this dissertation would not have been possible. Thank you to**:**

- Proff. P. Stadler and J.P. Schoeman – respectively former head and current head of the Department of Companion Animal Clinical Studies, Faculty of Veterinary Science, University of Pretoria, who allowed me to complete my studies in small animal surgery

- Prof. A. Carstens – my promoter, who was always there to help when necessary, to motivate and encourage when needed most, and who was always understanding

- Prof. G.L. Coetzee – my veterinary co-promoter, who inspired me to become a surgeon, and for his valuable input in the clinical aspects of this study

- Dr. N.D.L. Burger – my engineering co-promoter, for his valuable input in the technical aspects of this study

- Prof. P.N. Thompson – who performed the initial statistical analysis on such short notice

- Mr. J. Grimbeek – who performed the final statistical analysis with precision and in so much detail, sacrificing precious family time to do this

- Prof. R.M. Kirberger – my guidance committee chairman, who was always supportive, and for his constructive advice

- Sr. B. Olivier, Sr. L. Odendaal, and Sr. M. McClean – radiographers, for all their patience in taking series upon series of radiographs

- Mr. R. Mienie, Mr. S. Vermeulen, and Mr. P.J.J. Botha – mechanical engineers, who were responsible for the initial design of the test configuration, the performance of the biomechanical tests, and the finer data calculations from the graphs

- Mr. J. Setati and Mr. W. Chiloane – my assistants, who meticulously helped me with the preparation of the specimens

- Colleagues in private practice – who supplied me with many of the dachshund cadavers

- University of Pretoria – for financial support to complete this project

- Our heavenly Father – for giving me the opportunity and the talents to do advanced studies in small animal surgery

LIST OF TABLES

LIST OF FIGURES

LIST OF ABBREVIATIONS

A	Cross sectional area through which a load is applied
A_0	Original cross-sectional area through which a load is applied
AMI	Area moment of inertia
ANOVA	Analysis of variance
AO/ASIF	Association for the Study of Internal Fixation
ASTM	American Society for Testing and Materials
BPS	Bone plate and screws
CACS	Companion Animal Clinical Studies
DCP	Dynamic compression plate
ΔL	Amount by which the length of an object changed
δ	Stress (or applied load)
δL	Deformation change of specimen
E	Young's modulus of elasticity
ε	Strain (or deformation)
F	Load
GPa	Gigapascal
IM	Intramedullary
IPW	Intramedullary pin and cerclage wires
kN	Kilonewton
kJ	Kilojoule
kPa	Kilopascal
K-wire	Kirschner wire
L	Length of specimen
L_0	Original length of specimen
LC-DCP	Limited contact dynamic compression plate
LCP	Limited contact locking (threaded) auto compression plate
m^2	Square meter
MPa	Megapascal
N	Newton
OVAH	Onderstepoort Veterinary Academic Hospital
p	Exceedance probability

Pa	Pascal
PMI	Polar moment of inertia
SOP™	String of Pearls™ universal interlocking plate system
SPCA	Society for the Prevention of Cruelty to Animals
SD	Standard deviation
Std. Dev.	Standard deviation

CHAPTER ONE: INTRODUCTION

1.1. Background

Tibial fractures of diverse aetiologies, displaying various fracture patterns, are a common reason for dogs presented for veterinary attention throughout the world.

The dachshund, a chondrodystrophic dog breed, presents a unique challenge in the treatment of tibial fractures. Due to its unusual angular anatomic structure[51,52] (see Figure 1.1), the dachshund tibia is predisposed to a high frequency of nearly equally represented oblique, spiral and comminuted fracture patterns, especially in the middle third of the diaphysis[9,50,51,52,69,73].

FIGURE 1.1. Mediolateral view of a dachshund tibia (left) and a tibia of a typical non-chondrodystrophic dog breed (right), indicating the difference in shape. Note the unusual angular anatomic structure of the dachshund tibia.

Various methods of fixation have been used successfully depending on the nature and location of the fracture involved and the signalment of the patient[25,29,51,52]. Surgical methods of fixation currently in use are different kinds of bone plates, screws, intramedullary pins, cerclage wires, external skeletal fixation, interlocking nails, and various combinations of these[2,9,10,25,29,42,45,51,59,70,73].

1.2. Problem statement

Optimal intramedullary pin insertion in the dachshund tibia is technically demanding due to the curvature of the bone. In addition, due to the irregular shape of the tibial diaphysis, cerclage wiring in this breed has a higher risk of failure by premature loosening [51,52].

No published comparative information is available regarding the biomechanics of intramedullary pinning with cerclage wires, and lag screw with neutralization plate fixation of oblique diaphyseal fractures of the tibia of chondrodystrophic dog breeds.

This study was undertaken to shed more light on the mechanical behaviour of intramedullary pins and cerclage wires, in comparison to bone plates and screws, when applied *in vitro* to oblique diaphyseal fractures of dachshund tibiae.

1.3. Hypothesis

In the treatment of oblique mid-diaphyseal fractures of the tibiae of dachshunds**:**

- pre-bending of an intramedullary Steinman pin conforming to the shape of the medullary cavity, inserted manually in a normograde fashion and filling approximally 40% to 60% of the medullary cavity at its narrowest point, combined with a standardized application of full cerclage wires,

will result in equal plastic deformation and equal strength and effectiveness as**:**

- the use of a lag screw to achieve compression at the osteotomy site, combined with an orthopaedic bone plate, contoured to fit the medial surface of the bone and attached to it with cortical screws in a neutralization mode.

1.4. Aim

The aim of this study was to compare the breaking strengths and modes of failure between the two methods of repair of oblique diaphyseal tibial fractures of dachshunds.

1.5. Objective and value of this study

The objective of this study was to make recommendations as to treatment options of tibial fractures in dachshunds with specific reference to oblique diaphyseal fractures.

Many small animal practitioners do not have access to the specialized and costly equipment necessary to apply bone plates, or lack the essential skills to perform such operations. However, many practitioners have access to, and are skilled in using the simpler, more affordable equipment necessary to place an intramedullary pin and cerclage wires. For those practitioners in particular, the results from this study will be of value.

CHAPTER TWO: LITERATURE REVIEW

2.1. Introduction

Dachshunds form part of the chondrodystrophic group of dogs, that have a disorder of cartilage formation as a common characteristic[6,7], resulting in angular deformities of the limbs. Basset hounds, bulldogs, pugs, pekingese, beagles and Welsh corgis also display this characteristic[6,7,25].

2.2. Anatomic structure of the tibia

Proximally the tibia has two flat condyles that make up the tibial plateau. These condyles articulate with the femoral condyles via the menisci. The tibial tuberosity, which continues distally as the tibial crest before it tapers back to the diaphysis, is located just distal to the cranial border of the tibial plateau. The proximal tibial metaphysis is relatively flat medially, but concave both caudally and laterally. These surfaces blend distally into the tibial diaphysis, which is almost uniform in diameter, but slightly S-shaped in chondrodystrophic dog breeds in particular – it curves from proximomedial to distolateral in the proximal half and then back from lateral to medial in the distal half. Viewed from the medial or lateral side, an S-shape is also apparent, in which the concavity is mainly cranioproximal and the convexity caudodistal. The distal tibia flares slightly to form the distal articular surface[45].

2.3. Tibial fractures

Fractures of the tibia are relatively common in dogs, comprising between 14.8%[46,52] and 21% of long-bone fractures and 11.7% of all appendicular fractures[50]. The tibia is the third most common long bone fractured after the femur and radius/ulna[50,70] while diaphyseal fractures account for the majority (73% to 81%) of all tibial fractures in the dog[10,21,50,70]. In all breeds of dogs of all ages, the unusual angular anatomic structure of the tibia[51,52], leads to a high frequency of oblique, spiral and comminuted fracture

patterns, especially in the middle third of the diaphysis[9,50,51,52,69,73]. In the immature animal, proximal and distal epiphyseal fractures of the tibia are more common[70,73].

Concurrent fracture of the fibula almost always occurs with tibial fractures in mature animals[51,52,73]. In immature animals the fibula is often spared and aids as an internal splint after reduction[73]. Repair of the fibula is generally not necessary unless the proximal fibula or the lateral malleolus is involved[51,52]. While methods for tibial fracture repair are similar to those used for other appendicular fractures, some unique considerations, both anatomically and functionally, must be considered before its repair[70]. Stable, closed, reducible diaphyseal fractures of the tibia can be treated by closed reduction and some form of external support[50,51,52,59,73]. Open reduction and internal fixation must be employed for all unstable or nonreducible fractures. Oblique and spiral fractures with minimal comminution – including comminuted fractures that can be reduced to a single oblique or spiral fracture line[70] – are receptive to fixation by intramedullary pin and full cerclage wiring[51,52].

2.4. Biomechanical considerations

Consideration of mechanical influences on bone and fixation implants during normal physiologic and nonphysiologic use is important since excessive load may result in failure (fracture) of the bone and/or implant[69].

2.4.1. Biomechanical considerations of bone

Bone, as biological material, can absorb large amounts of load associated with normal physiologic activity, e.g. walking or running, but is less capable of tolerating a nonphysiologic load, e.g. bending[31].

Bone is not totally rigid and can deform due to loads applied to it. When mild deforming loads are removed from bone, it resumes its original shape. This is called *elastic deformation*. Large loads will deform bone permanently, i.e. to a point where it cannot resume its original shape. This is called *plastic deformation*. Even larger loads will result in failure of bone and cause a *fracture*. The relationship between load (force) and

bone deformation is described in graphic form as a *force-deformation* curve[27,31,69]. The structural strength of an object can be determined from such a graph by the load the structure can withstand, the deformation the structure undergoes, and the amount of energy the structure absorbs before failing[69].

2.4.1.1. Stress-strain graphs

Stress-strain graphs are valuable graphic representations of a material's biomechanical properties[64], produced by applying progressive compressive or tensile loads to the material[79]. Stress-strain testing is detailed by standards-setting organizations, notably the American Society for Testing and Materials (ASTM)[64]. To provide a standardized representation of the mechanical behaviour of a material (as opposed to its structural behaviour), it is necessary to normalize the force-deformation parameters and eliminate the influence of structural geometry and dimension. When bone specimens of relatively uniform size and shape are tested, the load (F) per cross sectional area (A) can be plotted against the amount of deformation change (δL) in relation to its original length (L) to generate a *stress-strain* graph[27,31,69] where the load applied to bone is expressed as stress and its deformation as strain.

An example of a classical stress-strain graph is portrayed in Figure 2.1.

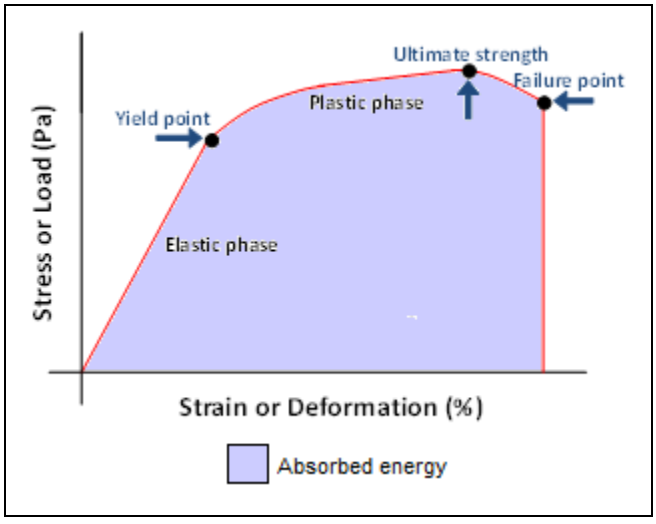

FIGURE 2.1. Example of a classical stress-strain graph. (Redrawn from Kraus[31]).

Stress (δ) is a measure of the internal forces or internal interactions that result when an object is deformed, i.e. a measure of how strong a material is[69]. Stress is expressed as load per unit area [69,77], or the amount of pressure the material can withstand without undergoing physical change[77]. Stress is based on the original cross sectional area without taking into account changes in area due to applied load[28]. The metric unit for stress is Pascal (Pa), which is one Newton (N) per square meter (m^2)[77].

Strain (ε) is defined as the percentage change in length[77], or the ratio of change in length of an object relative to its original length, caused by stress applied to it in the form of pressure. Strain is dimensionless (has no units) and is expressed as percentage (%)[28,69,77].

The area under the stress-strain graph represents the amount of energy absorbed by that object (e.g. bone) prior to its failure, or the amount of energy necessary for that object to fail[27,31,69]. (See Figures 2.1 to 2.3).

Within the elastic deformation phase of the stress-strain graph, the bone imitates a spring, i.e. the deformation in the bone increases linearly with increasing load, and after the load is released, returns to its original shape, thus releasing much of the energy imparted to it[27,31,69,77]. As the load on the bone increases, the bone deforms to a specific point where it will not fully resume its original shape after the load is removed. This point is called the *yield point*, also indicating the end of the elastic phase[27,31,69]. After this point, the bone is in its plastic deformation phase in which it will remain deformed after the load is removed. Here the bone undergoes a rearrangement of its internal molecular or microscopic structure, in which atoms are moved to new equilibrium positions[64].

The amount of post yield strain that occurs in a material before it fails is a measure of the *ductility* of the material[77]. Ductility can be defined as the extent to which a material can sustain plastic deformation without failure[28]. The opposite of ductility is *brittleness*, when a material requires very little post yield strain to fail. Bone, in general, is a classic example of a brittle material[77], while most metals tend to be ductile.

Ductile materials characteristically retain elastic behaviour in the plastic deformation area, implicating that after a certain degree of plastic deformation, the material will return to a less deformed state when the load is removed, although not to its original state. This behaviour is also typical of viscoelastic materials, of which bone is one example[22,72,77]. (See Figure 2.2).

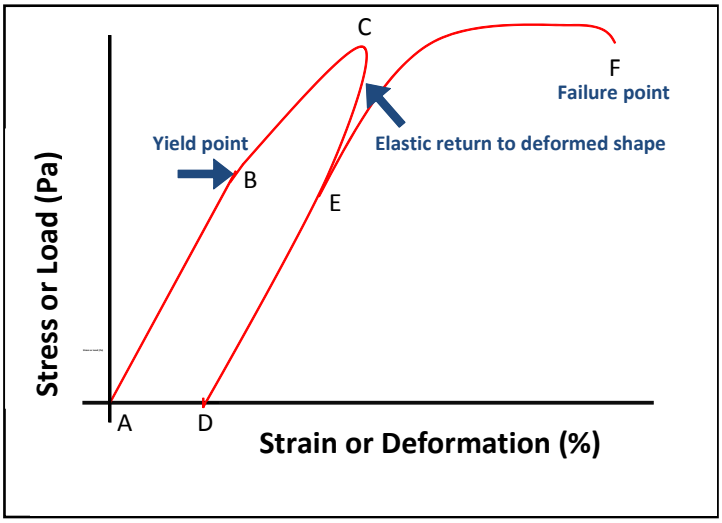

FIGURE 2.2. Elastic behaviour of a structure after some plastic deformation. (Redrawn from Finlay[22]). (A = Zero point (original shape); B = 1st yield point; C = 1st plastic deformation; D = Point of return to deformed shape; E = Yield point of deformed specimen; F = Failure point after 2nd plastic deformation; A - D = Deformation offset.)

When a structure is loaded beyond the yield point (B), plastic deformation occurs. Especially in the case of ductile materials, the structure retains its spring-like action that resulted in the initial elastic deformation. When the load is removed after some plastic deformation (C), the structure returns by the same slope than the elastic deformation, closer to the original shape or length, but with some plastic deformation (D). This is important in the use of cerclage wires. When the wire is tightened, it retains the spring like action where its mechanical effect will cause static compression of the bone fragments[8,72]. When the cerclage wire is distracted, such as with bending forces on a bone, the wire will again go into elastic (D-E) and plastic (E-F) deformation. Loosening of the wire will occur if the elongation of the wire (plastic deformation after elastic return) exceeds the circumference of the bone[40].

A number of terms have been defined for the purpose of identifying the stress at which plastic deformation begins:

Yield strength is defined as the stress at which a predetermined amount of permanent deformation (strain) or *offset* occurs. Offset yield strength can be defined as an arbitrary approximation of the elastic limit[28], and is an indication of the maximum amount of stress that can be developed in a material without causing plastic deformation and is a practical approximation of its elastic limit (*vide infra*). To determine yield strength, the predetermined amount of permanent strain is set along the strain axis of the stress-strain graph, to the right of zero, and a straight line is drawn at the same slope as the initial portion of the stress-strain graph. The point of intersection of this new line and the original stress-strain curve is projected to the stress axis. This stress value is the yield strength. This method of plotting is performed for the purpose of subtracting the elastic strain from the total strain, leaving the predetermined offset as a remainder[79]. Some materials do not exhibit a clear transition between the elastic and plastic phases, therefore, 0.2% strain offset (the stress needed to induce plastic deformation) is typically taken to be the stress needed to induce a specified amount of permanent strain[64,69].

Alternative values are sometimes used instead of yield strength. Several of these are briefly discussed below.

The *yield point* was defined earlier[27,31,69], but it can also be recognized as a drop observed in the load (sometimes a constant load), while the strain continues to increase.

The highest value, at which stress is directly proportional to strain, is called the *proportional limit,* i.e. the highest stress at which the curve in a stress-strain graph remains in a straight line[79]. The proportional limit is not usually used in specifications because the deviation begins so gradually that controversies are sure to arise as to the exact stress at which the line begins to curve.

Studies of stress-strain graphs show that the yield point is so close to the proportional

limit that for practical purposes the two may be taken as one. In addition, it is also much easier to locate the former[28,77].

The highest stress that can be applied without causing permanent deformation is called the *elastic limit*. Elastic limit is used as a descriptive, qualitative term as it cannot be determined from the stress-strain graph. The method of determining the elastic limit would have to include a succession of slightly increasing loads with intervening, and complete unloading for the detection of the first plastic deformation. Like the proportional limit, its determination would result in controversy.

The *strength limit* is the stress generated by a compressive load applied to a bone specimen, when the first cracks appear in the bone[79].

The maximum stress a bone can sustain before failure is called the *ultimate strength*, and the *breaking strength* is the stress at which the bone actually fails or fractures[77]. After reaching its point of ultimate strength during the plastic phase, further deformation produced by an external load[79] will lead to failure[27,31,69] at the so-called *failure point*. In bone the ultimate strength and the breaking strength at the failure point usually have the same value, but this is not necessary true in all materials or combinations of materials, especially when a metal implant is attached to bone in the repair of a fracture. Strength, as it is defined above[77,79], is an intrinsic property of bone, i.e. these strength values are independent of the size and shape of the bone. The load required for the bone to fail is different from the intrinsic strength, because the breaking load that causes failure will vary with bone size and shape[77].

The material properties of bone tend to differ depending on the rate at which a specific load is applied to it. If a load is applied rapidly, bone tends to absorb more energy and will behave with more stiffness and higher ultimate strength. Any material with such a load-rate dependent property is referred to as *viscoelastic*. Furthermore, bone is also *anisotropic*, i.e. exhibiting different mechanical properties in different directions[27,31,69].

Every bone is a complex structure with a collection of components each having different material properties. For example, the metaphysis of the tibia has different material

properties than its diaphysis. A single bone is composed of both cortical and cancellous bone, with porosity ranging from 3% to 90%. The material properties of cortical and cancellous bone are different and reflect their general biomechanical purposes. The stress-strain graph is a general engineering description of the bone's material properties, keeping in mind the heterogeneous nature of bone[27,31].

The metaphysis is composed mostly of cancellous bone[27,31,69], which is made up of individual trabeculae, each with its own stiffness, together forming a structure that has its own unique stiffness. Cancellous bone therefore has a *material* stiffness, which is the stiffness of each trabecula, and a *structural* stiffness, which represents the stiffness of the entire trabecular structure. The majority of biomechanical studies of cancellous bone concentrate on its structural properties because the material properties of the different trabeculae are difficult to measure individually. These structural properties vary in different anatomical regions depending upon the cancellous bone density and trabecular orientation[77]. When a large compressive load is applied to bone, the fine trabeculae of the metaphysis will collapse. The wide metaphysis, though early to deform, will continue to deform without complete collapse. Here the elastic phase of the stress-strain graph is short while the plastic phase is relatively long[27,31,69]. (See Figure 2.3a). This material property is helpful in absorbing loads across joints and preventing direct damage to the joint cartilage[27, 31].

The diaphysis, on the other hand, is composed of cortical bone where large loads are needed to deform the bone[27,69]. Nearly 80% of the skeletal mass is represented by cortical bone. It provides strength in areas where bending or any other load would be undesirable, such as in the diaphysis of long bones[77]. Cortical bone is normally rigid, yet brittle, with little plasticity, resulting in a long elastic phase of the stress-strain graph and a very short plastic phase. Once enough strain has occurred, the diaphysis will fracture[27,31,69]. (See Figure 2.3b).

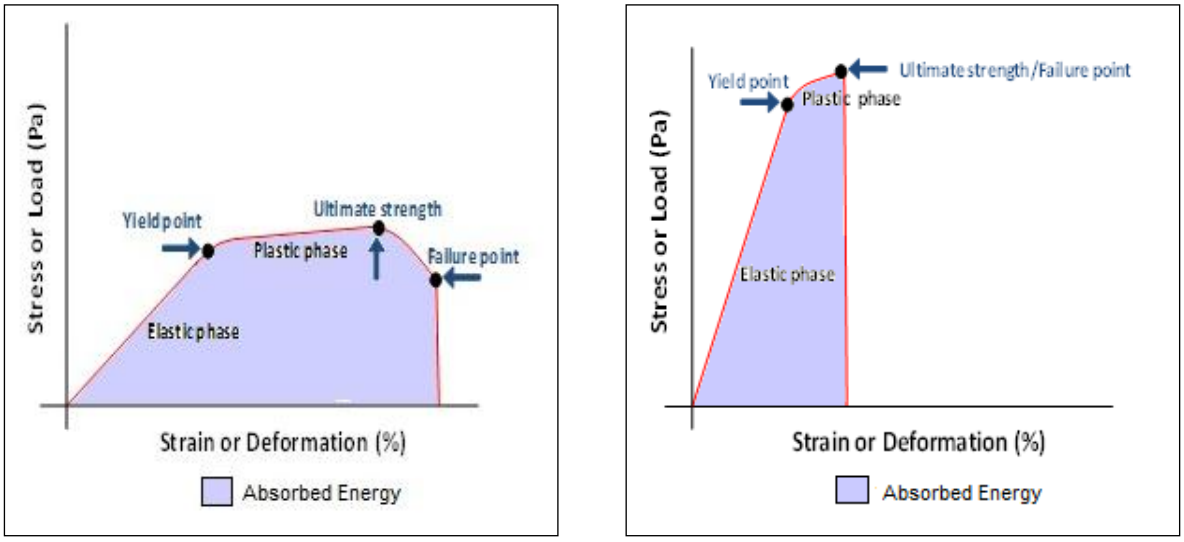

FIGURE 2.3. Stress-strain graphs for cancellous bone (metaphysis) (a) and cortical bone (diaphysis) (b). (Redrawn from Kraus[31]).

Due to the fact that all orthopaedic implants are to some degree fixed to the bone during the repair of fractures and therefore biomechanically united to form a bone-implant composite, the combination acts as a single unit and not as separate entities when stress is applied. Therefore, a single stress-strain graph is representative of both the bone and the metal components of such a specimen[36,41,42].

2.4.1.2. Modulus

The elastic phase of the stress-strain graph is generally linear, i.e. increased loads result in equivalent degrees of deformation[27,31,69]. The slope of the elastic phase represents the intrinsic stiffness or rigidity of the structure[77] and is referred to as the *elastic modulus* or more commonly as *Young's modulus of elasticity*. Modulus is a measure of the stiffness of an elastic material and is a quantity used to characterize materials[27,69].

Young's modulus can be experimentally determined from the slope of a stress-strain graph created during a compression or tensile test conducted on a material, using any linear area of the elastic phase of the stress-strain graph in the determination thereof[31]. (See Figure 2.4).

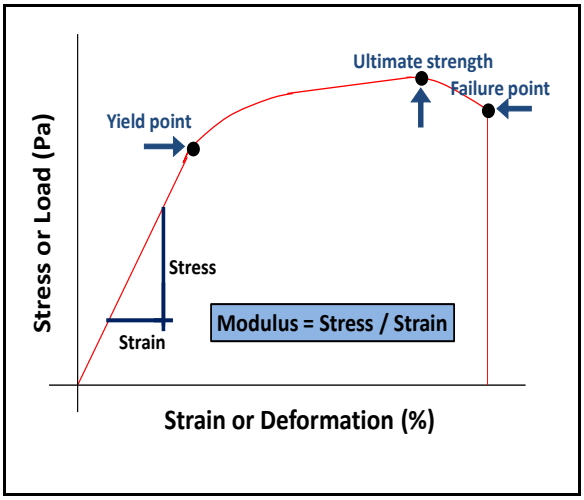

FIGURE 2.4. Young's modulus of elasticity, a measure of the stiffness of a material, is determined by using any linear area of the elastic phase of the stress-strain graph. (Redrawn from Kraus[31]).

Young's modulus of elasticity is calculated according to the following formula**:**

$$E = \frac{\delta}{\varepsilon} = \frac{\frac{F}{Ao}}{\frac{\Delta L}{Lo}} = \frac{FLo}{Ao\Delta L}$$

where E = Young's modulus, δ = Stress (or applied load), ε = Strain (or deformation), F = Load applied to the object, A_0 = the original cross-sectional area through which the load is applied, ΔL = the amount by which the length of the object changed, and L_0 = the original length of the object[69].

The metric unit for Young's modulus is Pascal (Pa). Due to the magnitude of Young's modulus, more manageable units of expression are often used, such as kPa, MPa or GPa[77].

In physical terms, Young's modulus is defined as the ratio of the uniaxial stress over the uniaxial strain in the range of stress in which Hooke's law of elasticity operates. Hooke's Law of elasticity is an approximation that states that the extension of a spring is in direct proportion to the load applied to it. Many materials, such as bone and metal,

obey this law, providing that the applied load does not exceed the material's elastic limit. Hooke's law in simple terms states that stress is directly proportional to strain[28,77].

The stiffer a material, the steeper the slope of the elastic phase of the stress-strain graph, and subsequently the greater the modulus[27,69]. The behaviour of three different materials – a soft metal, glass and cortical bone – was studied by Nordin and Frankel[44] to compare the materials' individual elastic moduli. (See Figure 2.5). Of these three materials, metal had the highest modulus and at stresses beyond its yield point, exhibited typical ductile behaviour by undergoing large plastic deformation before failure. Glass had a higher modulus than bone, (but less than metal), and underwent brittle failure, but without any discernable plastic deformation. Bone had a much lower modulus than metal or glass, but also underwent brittle failure after a period of plastic deformation. These differences in stiffness can result in a modulus mismatch when metal devices are used to repair bone fractures.

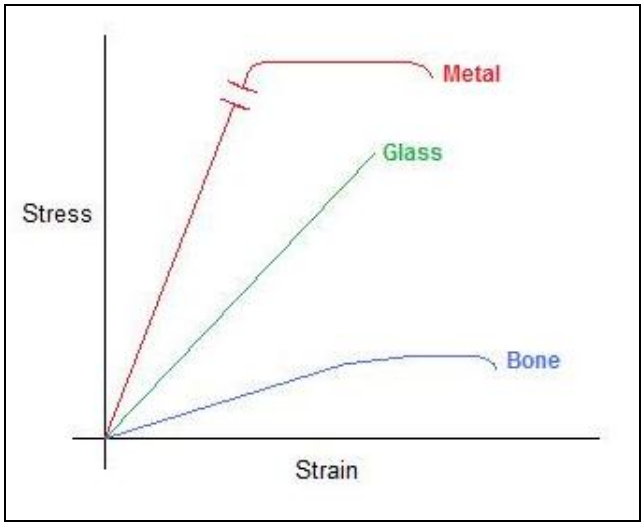

FIGURE 2.5. Stress-strain graphs of three different materials. (Redrawn from Nordin and Frankel[44]).

2.4.2. Biomechanical considerations of metal implants

Implants used in fracture repair must bear all or part of the load normally carried by the bone[16,42]. The majority of implants currently used in the management of bone fractures in small animals are manufactured from iron-based alloys, especially 316L stainless

steel[36,41,42,58,67], known for its superior corrosion resistance. Of the four basic groups of stainless steel, the austenitic group is mostly used for the manufacturing of orthopaedic implants[40].

Specifications for iron-based alloys have been laid down by the ASTM. Alloys used in the manufacturing of orthopaedic implants have to comply with ASTM standards F138 and F139[40]. Among the specifications for these alloys are combinations of properties that permit the manufacture of properly shaped and sized implants, the need for suitable mechanical properties relative to allowable sizes for implantation, and compatibility *in vivo*, often for extended periods of time[32,40].

Cost is a major factor limiting the use of implants other than stainless steel in veterinary orthopaedics. For example, titanium plates and screws are widely used in human orthopaedics and are available for use in veterinary patients, but although they perform marginally better than 316L implants, they are significantly more expensive[42,71].

The composition of 316L stainless steel implants used in this study is given in table 2.1.

TABLE 2.1. Chemical composition of 316L stainless steel[40].

Chemical Composition (%)	
Iron	55 - 60
Chromium	17 - 20
Nickel	10 - 14
Molybdenum	2.8
Manganese	1.7
Silicone	0.57
Copper	0.1
Nitrogen	0.095
Phosphorous	0.025
Carbon	0.024
Sulfur	0.003

316L stainless steel is a relatively strong material, being able to withstand ultimate loads of up to 700 MPa during tension. This compares well to cortical bone, which is able to withstand loads of 150 MPa during compression, and a little less during tension[42]. The inherent strength of 316L allows implants to be made small enough to allow implantation, while remaining strong enough to resist most of the biomechanical forces acting on the bone-implant composite during the process of fracture healing[36,41,42].

The material properties of metal implants are not only determined by their composition, but also by the manufacturing process. Melting and casting of the alloy is followed by forging using compression, after which it is cold worked to elongate the grain structure into fibrous shapes parallel to the long axis of the implant and anticipated deforming loads *in vivo*. This micro structure of the implant provides optimum strength to prevent

breakage. Cold working also increases the stiffness of the implant and thereby reduces its ductility. A certain degree of ductility is, however, essential to prevent brittle fracture of an implant during *in vivo* cyclic loading and to allow contouring of the implant at surgery. The use of heat can further refine an implant to increase its ductility and to obtain the desired properties for different implants. For example, 316L cerclage wire is more ductile than a 316L bone plate, which in turn, is more ductile than a 316L Steinmann pin[72].

2.4.2.1. Implant failure

Implant failure can occur some weeks after an apparently successful fracture repair. Loads well below those needed to fracture an implant have the potential to alter the implant material permanently. Cyclic loads applied to a metal, even if not enough to cause it to break, can cause microscopic cracks in the metal, which will gradually lengthen, sometimes only a fraction of a micron, each time the load is re-applied[42]. The fatigue characteristics of a metal can be determined experimentally and are described graphically as stress versus number of cycles[36,41,42]. An example of this is shown in Figure 2.6, which was determined experimentally for 316L stainless steel[42].

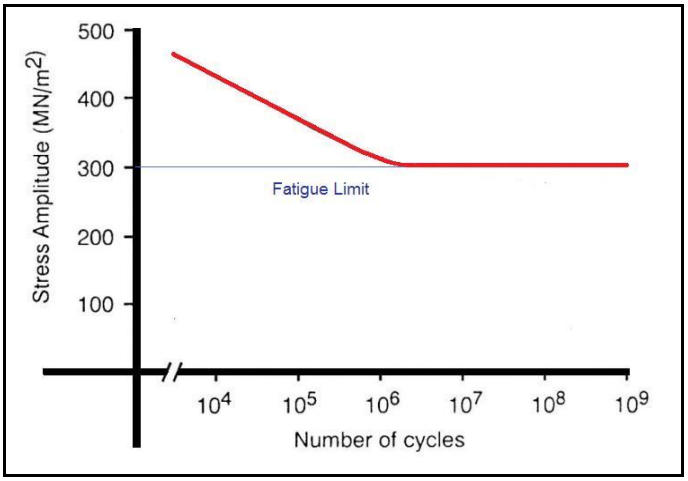

FIGURE 2.6. Stress versus number of cycles for 316L stainless steel. (Redrawn from Ness[42]).

It is obvious from this graph that larger loads lead to earlier failure, and that there is an area to the right (larger than 1 x 10^6 cycles) of the fatigue limit where fatigue failure will

never occur, no matter how often loading is applied. Loading forces higher than those indicated on this curve, will lead to permanent plastic deformation and/or failure (breaking) of the metal. The life span of an implant is therefore directly related to the cyclical loading to which it is subjected. The number of cycles to failure (i.e. time to failure) will significantly be reduced by any form of stress concentration in a metal implant[41,42].

In the clinical situation, size and distribution of loading forces through the metal implant will be influenced by its relationship to the bone[36,42].

Material failure due to metallurgic imperfections or manufacturing faults, although rare, can lead to premature failure of an implant. Electrochemical or oxidation-reduction corrosion of the metal due to oxidation and ionization in the oxygen rich and ionic extracellular fluid in which it is continually bathed *in vivo*, can also contribute to material failure. By far the most important mode of implant failure encountered in small animal orthopaedics, is *fatigue failure*[36,41,42].

True stress is not uniform throughout any specimen – there will always be some location where the local stress is at its maximum, for instance in an area of a notch or some other defect at the surface. Once the maximum stress is reached, the localized flow at this site can no longer compensate by further *strain hardening* (increase in strength and hardness of a metal due to a mechanical deformation in the metal's microstructure). This soon leads to *neck* formation in the gauge length of the specimen, after which all subsequent deformation takes place in the neck, causing the neck to become progressively smaller. With true stress increasing all the time, the specimen will soon fail[64]. (See Figure 2.7).

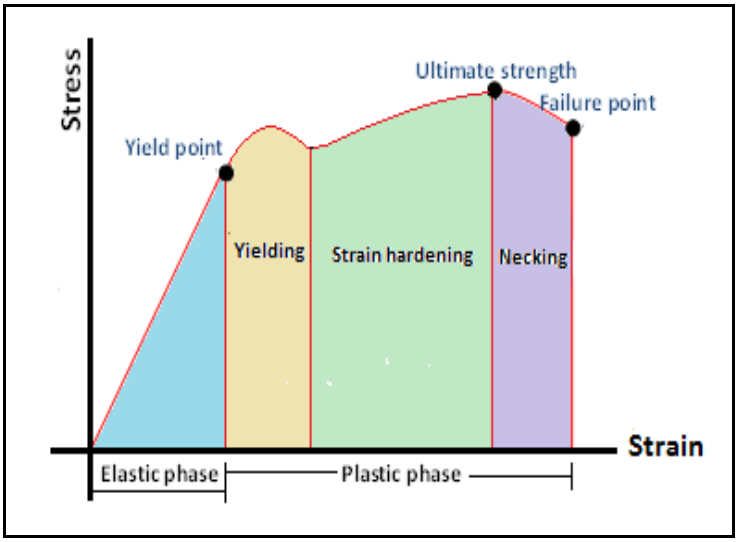

FIGURE 2.7. Stress-strain graph demonstrating strain hardening and necking. (Redrawn from Kraus[31] and Roylance[64]).

Acute material failure of an implant is not common in small animal orthopaedics, because this involves a process where larger amounts of energy are required than what are generally present in fractures of this kind. Reduced area moment of inertia (AMI) of an implant, i.e. reduced ability to resist bending, also plays an important role in premature implant failure. Area moment of inertia depends primarily on the mass of the implant material and the distance from the neutral axis of the bone-implant composite, but open fracture gaps or an open opposite (*trans*) cortex can also influence the AMI by reducing the strength of the bone-implant composite in that area. Low AMI will accelerate fatigue failure and will permit movement of the fracture, delaying fracture healing and therefore further increasing the risk of implant failure[36,41,42].

2.5. Loads acting on bone

A final consideration is bone strength if a load is applied in a physiologic direction, and bone weakness if a load is applied in an abnormal, nonphysiological direction. For example, a tibia can tolerate large stresses if an axial load is applied, but tolerates much less stress with a bending load[27,31,69].

Long bones exhibit specific fracture patterns as a result of different modes of loading. Several internally and externally generated loads can act on bone *in vivo,* arising either

individually or more typically in combination with one another[57]. Five individual loads acting on long bones are usually recognized, i.e. compression, tension (distraction), shearing, bending (angular or bowing), and torsion[17,21,27,50,51,52,59,69,73]. (See Figure 2.8).

Axial loads, either *compression* or *tension*, occur along the long axis of the bone, while *shearing* occurs transversely, *bending* in a craniocaudal or mediolateral plane, and *torsion* in either direction around the long axis of the bone [69].

Compression occurs when two opposing loads act on a bone along a single axis[27,31,50], and is a primary disruptive load present in all long bone diaphyseal fractures, owing to load generated by weight bearing and muscle contractions surrounding the bone. Compressive loads can be beneficial in transverse and short oblique diaphyseal fractures where the fragment ends interdigitate and axial alignment is maintained, or detrimental in short oblique diaphyseal fractures where the fragment ends do not interdigitate, long oblique fractures, and comminuted fractures in which anatomical reconstruction is not possible [69].

Resistance against compression is directly related to a bone's mineral content. Pure compressive loads seldom cause fractures in animals because bone is under normal circumstances quite resistant to this normal physiologic type of load. However, when larger than normal compressive loads that exceed absorption (by the elastic phase of the stress-strain graph) are applied, most of the energy is released into the adjacent bony tissue, disrupting the structure of the bone, often leading to short oblique fractures[31,69]. (See Figure 2.8a).

Tension, the opposite of compression, occurs when two opposing loads pull the bone apart[27,31,50]. Pure tensile loads are not seen in the diaphysis of long bones, but generally at the end of long bones where tendons and ligaments insert, and on the convex surface of bones undergoing bending deformation[69]. Resistance against tension is mainly related to the arrangement and properties of collagen. Tensile loads generally result in failure perpendicular to their direction. These loads are generally not physiologic and therefore, bone is inherently weaker against them. Avulsion fractures are examples of the result of tensile loads[31,69]. (See Figure 2.8b).

Shearing occurs when loads in opposite directions at different levels act on a bone. The opposing loads are due to the inherent resistance of constituents of bone to slide across one another. The bone fails or fractures when bonds between the constituent parts fail, as in tension. Shear loads are also generally not physiologic; therefore, long oblique fractures usually occur easily secondary to these loads[27,31,50,69]. (See Figure 2.8c).

Bending results when tensile and compressive loads act simultaneously on bone[27,31,50]. (See Figure 2.8d). Bending loads are the result of eccentric loading of long bones, their normal curvature, and the spanning of these bones by large muscle masses[69].

Because bending and tensile loads are opposing forces, the plane within the bone between bending and tensile loads contains no load and is called the neutral plane. The opposing loads are the bone's strength against compression (great) and the bonding of its constituent parts (weak). The bone will fail first on the tension side. Since many long bones, including the tibia, have some curvature, forces acting from each end of the bone result in bending loads as well as compressive and tension loads. The greatest tensile load is found on the convex side of the curved bone, whereas the greatest compressive load is on the concave side. The fracture line will progress across the bone transversely or slightly obliquely, resulting in transverse, short oblique and/or comminuted fractures of the concave aspect, often with some "butterfly" fragments and greenstick fractures (in young animals) [27,31,50,69]. (See Figure 2.8e).

Torsion occurs when rotating loads in opposite directions act on the ends of a bone structure. The opposing loads tend to be complex and depend on the geometry of the bone. Shear and tensile loads are the major constituent loads; therefore, the bonding substances of bone act as the opposing forces[27,31,50]. Shear loads are distributed about the neutral axis along the entire cross-sectional area of the bone and roughly at 45 degrees to the axis of rotation[69]. Because strong torsional loads are not generally physiologic in nature and an angled distal limb easily acts as a rotational lever arm, fractures due to torsion are common and usually result in spiral oblique fractures[27,31,50]. (See Figure 2.8f).

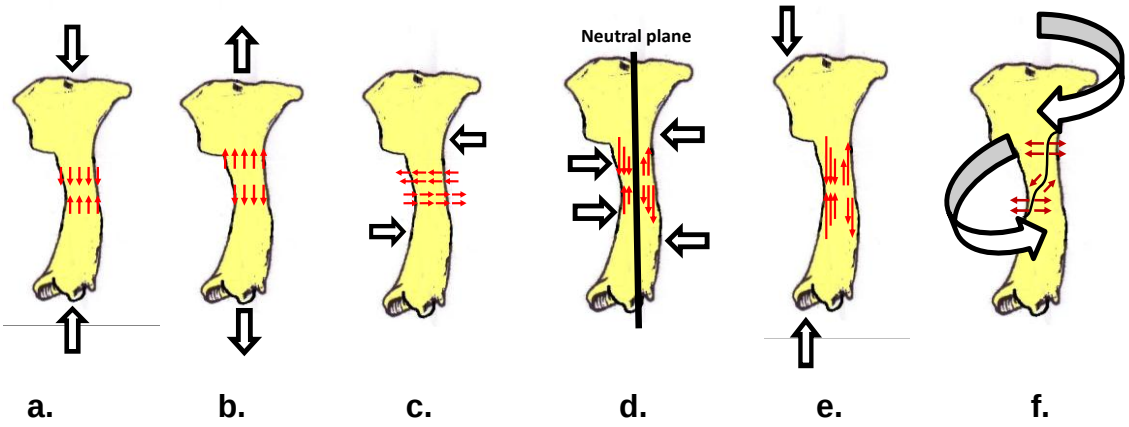

FIGURE 2.8. Loads acting on bone. (a). Compression. (b). Tensile (distraction). (c). Shearing. (d). Bending. (e). Bending loads on each end of a curved bone. (f). Rotational (torsion). (Redrawn from Kraus[31]). (Open arrows = direction of loads; red arrows = direction of movement of bony tissue).

Because of the complex shape of bone, however, most fractures result from a combination of all these loads[31]. For instance, the dachshund tibia often fails in shear when subjected to a compressive load. This is because simple compression creates shear stress at a 45° angle to the direction of loading, and since most materials are weaker in shear than in compression, failure occurs in shear. Compressive, tensile, and shear stresses invariably occur in combination, even under the simplest loading schemes[77].

The metaphysis of long bones are comprised of trabecular bone that is able to absorb and transmit energy and compressive loads generated by normal weight bearing. Because the resistance of trabecular bone is less than that of cortical bone, the metaphyseal region has to be wider than other regions of long bones[5,15,39,49]. The fact that long bones are thinner in the diaphyseal area than in the metaphyseal or epiphyseal areas, but still maintain adequate strength is due to the compact nature of their bone material and their strain behaviour. The compressive load of diaphyseal bone reduces the strain in bending and thus increases its capability for elastic or plastic bending without a brittle fracture[15,39,49].

The shape of the diaphysis of most long bones is cylindrical with a compromise between a square and a triangle in cross section. Its shape is dependent on the type of

loads it is designed to resist. A cylindrical shape is best for resisting torsional loads and a square shape for resisting bending loads that are applied parallel to its sides. The diaphyses of long bones are also tubular. This shape is better able to resist torsional and bending loads than a solid cylinder, since it distributes its mass at a distance from the neutral axis of the bone[15,44,49].

In addition, the heterogeneous nature of bone as a material allows for different areas of bone to have different strengths in response to different loads. Loads will tend to concentrate and propagate along the weak areas of bone[31]. A bone fractures when a load greater than its tolerance is applied to it. The resultant fracture pattern is a function of the type of load, the amount of energy applied, the viscoelastic properties of the bone and in a lesser degree, the amount of soft tissue covering the area.

When loads are applied to a limb in weight bearing, the load is transmitted along the bone, resulting in stresses that tend to misalign or disrupt the fracture site. These stresses are also present in the absence of weight-bearing because of muscle tension[30,31].

2.6. Loads acting on a bone-implant construct

After internal fixation, the use of the affected limb results in a complex array of loads within the bone-implant construct, caused by weight-bearing and muscle contractions during each gait cycle. A combination of three loads normally acts on such a bone-implant construct (hereafter referred to as “specimen” or “test specimen”), i.e. axial compression, bending and rotation[42,58,59]. In specific instances, fragments associated with the attachment of major muscle groups may also undergo tension.

Axial compression acting on a reconstructed fracture will cause collapse and shortening, with weight bearing and muscle contraction contributing to this component. The amount of purchase obtained by an implant in the major proximal and distal fragments, as well as the completeness of the reconstruction will influence the ability of the fracture repair to resist compression[42,58].

Bending loads, owing to eccentric loading of the curvature of the bone, are always present when a bone that bears weight is not placed perpendicular to the ground. Additionally, the spanning of bones by large muscle masses leading to eccentric muscle contractions can cause bending loads in any direction[10,16,45,50,58]. An implant's resistance to bending is determined by its elastic modulus and its AMI[41,58].

Rotation of the bone is caused by changes in the direction of the body while the affected limb bears weight[58,59]. Polar moment of inertia (PMI) represents the ability of a structure to resist deformation by torsional forces and is dependent on the distribution of material in the structure. Polar moment of inertia therefore quantifies the way in which the structure is distributed around the centre of the rotational effect. Rotational stability is estimated by how well the implant engages the primary fracture fragments and by interaction of the fracture fragments with one another. Polar moment of inertia of the implant is not usually a weak point in the construct[58].

The two most important factors to consider during internal fixation procedures are to minimize any additional trauma to an already traumatized area, and also to provide and secure an optimal biological and mechanical environment in which healing of the fractured bone can occur.

In general, bone fractures will heal well if**:**

- Fracture fragments are adequately vascularized;
- Fracture fragments are adequately stabilized in terms of alignment and movement, with fracture gap(s) that are relatively small; and
- Infection does not occur[10,12,17,26,27,31,50,59,69].

2.7. Blood supply

All physiological processes within bone, including the ability to heal, are dependent on its blood supply. In the diaphysis of mature long bones, the afferent blood supply, which is of frequent concern in orthopaedics, is derived mainly from the principal nutrient artery, and supplemented through anastomoses with the metaphyseal arteries[24,82]. In areas where the medullary circulation is intact, the cortex is mainly

supplied by these medullary blood vessels, except in areas of ligamentous, fascial or strong muscular attachments[24,26,82]. In these areas, a minor component of the afferent system, the periosteal arterioles, run perpendicularly to the cortex and supply its outer layers[24, 82]. According to research by Gothman (1962), there are no longitudinal periosteal blood vessels[24]. Under normal circumstances the direction of blood flow through the cortex is centrifugal, i.e. from medulla to periosteum, with venous drainage from the periosteal surface.

Blood flow in immature bone is greater than in mature bone and is centred around areas of active growth. Here, the epiphysis and metaphysis are supplied separately and the periosteum has an extensive longitudinal system of blood vessels. At maturity, the metaphyseal and epiphyseal blood supply become one and the periosteal supply atrophies to only a vestige[82].

With bone fractures, the afferent blood supply increases at the sites of healing. When needed, a variable and transitory supplemental extraosseus blood supply can be derived from the periosseous soft tissues. The function of this new extraosseous system is to supply blood to detached bone fragments, periosteal callus and the cortex when devascularized by trauma or surgical intervention. This transient extraosseous blood supply subsides as soon as the normal components of the bone's blood supply are re-established[24,26,82].

To some degree, every method available to stabilize fractures has the potential to compromise the local blood supply to the bone. For example, the insertion of an intramedullary pin will disrupt the medullary blood flow; the extent thereof depends on the size of the pin – the larger the pin in relation to the medullary cavity, the greater the vascular damage[82].

2.8. Treatment of fractures

It is essential to consider the loads acting on a long bone fracture site when selecting an implant for fracture stabilization[31,50]. First, the biomechanics of the injury should be evaluated to ascertain which types of loads caused the fracture. Next, the secondary

loads acting on the fracture segments should be assessed so that they can be adequately neutralized by the specific therapy[13,17,69]. The type of therapy is also based on the type of bone healing (primary or secondary) best suited to the patient and the fracture. An appropriate fracture fixation technique is also based on the effects of the stabilization device on bone healing and vascular supply to the area of the fracture[13].

When the loads acting on a fracture are inadequately neutralized during fracture stabilization, delayed union, malunion or even non-union may result. Infection is an additional compromising factor that can lead to the formation of non-union in an already inadequately stabilized fracture[17].

The goal of any fracture treatment is early ambulation and complete return to full function[13]. The surgeon must always aim to obtain a load-sharing system between the bony column and the implant that is mechanically stable and to maintain axial and rotational alignment throughout the entire healing period[17,69]. Stability of a fixation depends on the stiffness of the fixation device, the stiffness of the device-bone interface, and the effectiveness of the device to specifically neutralize disruptive forces acting on the fracture[69].

Various methods of fixation can be used successfully depending on the nature and location of the fracture and signalment of the patient[25,29,51,52]. Familiarity of the surgeon with different techniques and equipment is important in determining the selected method of repair[29]. Methods of fixation currently in use in veterinary orthopaedics are: Bone plates, screws, intramedullary pins, cerclage wires, external skeletal fixation, interlocking nails, and various combinations of the above[2,4,9,10,11,19,20,25,29,30,38,42,45,51,58,59,70,73,75].

Intramedullary pins and orthopaedic wire are widely available, are relatively inexpensive, and many surgeons are skilled in their use. Hence, intramedullary pins and cerclage wires are commonly used for fixation of tibial fractures, usually with fairly good results[9,10,18,26,29,37,50].

2.8.1. Intramedullary pinning

An understanding of how intramedullary (IM) pins resist the various loads acting on a long bone fracture is needed. The goal of IM pinning is to fill the area of the fracture with a pin (or pins), as this gives rigidity to the pin-bone unit[50]. As long as the tubular nature of the fractured bone is restored, IM pins can be used in most long bone fracture types, including highly comminuted fractures[73].

Bending loads, that are present in most fractures, regardless of the fracture type, are well counteracted when a round pin of adequate diameter is well anchored both proximally and distally into the cancellous bone[10,18,50,59]. Its ability to resist bending loads is directly proportional to its diameter (large AMI) and to the ratio of its diameter to the medullary diameter[41,42,48,58]. As the medullary diameter becomes larger in comparison to the pin diameter, it becomes mechanically more difficult for the pin to control any bending loads[65]. Transverse shearing loads, together with bending loads, are furthermore best neutralized when it is also possible to have intimate contact between the pin and the inner (endosteal) cortical surface. This allows for effective load transfer across the fracture site, owing to the development of adequate shear resistance between the pin and bone[48], but does compromise some of the medullary blood supply[24,26,82].

Single IM pins lack the ability to resist rotational and axial (compression and tension) loads and need ancillary support to stop axial and rotational collapse. Rotational and axial loads are counteracted only by frictional forces between the bone and the pin, which is too small to be effective in most clinical situations[10,21] and to some degree by fragment interdigitation[78]. Tension loads are not present in most diaphyseal fractures[50].

Because of these deficiencies, IM pinning as the only method of fixation is only indicated in simple transverse diaphyseal fractures in which there is good interdigitation of the bone fragments[10,18,21,29,51,52,56,59,78].

The effect of IM pinning on the healing of fractures is important[82]. Except in cases where active reaming for seating of the pins has taken place, total destruction of the

medullary blood supply does not occur. Temporary disruption of the medullary blood supply occurs with any displaced fracture. The use of an IM Steinmann pin will reduce this supply initially, but will by no means completely destroy it. Hypertrophy of the medullary blood vessels will take place around the pin within the first 14 days after pin placement, unless the pin completely fills the medullary cavity, or if the inner cortex has been reamed out[17].

Correct technique of IM pin placement in the tibia is important to avoid iatrogenic damage to the intra-articular structures of the stifle[10,18,21,29,51,52]. The potential for interference with the femoral condyle, patella, patellar ligament, cranial cruciate ligament, bones of the tarsus and the synovial cavities needs to be minimized[25,37,70]. These potential idiosyncrasies occur partly because of the anatomic shape[45,73] of the tibia and the offset of the axial alignment of the medullary cavity in relation to the tibial plateau, particularly if heavy, nonflexible pins are used[73].

Two types of placing techniques are used to insert an IM pin in a long bone, i.e. normograde and retrograde. By using the retrograde technique, extension of the stifle joint is frequently prevented by the pin, which limits weight bearing. The resulting non-weight bearing lameness prevents the axial compression needed for pin fixation and results in muscle atrophy with subsequent decrease in blood supply[17]. It has been reported that a retrograde tibial pinning technique using a strict craniomedial direction may be acceptable, but that if incorrectly performed, injury to the stifle joint can occur[2,17,18,25,29,31,45,46,50,51,52,70]. A less frequently used option for retrograde tibial pinning where the pin exits the cranial border of the tibial tuberosity, has also been described[46].

Dixon *et al*[18] studied the effects of three different techniques of tibial retrograde IM pin placement on pin location and stifle joint injury and compared the results with normograde pinning. Their study showed that blindly advanced (non-directed) IM pins placed retrograde in the canine tibia exit significantly more caudal and lateral and have a significantly higher incidence of associated stifle joint trauma (damage of cranial cruciate ligament and femoral condyle articular surface) than non-blindly (directed) retrograde or normograde pins. It was concluded that although non-directed retrograde pinning cannot be recommended, retrograde pins directed craniomedially may be an

acceptable technique for the repair of proximal to mid-diaphyseal tibial fractures if care is taken to properly seat the pins proximally.

The majority of authors agree that the more acceptable technique for the pinning of a tibia is by normograde placement[2,9,10,17,18,21,25,29,31,37,45,50,51,52,59,70]. A number of techniques for normograde placement of intramedullary pins into the canine tibia have been described in the literature.

Currently, the technique most widely used, involves entering the tibia from the proximal (tibial plateau) aspect. With the stifle in 90° flexion, the medial collateral ligament and patellar ligament are palpated. The point of pin entry is slightly cranial to a point halfway between these two ligaments and just medial to the patellar ligament. This point is cranial to the menisci and cruciate ligaments and no weight-bearing cartilage is invaded. The pin is aimed in a disto-caudomedial direction[17,21,50,51,52,70]. The proximal end of the pin must be cut short enough (not longer than 5 mm) or bent 90° medially and then cut so that the rest of the pin does not damage the articular cartilage of the medial femoral condyle during extension of the joint. This can usually only be done by withdrawing, cutting and impacting the pin[17].

A variation of the above-mentioned technique, as described in older literature, involves entrance of the tibia on the dorsomedial aspect of the proximal tibial epiphysis[73]. The site of pin introduction is a small depression on the medial side of the proximal tibia equidistant from both the medial collateral ligament and the straight patellar tendon. The pin is introduced approximately at right angles to the tibial shaft until the tip of the pin is embedded in the subchondral bone. At that point, the pin is angled distally and parallel to the long axis of the bone and is driven into its final position. When placed properly, the pin is dynamic and has three points of contact: proximally at its entry point, against the lateral cortex of the diaphysis, and seated in the cancellous bone distally. Once the pin is in position, the proximal end can be bent and cut close to the surface of the bone to ensure that no contact is made with the femur and to facilitate later removal. With this technique, the end of the pin will be extra-articular and will allow for normal free motion of the stifle.

The distal seating of the pin should usually be at a site just proximal to the malleoli. It is important to remember that the malleoli hang like saddlebags over the tibial tarsal bone and if the pin is driven to the level of the distal malleoli, it will penetrate the joint[17].

In curved bones like the tibia of chondrodystrophic dog breeds, in order to fill the fractured area with a pin, will often mean inability to achieve proper anatomic reduction. For mid-diaphyseal tibia fractures in the majority of other dog breeds, it is generally recommended to fill about 60% to 75% of the medullary cavity at its narrowest point[50]. Due to the exaggerated S-shaped curve of the tibia in chondrodystrophic dog breeds, a flexible pre-bent IM pin with a diameter not exceeding 60% of the diameter of the medullary cavity at its narrowest point, appears to work better in these breeds, since heavier pins do not allow for easy application and can cause forced straightening of the tibia's curve, resulting in a valgus deviation. Gentle manual advancement of the pin after penetrating the proximal cortex in both normograde techniques, allows it to bend slightly and to better conform to the normal anatomic conformation of the tibia[50,73].

2.8.2. Cerclage wiring

The use of cerclage wiring as ancillary treatment with IM pins refers to a flexible stainless steel wire that completely (full cerclage) or partially (hemicerclage) passes around the circumference of a bone and is then tightened to provide static interfragmentary compression of the different loose bone fragments[50,58,59]. Cerclage wires effectively counteract bending, shear, and rotational loads, and also provide interfragmentary compression of the fracture fragments[10,21,27,45,50,51,52,59,73].

Because of the stresses produced by early weight bearing, it is not recommended to use full cerclage or hemicerclage wires as the only method of fixation in any type of oblique diaphyseal fracture[50,51,52,59,73]. In addition, wires are often stressed during placement and tying, and are therefore susceptible to fatigue failure. Small nicks and notches in the wire also weaken a wire's resistance to repetitive loading[58].

Cerclage wires are used primarily as ancillary fixation devices with IM pins and bone plates on long oblique, spiral and certain comminuted or multiple diaphyseal fractures.

In addition, cerclage wires are used intraoperatively to aid in holding fracture fragments together while the primary fixation is applied[50,59].

Cerclage wire fixation should be restricted to those oblique diaphyseal fractures where the length of the fracture line is at least twice the diameter of the bone (or longer), ensuring that tensioning of the wire produces stable interfragmentary compression rather than shearing[50,59,62]. At least two wires should be used, but more than two cerclage wires are recommended. They should be spaced about half a bone diameter apart[59], starting and ending approximately 0.5 cm from the tips of the fragments and be perpendicular to the long axis of the bone[17]. Blass *et al*[8] and Rooks *et al*[62] independently recommend the use of monofilament stainless steel wire of 0.8 to 1.0 mm (20 to 18 gauge) for use in small to medium sized dogs. Roe[59] supports this and concludes that there are no rules for the appropriate size for a particular situation other than to use the biggest diameter of wire that seems appropriate to the size and strength of the bone.

Techniques of application of cerclage wires currently most popular in the veterinary literature include the twisting method and the bent eyelet wire method, where a single wire loop encircles the bone in each case. Both produce equally good clinical results if applied correctly, although more tension is produced in the wire with the eyelet method[8,14,60,68]. However, the yield point (the stage where the wire begins to deform and the free arm unbends due to tension) is lower for the eyelet than the twist method[8,60,62,68].

Modifications of the eyelet and twisting methods, where both free ends of the wire encircle the bone in each case, have been described. The double loop, double wrap, and loop-twist techniques, are examples of these methods. The double loop cerclage is formed from a single length of wire, folded near its centre with both free ends passing through the centre fold before tightened with a single eyelet tightener with two cranks or a double loop tightener. The double wrap cerclage is formed from a single eyelet cerclage where the wire is of sufficient length to encircle the bone twice before placing the free end through the eyelet and tightening it with a single eyelet tightener. The loop-twist cerclage is formed by creating a small loop in the wire by folding a single wire

in half. Both free ends of the wire encircle the bone, with one end passing through the loop before it enters the tightener to be attached to the second crank, after which it is tightened and bent over, but not cut. The second crank is tightened to take up the slack and the instrument is rotated on its axis to complete the twist. These methods generate superior tension and resist greater loads before loosening than the single looped twisting or eyelet methods. The main disadvantage of these methods is that they take up more space around the bone, hence limiting the number of cerclage wires that can be applied. This method may lead to less effective fixation, especially in smaller veterinary patients[8,60,62].

The effects of cerclage wiring on fracture healing has been reported[56,57,76,80,81]. Failure of fracture healing is usually not due to vascular compromise by the cerclage wire, but due to failure to apply cerclage wires correctly[24]. Due to the fact that the actual contact area of the cerclage wire with the underlying bone is less than the diameter of the wire, it minimally interferes with cortical blood flow[24,26], even when parts of the bone surface are grooved for anchoring of the wires. The key in preserving the cortical blood supply is that all cerclage wires must be tight around the bone, since a moving wire will disrupt the periosteal capillary network, devascularizing the underlying bone and disrupting periosteal callus formation[50,56,57]. If a wire is loose or broken, the fracture may be unstable at the fracture line, which can lead to excessive bone movement with a resultant delayed- or nonunion. Movement of the wire can interfere with bone vascularization by shearing off capillaries arising from the soft tissues that form the transient extra-osseous blood supply[24,82].

2.8.3. Bone plates and screws

Bone plates and screws are considered as the most sophisticated and reliable form of internal fixation currently available (Coetzee GL, University of Pretoria, Pretoria, South Africa, personal communication, 2007). Stable internal bone plate and screw fixation allows for early joint mobilization, full weight bearing, and union of the fracture[16,50,59].

2.8.3.1. Bone plates

When applied correctly, bone plates produce excellent stability of the fracture site [50,59]. They are effective in resisting all loads that need be counteracted – compression, tension, and rotation, and if the bone is anatomically reconstructed, also bending and shearing loads[42,50,58,59].

Bone plates are most susceptible to bending loads because of their eccentric placement relative to the central axis of a bone. When fractures are anatomically reduced with fragments compressed by the plate, the bone and plate share the load, their AMI is large, and the construct is strong. When it is not possible to reconstruct the bone, the plate alone has to resist all the bending forces. A screw hole, especially when located within the area of the fracture, is the weakest point on a plate due to stress concentration and greatly reduced AMI at that point[36,41,58].

Various types of bone plates are available, which are primarily copies of the original system developed by the Association for the Study of Internal Fixation (AO/ASIF). Based on their function and modes of application, three main groups of bone plates are recognized in veterinary orthopaedic surgery, i.e. dynamic compression plate (DCP), neutralization plate and buttress plate[50,59]. Due to its versatility, DCPs can be used in all three modes of application[16,50,59].

DCPs have oval, sloped screw holes whereas true neutralization plates have round holes; other plates can have either oval or round screw holes or combinations thereof incorporated in their design[16,59].

The principle of the DCP is to stabilize and compress a fracture with good bone contact between the major fragments, e.g. transverse or slightly oblique fractures, by driving the bone ends together by means of tightening of eccentrically placed screws in the oval, sloped screw holes. This causes the bone fragment that the screw engages, to move with it relative to the plate, so that the fracture gap is narrowed[16].

A neutralization plate (either a DCP applied in neutralization mode or a true neutralization plate) refers to the application of the plate without compression. The plate splints the bone to support and neutralize the different forces acting on the reconstructed cylinder of bone. It is used when the fracture plane is oblique, because applying compression in a dynamic compression mode will cause the fragments to overlap one another. In these cases, compression of the fracture line and holding the fragments together is best achieved with lag screws or cerclage wires. However, they are never able to resist the bending forces on a weight-bearing bone on their own and therefore the additional application of a neutralization plate is imperative[50,59].

When a bone cannot be reconstructed in the area of the fracture, the plate is applied in buttress mode to maintain axial alignment. No compression is afforded to the fracture and the plate acts as a bridge. The plate is securely attached to the major proximal and distal bone fragments and must bear the entire load on the bone until the callus bridges the gap and matures. In some situations, a lengthening plate may be used so that a solid portion of plate spans the comminuted section of bone[16,50,59].

Other plate types were developed to address certain deficiencies in the standard bone plate systems during specific applications[50,59]. An example of these, is the limited contact dynamic compression plate (LC-DCP), where stress concentration in the area of the screw holes is reduced, the AMI is similar over the length of the plate, the amount of devitalized cortical bone due to interference with periosteal blood supply is reduced, and which has superior fatigue resistance compared to DCPs[36,41,58]. Another recent development is the limited contact locking (threaded) auto compression plate (LCP) which allows the surgeon to use locking screws, compression screws or both at any location[23,71]. Other examples are reconstruction plates, lengthening plates, T - and L plates, pancarpal - and pantarsal arthrodesis plates, acetabular plates, triple pelvic osteotomy plates, tibial plateau leveling osteotomy plates[16], “C” and Mennen clamp-on plates[17], the clamp and rod internal fixation system (CRIF), and the String of Pearls™ (SOP™) universal interlocking plate system[43]. Biodegradable, self-reinforced polylactide bone plates are increasingly being used in human orthopaedics and are also available for use in veterinary patients, notably in toy breed dogs, in combination with metal screws. However, these plates are usually not strong enough when used as a

single plate and clinical use in veterinary patients has been limited due to their relatively high cost. Semitubular plates are standard plates in the AO/ASIF system, but due to its relative weakness compared to DCPs, are not often used in veterinary orthopaedic surgery[23,43,50,59,66,74,85].

The AO/ASIF group has developed guidelines for selection of the plate size for various bones based on the weight of the patient[50].

2.8.3.2. Bone screws

Screws in orthopaedic surgery are used to hold a plate to the bone in a lag fashion[58,59], and to compress or hold bone fragments together. In most instances of individual use, they are applied in lag fashion so that fragments are compressed[12,58,59,67].

Two basic types of bone screws are used in orthopaedic surgery, i.e. cortical and cancellous[12,16,59,67]. Cortical screws are always fully threaded. Their core diameter is relatively thick and the pitch of the threads relatively shallow. Cortical screws are designed for primary use in the dense diaphyseal bone. Cancellous screws are either fully threaded or partially threaded, but with relatively few threads per unit length. Their core diameter is relatively thin and the pitch of the threads relatively high with deep threads. Cancellous screws are designed for use mainly in the metaphysis or epiphysis where the cortex is thin with an abundant amount of cancellous bone present, in very young animals with soft cortical bone, or in cases where threads for cortical screws have been stripped[12,16,45,59,67].

Cortical screws are frequently used in a lag fashion by overdrilling the *cis* cortex. The hole in the *trans* cortex is determined by the core size of the screw and tapped with a tap that corresponds to the thread of the screw[12,59,67]. A lag screw's thread purchases only the *trans* cortex. Lag screws, or the use of the lag screw technique, are the most efficient way of achieving interfragmental compression and stability[12]. Static interfragmental compression is achieved by tightening the screw. Maximal interfragmental compression is achieved when the screw is inserted through the middle of the fracture line equidistant from the fracture edges and directed more or less at right

angles to the fracture plane. When a screw in lag fashion is inserted in any other direction, shearing loads will be introduced and the fragments will shift[12,59,67]. (See Figure 3.16).

In oblique, spiral or multiple diaphyseal fractures, the bone fragments should be held in place by lag screws, or using the lag technique with a gliding hole. However, lag screws do not provide a great deal of strength. They are therefore protected from weight-bearing by a bone plate applied in a neutralization mode[12].

2.9. Test methods

A variety of test methods for evaluating different aspects of specimens under specific test conditions have been described. The ASTM specifies the test method (e.g. axial compression), the specimen type (e.g. dog bone) and the loading conditions (e.g. end support) for test specimens[1,28,74,83,84]. For the purpose of this study, two test methods are mentioned. The test method used in this study was the two point single cycle axial compression test loaded under displacement control[74]. The test specimens were placed in custom made test cups with the two opposite ends firmly fixed in the direction of the linear axis, loaded by increasing compressive forces until these forces reached the values at which the specimens failed[79]. This method was derived from ASTM D 695-02a and ASTM D 6641[1,83,84], which are test protocols that have previously been validated.

Compressive tests are performed to determine the strength (a measure of how well a material withstands axially directed “pushing” forces) and to characterize how a material behaves under various loaded conditions[28]. The specimen is compressed, and deformation at various loads is recorded. A transducer connected in series with the test specimen provides an electronic reading of the load corresponding to the displacement[64]. The ASM Handbook®, Volume 8 (Mechanical Testing and Evaluation) states that axial compression testing is a useful procedure for measuring the plastic flow behaviour and ductile fracture limits of a material[3,28,32].

An alternative test method, the cyclic fatigue method[28,74], which could perhaps be considered more physiological in terms of the magnitude of forces exerted on a dachshund tibia during normal walking or running, was initially considered as the test method of choice for this study. Cyclic fatigue testing can be defined as simply applying cyclic loading to a test specimen to understand how it will perform under similar conditions in actual use[28]. The ASTM specifies the cycle limit for a fatigue test on orthopaedic implants to be approximately one million cycles, even if skeletal healing time is normally much shorter *in vivo* (only approximately 150 000 to 250 000 cycles over a period of 2 to 3 months)[3].

The test signal to be used in such a study is also based on the specifications stated by the ASTM, i.e. the signal should be a sine wave that cycles between the desired maximum force and 10% of that maximum force[3]. Calculations obtained from Nordin and Frankel[44] further indicate that the force on the bone should be between 12 and 120 N. (See Figure 2.9).

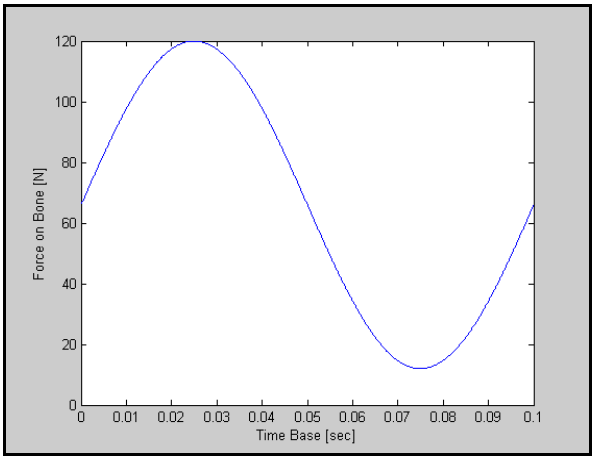

FIGURE 2.9. Required test signal for the study on dachshund tibiae, obtained from calculations by Nordin and Frankel[44].

2.10. Conclusion

Since no published comparative information is available on the biomechanics of IM pinning with cerclage wires, and lag screw with neutralization plate fixation of oblique diaphyseal fractures of the tibia of chondrodystrophic dog breeds, this study was

conducted to acquire more information on the subject.

In the literature, references to fractures of dachshund tibiae are very scarce. A case of a dachshund with a mid-diaphyseal spiral fracture of the right tibia was described, where only cerclage wires were used to achieve reduction. The patient's limb was placed in a light lateral splint post-operatively. Radiographs taken after 6 weeks showed bony callus formation and the complete absence of the original fracture line. It was concluded by the authors of that article that the exaggerated tibial curvature of dachshunds precluded the use of an IM pin in this dog breed[70].

On the contrary, Coetzee (University of Pretoria, Pretoria, South Africa, personal communication, 2007), proposed that a thinner than usual, pre-bent Steinmann pin, manually introduced in a normograde fashion, can be used in combination with two or three full cerclage wires in oblique mid-diaphyseal fractures of the tibia of chondrodystrophic dog breeds to provide a more rigid and reliable internal fixation technique.

CHAPTER THREE: MATERIALS AND METHODS

3.1. Principle

Twenty tibiae recovered from adult dachshund cadavers were studied (*vide infra*). The tibiae were randomly allocated into two groups consisting of ten bones each.

Oblique fractures running in a proximo-cranial-disto-caudal direction in the middle third of the tibial diaphysis were simulated by osteotomy of all bones. A ten year retrospective pilot study was performed by the author, evaluating radiographs of oblique and spiral tibial fractures in dogs on record at the Diagnostic Imaging Section at the Onderstepoort Veterinary Academic Hospital (OVAH) between 1998 and 2008. This study showed that the majority (87%) of these fractures had a proximo-cranial-disto-caudal configuration. Based on these results, it was decided to use a similar configuration for the simulation of fractures of all tibiae in this study.

Each osteotomized dachshund tibia was repaired using one of the following methods:

- **Group 1 (Experimental group, 10 tibiae):**

Pre-bent IM pin, selected on the principle of filling approximately 40% to 60% of the medullary cavity at its narrowest point (contoured according to the shape of the diaphysis of the bone, measured and confirmed on pre-osteotomized, mediolateral radiographs), combined with a set of three full cerclage wires of 1.0 mm in diameter. All osteotomized bones were repaired normograde, the pin entering at the proximal tibial plateau in a standard location[18,29,50,52].

- **Group 2 (Control group, 10 tibiae):**

A cortical screw, used in lag fashion, placed over the osteotomy line to achieve interfragmentory-compression, combined with a six hole, 2.7 mm DCP[50] and cortical screws. The bone plates were contoured to fit the medial surface of the bone with all

screws inserted in a neutral fashion, thereby creating a neutralization plate.

3.2. Inclusion criteria

To eliminate some of the variables due to age and size, only skeletally mature dachshunds (2 to 8 years old) of either gender were considered for this study. The animals were all free from obvious metabolic problems or other pelvic limb pathology causing osseous changes in their tibiae, i.e. all the tibiae were radiologically normal in appearance. However, minor osteophytic changes (< 2mm) were accepted for the purposes of this study.

3.3. Model system

This project was a prospective descriptive study on dachshund cadaver material.

Cadavers were obtained from the Pretoria branch of the SPCA and from private veterinary practices. The animals were humanely killed by an intravenous overdose of Sodium pentobarbitone (*Eutha-naze*®, Bayer (Pty) Ltd., Animal Health Division, Isando, South Africa), administered by a veterinarian for various reasons other than for the purposes of this study or tibial involvement. Where owners were involved, their consent was obtained for use of the pelvic limbs, by signing the Fracture Study Consent Form that was compiled for the purposes of this study. (See Appendix A). Where no owner could be identified, the consent form was signed by the responsible veterinarian in charge of the case.

The cadavers were weighed and the gender noted (see Tables 4.1 and 4.2) before the tibiae were dissected out and stripped of all surrounding soft tissue except the periosteum, using a scalpel blade and Metzenbaum scissors. The fibulas were removed by means of a scalpel or bone rongeur and discarded.

Each tibia was labeled for later identification, using a pencil on the bone itself. The bones were identified by the side (left or right) and the chronological number of the dog, e.g. R-2 (the right tibia of dog number 2) or L-7 (the left tibia of dog number 7). The

bones were then individually wrapped in paper towels, soaked in lactated Ringers solution (*Sabax Ringer-Lactate*®, Adcock Ingram Critical Care (Pty) Ltd, Johannesburg), packed in sealed plastic bags and stored in a domestic freezer (*Defy*® *Multimode*) at minus 20°C[35,47,52].

A study done by Roe *et al*[61] indicated that adult canine bone, aseptically collected, did not undergo any significant structural changes after 16 and 32 weeks of sterile storage at minus 20°C. Pelker[47] reported that storage of rat bone at minus 20°C for 4 weeks, did not detrimentally affect its biomechanical properties.

3.4. Experimental design

To obtain the required total of twenty suitable specimens, thirty four tibiae went through the different stages of pre-loading preparation. (See Section 3.5.2). Fourteen tibiae were eventually eliminated from the program before reaching the actual testing stage, due to bone fractures that occurred during either one of the preparatory phases.

The dachshund tibiae that reached the testing stage were numbered from 1 to 20 and randomly allocated to groups 1 or 2, by drawing their numbers out of a hat.

The bones were tested in a random sequence. After allocation of the bones to the two groups, the bones kept their original numbers. To determine from which group a bone was selected, the same method as before was applied for each bone, i.e. drawing a group number out of a hat (group 1 or 2), and then a number of an individual bone (e.g. R-2) from that group.

To allow comparison between bones and partial elimination of influences caused by additional variables, especially inter-dog variation, one standard size IM pin and bone plate respectively, were used throughout – the pin (a 2 mm Kirschner wire) filling approximately 40% to 60% of the medullary cavity at its narrowest point, and the bone plate being a size 2.7 mm, six hole DCP. (For the purposes of this study, all Kirschner wires used were referred to as IM pins). The IM pin was accompanied by three full cerclage wires of a standard size (1.0 mm), applied in a standard fashion around each

test bone in group 1. (See Section 3.5.3.).

A final year student in mechanical engineering, Mr. R. Mienie, was tasked with designing and building the pre-assembly testing cups (see Figure 3.1), serving as partial fulfillment of the requirements for his BEng(Mech) degree. The proximal cup was designed to allow the test specimen to be fixed at an incline of 20° craniocaudally by including an angled metal inlay in the design, with the distal cup in a standard horizontal position. Each tibia was fixed at its dorsal and ventral extremities in the cups before being integrated in the testing area of the *Schenck® 100kN* testing machine (see Figure 3.20) situated at the premises of the Faculty of Engineering, Built Environment and Information Technology, University of Pretoria.

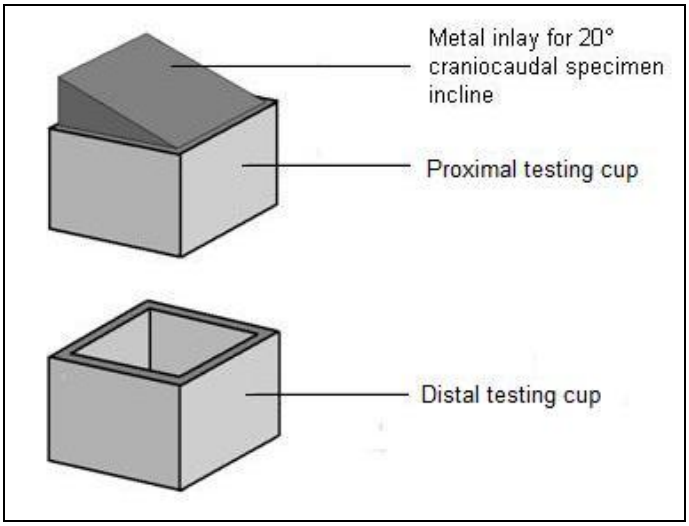

FIGURE 3.1. Diagram of pre-assembly testing cups as designed by Mr. R. Mienie.

A computer capable of monitoring stress and strain on the bone-implant composite was linked to the testing machine. The required parameters were measured and recorded every 0.01 seconds. The data obtained from each stage of the test was expressed on a spread sheet in *Microsoft Excel®*, from which a stress-strain graph was plotted for each bone. Mr. B.S. Vermeulen, a mechanical engineer from a private engineering company in Pretoria, CMTI Consulting (Pty) Ltd, performed the necessary biomechanical tests under supervision of co-promoter Prof. N.D.L. Burger and the author, and was responsible for the plotting of the stress-strain graphs.

3.5. Experimental procedures

3.5.1. Radiographs and photographs

Mediolateral and craniocaudal view radiographs of each bone were made pre-osteotomy, post-osteotomy, post-repair and post-test, and the method of failure noted. (*Siemens® Polymat 50, with FFD/SID 107cm, Bucky table grid 8:1, and moving focused grid).* A *Fujifilm® FCR IP Type CC* cassette was used throughout, with exposure factors of 44kV and 4mAs. Radiographs were digitally developed (*Fujifilm® FCR Capsula*) and stored in the digital PACS radiographic system of the Diagnostic Imaging Section of the Dept. CACS, OVAH.

Digital photographs (lateral, medial and cranial views) were also taken at each stage to illustrate the method of failure in more detail. (*Canon® Powershot SX120 IS*).

3.5.2. Specimen preparation

The *Schenck® 100 kN* testing machine was only capable of testing one bone per day. On the day of testing, an appropriate bone was removed from the freezer and thawed in a bath of lactated Ringers at room temperature[35]. The bone was transported in the bath of lactated Ringers, to the OVAH where the first mediolateral and craniocaudal view radiographs (see Figure 3.2) were taken by the Diagnostic Imaging Section of the Department of Companion Animal Clinical Studies (Dept. of CACS). Each pre-osteotomized tibia was radiographed individually to confirm physeal closure and to ensure that there were no other osseous changes indicating bone pathology. The first digital photographs of each bone were also taken. (See Figure 3.3).

a.  b. 

FIGURE 3.2. Mediolateral (a) and craniocaudal (b) view radiographs of a pre-osteotomized dachshund tibia.

a.  b. 

FIGURE 3.3. Digital photographs of a pre-osteotomized dachshund tibia, indicating the medial (a) and cranial (b) aspects.

The medullary, diaphyseal cortical, and bone diameter at its narrowest point, and the tibial length were accurately determined on each mediolateral view radiograph by the use of a Vernier™ caliper. To determine the true values, a magnification correction factor was calculated on the basis of the diameter of a twenty cent piece that was included on each radiograph.

Further preparatory procedures were then performed in the demonstration laboratory of the Small Animal Surgery Section of the Dept. of CACS at the OVAH.

The intended osteotomy line was pencil marked on the medial aspects of each defrosted tibia, drawing a line on the bone along its long axis which runs between the intercondylar eminences proximally and the medial malleolus distally. This line was divided into three equal segments with two intersecting lines drawn perpendicular to the first line to indicate the middle third of the tibial diaphysis. (See Figure 3.4).

FIGURE 3.4. Photograph of the medial aspect of the left tibia of a dachshund indicating the division of the tibia on its medial surface.

Each tibia was individually clamped in a bench vice (see Figure 3.5) and a standard mid-diaphyseal osteotomy of between 60º and 70º (to the long axis of each tibia) was performed in the middle third of the diaphysis in a proximo-cranial-disto-caudal direction

(see Figure 3.6) to simulate an oblique fracture, using an oscillating saw (*Stein MultiMaster*®, Sheffield, United Kingdom). (See Figure 3.7).

FIGURE 3.5. A tibia divided by pencil lines on its medial aspect, clamped in a bench vice.

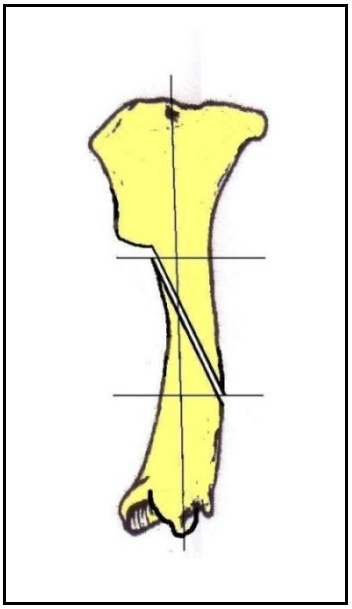

FIGURE 3.6. Diagram of the medial aspect of a right dachshund tibia with osteotomy in a proximo-cranial-disto-caudal direction in the middle third of the diaphysis.

FIGURE 3.7. Oscillating saw blade in position on the medial aspect of a tibia, at the start of the osteotomy.

A second mediolateral and craniocaudal view radiograph (see Figure 3.8) were made. The bone fragments were positioned in such a manner as to reconstruct the original shape of the bone. A second set of digital photographs were also taken at this stage. (See Figure 3.9).

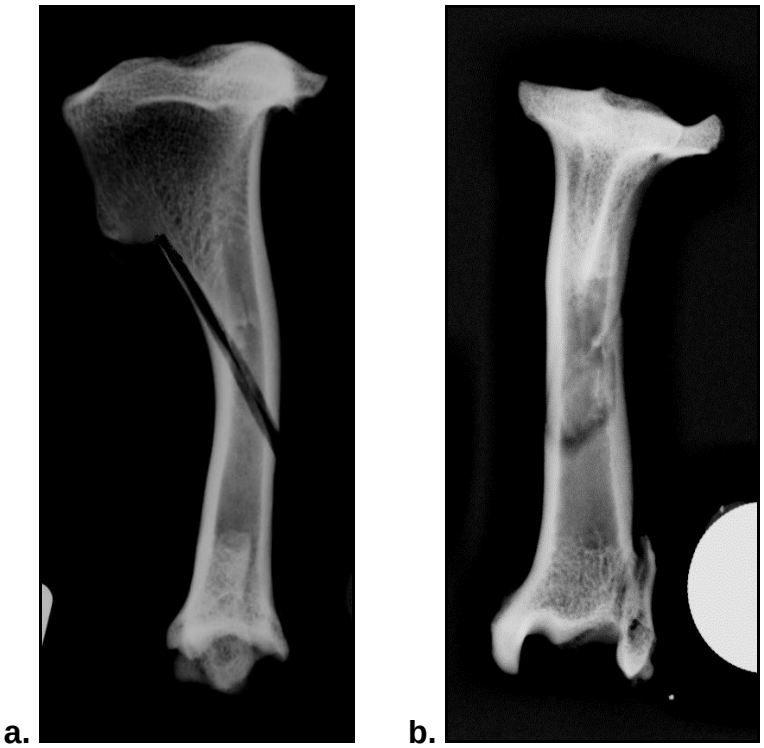

FIGURE 3.8. Mediolateral (a) and craniocaudal (b) view radiographs made of an osteotomized dachshund tibia.

a.  b. 

FIGURE 3.9. Mediolateral (a) and craniocaudal (b) photographs of an osteotomized tibia.

3.5.3. Osteotomy fixation

Implants and instruments used in the osteotomized bone fixations, are portrayed in Appendix B.

3.5.3.1. Group 1

The pre-bending of IM pins were performed to conform to the curve of the medullary cavity of each dachshund tibia on mediolateral view radiographs. The curve in the pins was then confirmed by comparing them to the shape of the diaphysis on the medial aspect of each bone specimen. The pre-bending was performed in the transverse plane only. (See Figure 3.10).

FIGURE 3.10. A 2 mm Steimann pin (K-wire) compared to the shape of the diaphysis of a dachshund tibia after being measured and pre-bent to conform to the curve of its medullary cavity on a mediolateral view radiograph.

All osteotomized bones for pinning (group 1) were repaired manually (i.e. not using any power tools) in a normograde fashion, entering at the proximal tibial plateau in a standard location. (See Figure 3.11). The areas of insertion of the medial collateral ligament on the medial tibial condyle and the patellar ligament on the tibial crest, were identified. The point of pin entry was slightly cranial to a point halfway between these two land marks and just medial to the patellar ligament. The pin was aimed in a disto-caudomedial direction[17,21,50,51,52,70], turning the chuck not more than an eighth to a quarter turn clockwise or anti-clockwise each time. The proximal end of the pin was cut not longer than 5 mm. This was only possible by withdrawing, cutting and again impacting the pin[17]. The IM pin was well and correctly seated in the medullary cavity before the first full cerclage wire was applied.

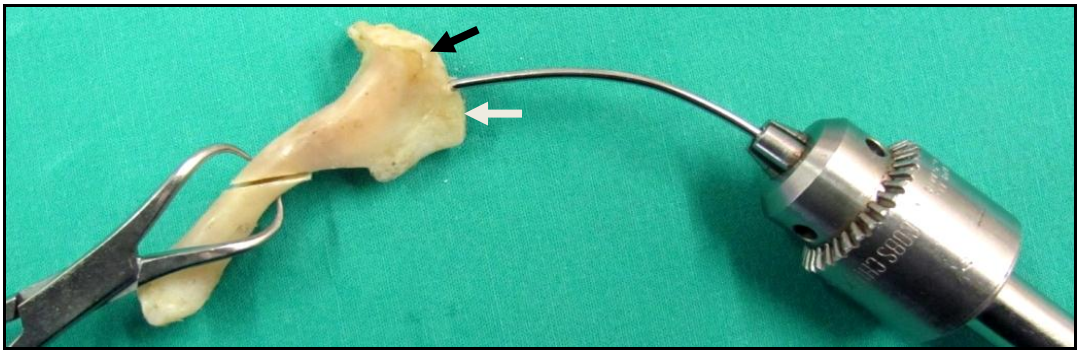

FIGURE 3.11. Pre-bent Steinmann pin introduced normograde, entering the tibia proximally (tibial plateau), aiming in a disto-caudomedial direction. The point of entry is slightly cranial to a point halfway between the medial collateral ligament (black arrow) and patellar ligament (white arrow) and just medial to the patellar ligament.

Three evenly spaced, 1.0 mm diameter cerclage wires were applied to the group 1 tibiae, making use of pre-prepared cortical grooves on the cranial, caudomedial and caudolateral aspects of the diaphysis to anchor the wires more effectively. The sharp edges of a small bone file were used for this purpose. (See Figure 3.12). The groove depth was standardized to be no deeper than one quarter to one third of the diameter of the cortex of the tibial diaphysis (i.e. less than 0.5 mm deep).

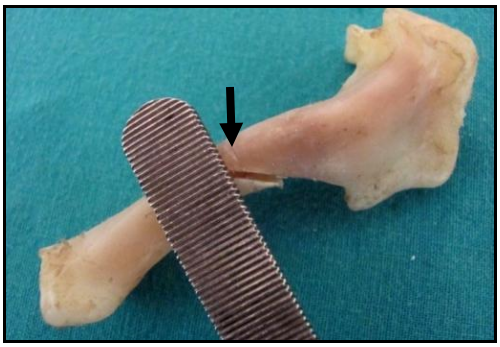

FIGURE 3.12. Bone file with cortical groove (black arrow) on the caudomedial aspect of the bone, perpendicular to its long axis.

The bent eyelet wire method, where a single wire loop encircles the bone in each case[8,14,60,68] was used to apply the full cerclage wires, using a wire loop tightener. (See Figure 3.13). The wire loop was placed caudomedially on the diaphysis, with the opposite end of the wire bent cranially after fixation for at least one third of the circumference of the bone on its medial surface. The wires were spaced not more than half a bone diameter apart[62], starting and ending not more than 0.5 cm from the tips of the fragments and perpendicular to the long axis of the bone[18].

FIGURE 3.13. Application of a cerclage wire around the tibial diaphysis using a wire loop tightener, illustrating the bent eyelet wire method.

A third mediolateral and craniocaudal view radiograph were made (see Figure 3.14) and a third set of digital photographs (see Figure 3.15) were taken as soon as the bone was repaired.

a. b.

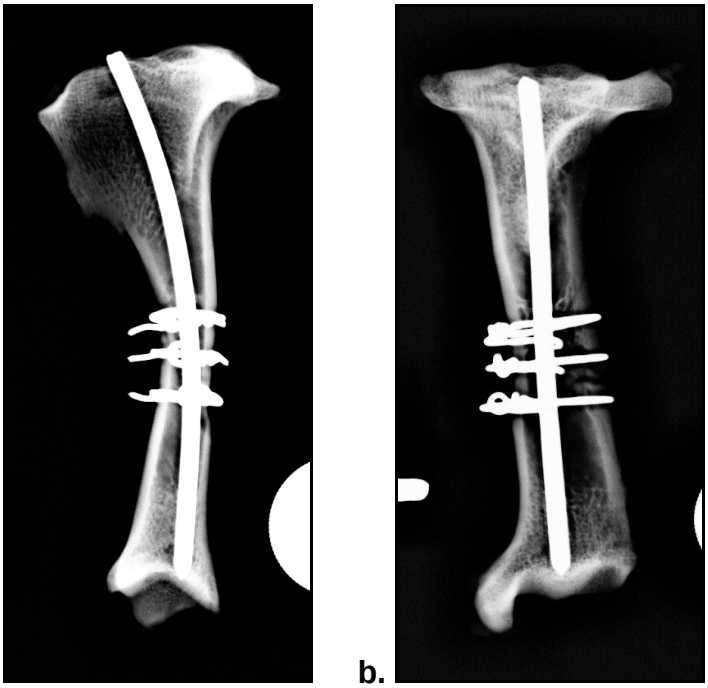

FIGURE 3.14. Mediolateral (a) and craniocaudal (b) view radiographs of an osteotomized dachshund tibia repaired with an IM pin and cerclage wires.

a. b. c.

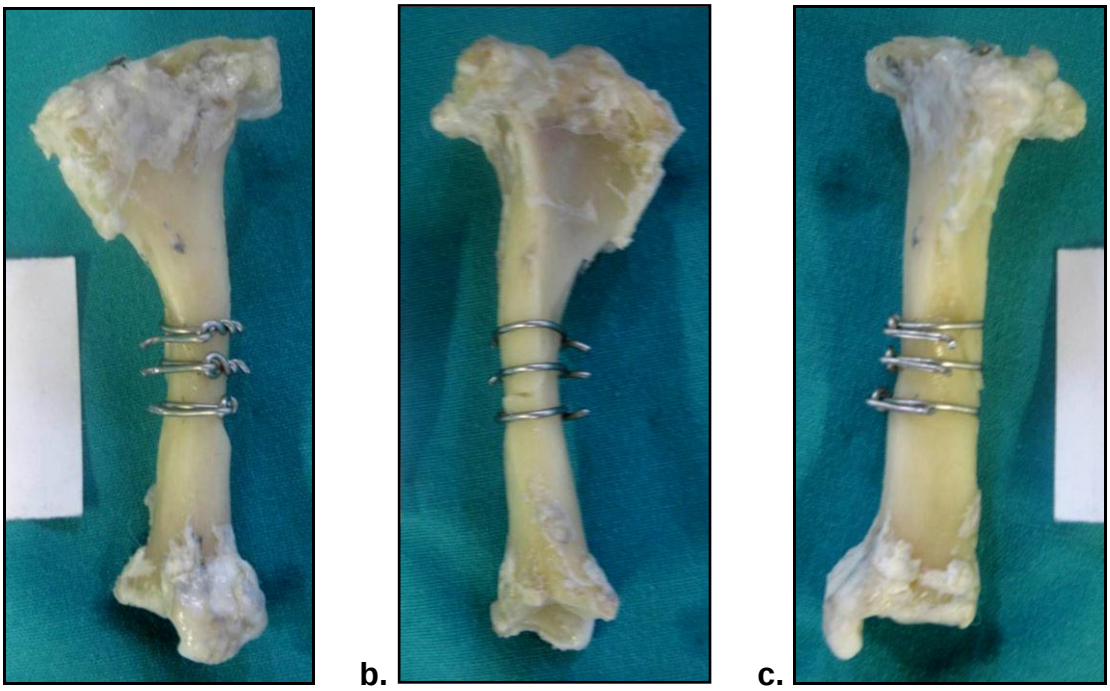

FIGURE 3.15. Medial (a), lateral (b) and cranial (c) photographic views of the same specimen as in Figure 3.14.

3.5.3.2. Group 2

All osteotomized bones for plating (group 2, the control group) were repaired by stabilizing the bone fragments with a lag screw. This stabilization was subsequently protected with a six hole, 2.7 mm DCP, contoured and attached to the medial aspect of the tibia with cortical screws in a neutralization mode.

In order to achieve compression at the osteotomy site, a 2.7 mm cortical screw was used as a lag screw by over drilling the screw hole in the *cis* cortex using a 2.7 mm drill bit, while the screw hole in the *trans* cortex was drilled with a 2 mm drill bit and tapped with a 2.7 mm tap. The lag screw (2.7 mm cortical screw) was inserted in a cranio-proximo-caudal direction, more or less perpendicular to the osteotomy line and in the middle thereof. (See Figure 3.16). During the application of the implants, the bone was kept hydrated with lactated Ringers to preclude thermal burns.

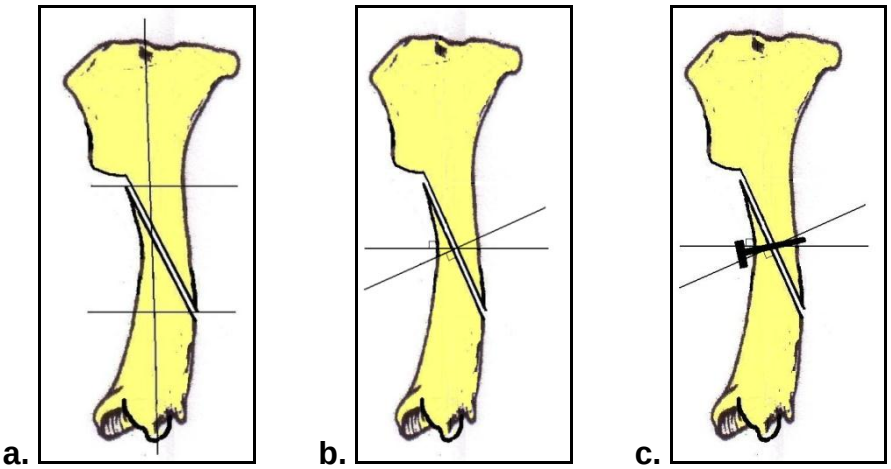

FIGURE 3.16. Diagram of the medial view of the right tibia of a dachshund with osteotomy in a proximo-cranial-disto-caudal direction in the middle third of the bone's diaphysis (a). Two lines drawn perpendicular to the osteotomy line and the *cis* cortex of the bone respectively, crossing each other in the middle of the osteotomy line (b). In order to achieve compression at the osteotomy site, a cortical screw in lag fashion was placed cranio-proximo-caudally, bisecting the two drawn lines in figure b (c).

The basic steps that were followed to apply the lag screw technique and bone plate and screws in each of the tibiae in group 2, are portrayed in Appendix C.

A third mediolateral and craniocaudal view radiograph were made (see Figure 3.17) and a third set of digital photographs (see Figure 3.18) were taken as soon as the bone was repaired.

a. b.

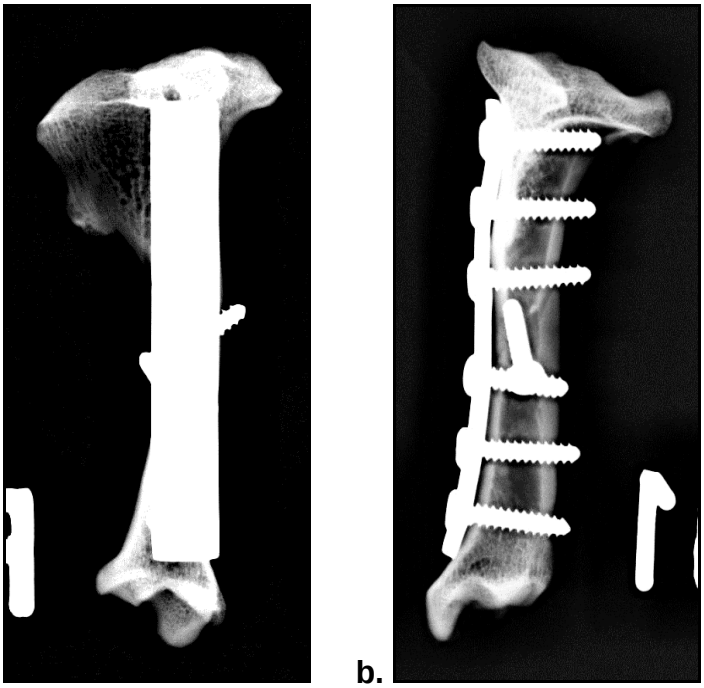

FIGURE 3.17. Mediolateral (a) and craniocaudal (b) view radiographs of a completed repair of the oblique osteotomy of a dachshund tibia using a bone plate and screws.

a. b. c.

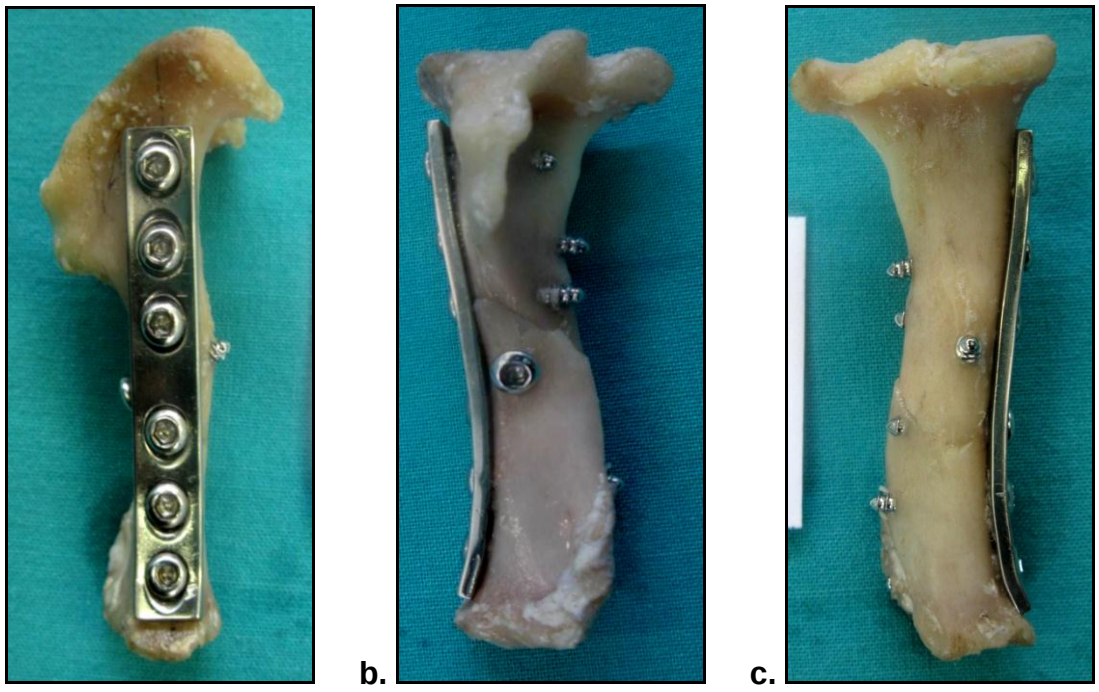

FIGURE 3.18. Medial (a), cranial (b) and caudal (c) photographic views of the same specimen as in Figure 3.17.

3.5.4. Testing

Testing took place at the venue of the Department of Mechanical and Aeronautical Engineering, University of Pretoria. The test specimens were transported from the OVAH to this venue as soon as the third set of radiographs and photographs were made, once again covered in a bath of lactated Ringers solution. The test preparation and procedure started immediately on arrival.

3.5.4.1. Single cycle compression until failure *versus* cyclic fatigue testing

A pilot study was performed by the author, wherein four specimens (two from each group) were subjected to a cyclic fatigue test method. A fixed[3,74] cyclical load (stress) was repeatedly applied to each bone-implant composite for one million cycles, or up to the point where the fixation failed or the test bone collapsed. No information was available on test frequencies for use in dachshund trials; therefore experimental testing was conducted to determine the test frequency, using ten live dachshunds running on a 5 meter long test track. These trials showed that their average frequency was between 9 Hz and 11 Hz, which converts to an equivalent of 9 to 11 steps per meter for the average dachshund. It was therefore decided that the test signal should be 10 Hz (Burger NDL, CMTI Consulting (Pty) Ltd, Pretoria, South Africa, personal communication, 2010).

However, all four tests resulted in similar stress-strain graphs, i.e. a horizontal line in a single plane, from which none of the study parameters could be determined. In none of these cases the *fatigue limit* (see Section 2.4.2.1. *Implant failure*) was exceeded, which means that only non-physiological loads, i.e. loads much higher than those used in the pilot study, would be able to cause plastic deformation and/or failure (fracture) of the implant[41,42]. It was concluded that no measurable effect was going to be obtained using the predetermined cyclic loads on any of the specimens over the specified one million cycles[3,74].

It was subsequently decided to abandon the use of the cyclic fatigue method for the purpose of this study due to the irregular shape of the stress-strain graphs, and to

replace it with the two point single cycle compression test[74]. This test method provides an excellent and simple way of determining breaking strengths of materials[28], such as the bone-implant constructs used in this study.

3.5.4.2. Test procedure

The *Schenck® 100 kN* testing machine (see Figures 3.20 and 3.22) that was used, is capable of simulating only compressive loads. The fixation of the test specimen at an incline of 20° craniocaudally (see Figures 3.1 and 3.21) resulted in a simulation of a combination of at least four of the five loads normally acting on long bones, (i.e. axial compression, bending, shearing and distraction). The *Schenck® 100 kN* testing machine was not able to simulate torsion. A load cell, which is a transducer that converts load (force) acting on it into a measurable, analog electric signal, was introduced in the testing system. (See Figure 3.22).

FIGURE 3.19. The *Schenck® 100 kN* compression testing machine, used in the testing procedures, linked to a computer to record the test data.

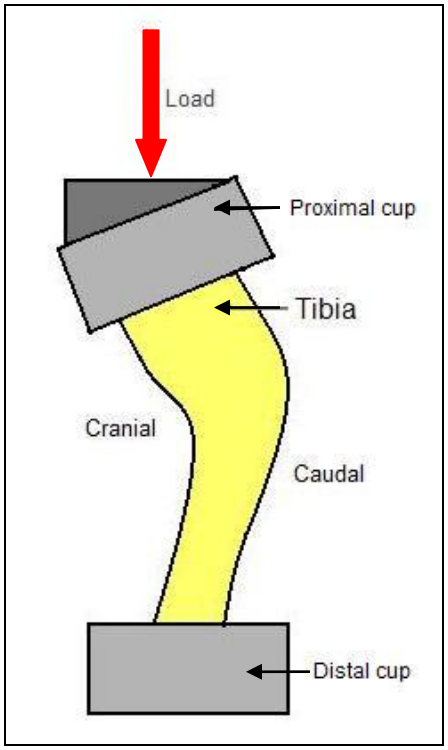

FIGURE 3.20. Diagram of the test specimen fixed at an incline of 20° craniocaudally. The red arrow indicates the direction of the applied load.

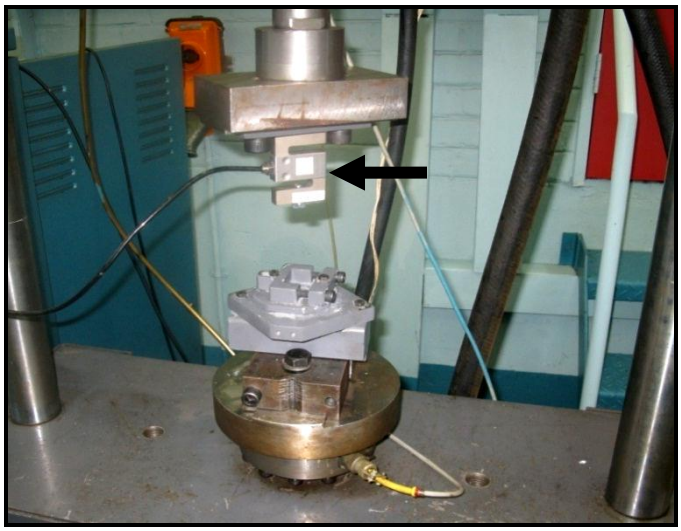

FIGURE 3.21. Close-up view of the testing area of the testing machine. The S-shaped load cell (black arrow) is clearly visible on this view.

An epoxy resin (*Pratley Quickset Putty®)* was used as potting material to fixate the tibiae at their proximal and distal ends in the testing cups to limit any undesired movement of the extremities of the bones in the testing machine during testing procedures. The bones were embedded in the potting material not deeper than 5 mm and in the case of the specimens in group 2, at least 3 to 5 mm away from the ends of the bone plates[74] to limit its influence on the strength of the diaphyses. The epoxy resin took approximately 1.5 hours to obtain full strength[53], during which time the bones were kept hydrated[54], by spraying the test bone with 10 ml lactated Ringers every 2 minutes.

After the epoxy resin had obtained 60% of its strength (within 20 minutes of application)[53], the bone was kept hydrated by covering it with a layer of cotton wool soaked in lactated Ringers, and wrapping the entire test specimen with a plastic wrapper (*Glad wrap® Non-toxic clear plastic wrap*) for the duration of the test. (See Figure 3.22).

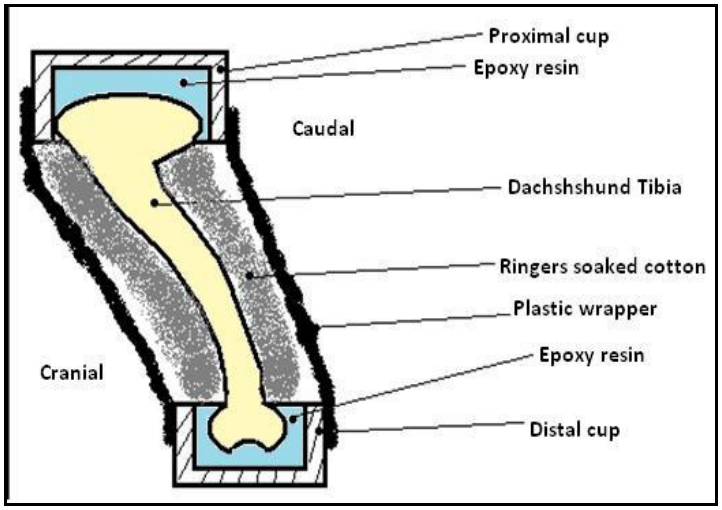

FIGURE 3.22. Diagram of a test specimen covered with a layer of cotton wool soaked in lactated Ringers and placed in a plastic wrapper.

After completion of these steps, a test specimen was placed within the test area of the *Schenck® 100 kN* testing machine for the actual tests to start. (See Figure 3.23).

a. 

b. 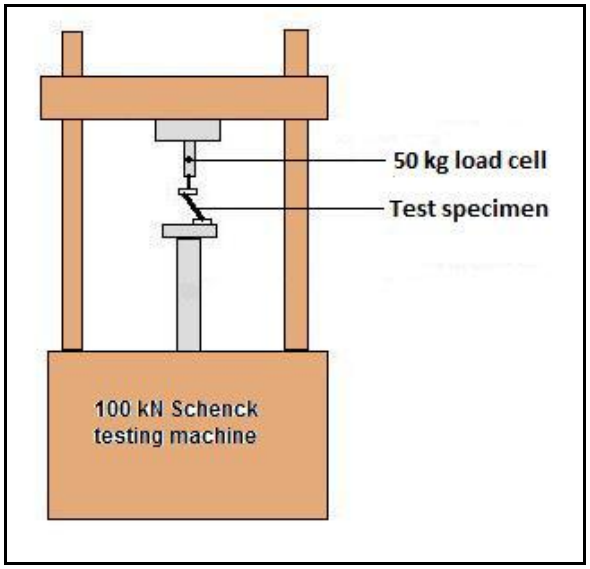

FIGURE 3.23. The test specimen placed in the testing position inside the testing machine (a). Diagram of the test setup (b).

Each test specimen was loaded under displacement control[74], increasing the load every 0.17 seconds, starting at 0 Pa. Displacement took place at 0.01 mm per increment, up to the point of implant failure or test specimen collapse.

3.5.5. Data captured

The following data was captured every 0.11 seconds (8.75 Hz) throughout each test by analog to digital conversion[74] and was subsequently transferred to a computer program (*Microsoft Excel*®) in order to draw a stress-strain graph for each specimen (also see Appendix D)**:**

- Stress (load) *(Pa)*
- Strain (deformation) *(%)*
- Displacement *(mm)*

The following were determined**:**

- Strength of the different bone-implant composites in the two groups.
- How and at what stage during the test procedure the implants would fail.

After completion of the biomechanical tests, each test specimen was removed from the

testing machine and transported in its cotton wool layer to the Diagnostic Imaging Section of the OVAH for a fourth mediolateral and craniocaudal view radiograph (see Appendix E), taken to determine the modes of failure for each specimen. Digital photographs (see Appendix E) were also taken of the test specimens in the unlikely event of the bone shattering beyond the protecting cotton wool layer, and for the purpose of more accurately determining each mode of failure. After removal of the cotton wool layers, it was however noted that no bone has shattered beyond its cotton wool covering layer.

3.5.6. Stress-strain graphs

A stress-strain graph was plotted from the raw data obtained for each specimen. (See Appendix D). Each stress-strain graph was individually examined with the aid of a dedicated computer software program (*MATLAB*®, MathWorks, Natick, Massachusetts). The inflection points were implisitly determined where the data showed sudden change in the curves. The following values were accurately determined in this way (see Tables 4.3 to 4.6)**:**

1) Stress at**:**
   - Yield point;
   - Ultimate strength;
   - Failure point
2) Strain at**:**
   - Yield point;
   - Ultimate strength;
   - Failure point

The following were also determined from the stress-strain graphs for each specimen (see Tables 4.7 and 4.8)**:**

1) Energy absorbed by the bone-implant-composite
2) Young's modulus of elasticity.

3.5.7. Statistical methodology

Descriptive statistics were initially performed to describe certain characteristics of the data, e.g. mean values, median values, standard deviation, etc. Some of these measures were, where applicable, represented in the form of scatter graphs and bar graphs.

A parametric analysis of co-variance (ANCOVA), a statistical method for testing whether certain factors have an effect on the outcome variables after removing the variance for which quantitative predictors (co-variates) account, was performed. Treatment methods and gender groups were used as factors, and mass and age of the animals as co-variates. Results were considered as significant on a 5% level of significance. P-values significant on the 10% and 1% levels were also indicated. Pearson correlations were used to interpret the linear relationship between the co-variates (body mass and age) and the outcome variables. Provision was made to meet the assumptions of normality of the data for the purposes of ANCOVA, by applying a normalization procedure.

CHAPTER FOUR: RESULTS

4.1. Data Presentation

Raw data obtained from the biomechanical tests and other observations were presented in the form of line graphs, tables, radiographs and photographs, from which the data to perform the necessary statistical analyses and the plotting of the relevant scatter graphs and bar graphs were gathered and refined.

4.2. Bone measurements and other parameters

The following bone measurements and other parameters were respectively identified from each cadaver, the pre-fracture and post-fixation radiographs and photographs, and the testing procedures**:**

- Age (see Tables 4.1 and 4.2);
- Gender (see Tables 4.1 and 4.2);
- Body mass (see Tables 4.1 and 4.2);
- Diameter of medullary cavity at its narrowest point (to aid in pin selection) (see Tables 4.1 and 4.2);
- Mean diaphyseal cortical width in that area (see Tables 4.1 and 4.2);
- Diameter of the whole bone in that area (see Tables 4.1 and 4.2);
- Length of bone (see Tables 4.1 and 4.2);
- Modes of failure of each specimen (see Tables 4.10 and 4.11).

TABLE 4.1. Group 1: Age, gender, body mass, medullary diameter, cortical width, and bone diameter at the narrowest point, and tibial length of the dachshund specimens. (n = 10)

Group 1 (IM pin and wires)								
Specimen no.	**Specimen ID**	**Age (years)**	**Gender (M/F)**	**Body mass (kg)**	**Medullary diameter (mm)**	**Cortical width (mm)**	**Bone diameter (mm)**	**Bone length (mm)**
1	**L-2**	4	M	11.70	5.345	1.296	6.641	72
2	**R-2**	4	M	11.70	5.099	1.484	6.583	72
3	**L-3**	7.5	M	8.65	3.801	1.831	5.632	75
4	**R-6**	5	F	6.55	3.017	1.689	4.706	75
5	**L-7**	3.5	M	9.45	3.476	1.632	5.108	76
6	**R-7**	3.5	M	9.45	3.508	1.681	5.189	76
7	**L-11**	6	F	7.20	2.950	1.681	4.631	65
8	**L-13**	2.5	M	7.00	3.252	1.515	4.767	70
9	**R-15**	4	F	5.50	3.603	0.975	4.578	56
10	**R-16**	6	F	5.20	2.095	1.629	3.724	66
Mean		**4.6**	**-**	**8.24**	**3.615**	**1.541**	**5.156**	**70.3**
Median		**4.0**	**-**	**7.93**	**3.492**	**1.631**	**4.938**	**72.0**
Std. Dev.		**1.5**	**-**	**2.34**	**0.972**	**0.246**	**0.912**	**6.4**

L = left; R = right; F = female; M = male

TABLE 4.2. Group 2: Age, gender, body mass, medullary diameter, cortical width, and bone diameter at the narrowest point, and tibial length of the dachshund specimens. (n = 10)

Group 2 (Bone plate and screws)								
Specimen no.	**Specimen ID**	**Age (years)**	**Gender (M/F)**	**Body mass (kg)**	**Medullary diameter (mm)**	**Cortical width (mm)**	**Bone diameter (mm)**	**Bone length (mm)**
11	**R-5**	3	F	6.80	5.029	1.352	6.381	68
12	**L-6**	5	F	6.50	3.451	1.562	5.013	75
13	**L-8**	7	F	6.50	3.939	1.402	5.341	74
14	**R-8**	7	F	6.50	3.571	1.749	5.320	74
15	**R-11**	6	F	7.20	3.313	1.459	4.772	65
16	**L-12**	5	F	6.00	3.819	2.510	6.329	66
17	**R-12**	5	F	6.00	4.782	1.188	5.970	66
18	**R-13**	2.5	M	7.00	3.276	1.579	4.855	70
19	**L-15**	4	F	5.50	3.232	1.203	4.435	56
20	**L-16**	6	F	5.20	2.155	1.446	3.601	66
Mean		**5.1**	**-**	**6.32**	**3.657**	**1.545**	**5.202**	**68**
Median		**5**	**-**	**6.50**	**3.511**	**1.453**	**5.167**	**67**
Std. Dev.		**1.5**	**-**	**0.64**	**0.817**	**0.379**	**0.868**	**5.7**

L = left; R = right; F = female; M = male

The raw data obtained from each stage of each test was transferred to a *Microsoft Excel*® spread sheet and displayed in the form of a stress-strain graph for each specimen. (See Appendix D). Each graph can roughly be divided into two main portions – a linear elastic section, and a non-linear plastic section[27,31,69].

The following stress and strain values for each specimen were determined from the individual stress-strain graphs**:**

- Yield point (see Tables 4.3 to 4.6);
- Point of ultimate strength (see Tables 4.3 to 4.6);
- Failure (fracture) point (see Tables 4.3 to 4.6);
- Energy absorbed by the bone-implant composite (seeTables 4.7 and 4.8); and
- Young's modulus (see Tables 4.7 and 4.8).

Using the respective yield point values as guideline, the following areas could also be identified from each graph**:**

- Elastic zone; and
- Plastic zone.

TABLE 4.3. Stress at yield point, ultimate strength, and failure point for the specimens in group 1. (n = 10)

Stress values: Group 1 (IM pin and wires)				
Specimen no.	**Specimen ID**	**Yield point (MPa)**	**Ultimate strength (MPa)**	**Failure point (MPa)**
1	**L-2**	0.353	0.475	0.407
2	**R-2**	0.288	0.470	0.469
3	**L-3**	0.356	0.474	0.475
4	**R-6**	0.352	0.392	0.137
5	**L-7**	0.163	0.245	0.247
6	**R-7**	0.130	0.153	0.134
7	**L-11**	0.473	0.477	0.477
8	**L-13**	0.480	0.486	0.486
9	**R-15**	0.151	0.178	0.135
10	**R-16**	0.479	0.482	0.485
Mean		**0.323**	**0.383**	**0.345**
Median		**0.353**	**0.472**	**0.438**
Std. Dev.		**0.137**	**0.136**	**0.161**

L = left; R = right

TABLE 4.4. Stress at yield point, ultimate strength, and failure point for the specimens in group 2. (n = 10)

Stress values: Group 2 (Bone plate and screws)				
Specimen no.	**Specimen ID**	**Yield point (MPa)**	**Ultimate strength (Mpa)**	**Failure point (Mpa)**
11	**R-5**	0.295	0.379	0.293
12	**L-6**	0.393	0.405	0.405
13	**L-8**	0.483	0.486	0.486
14	**R-8**	0.485	0.487	0.489
15	**R-11**	0.400	0.408	0.409
16	**L-12**	0.328	0.441	0.452
17	**R-12**	0.322	0.322	0.242
18	**R-13**	0.473	0.473	0.475
19	**L-15**	0.467	0.473	0.387
20	**L-16**	0.382	0.439	0.387
Mean		**0.403**	**0.431**	**0.403**
Median		**0.397**	**0.440**	**0.407**
Std. Dev.		**0.072**	**0.072**	**0.082**

L = left; R = right

TABLE 4.5. Strain at yield point, ultimate strength, and failure point for the specimens in group 1. (n = 10)

Strain values: Group 1 (IM pin and wires)				
Specimen no.	**Specimen ID**	**Yield point (%)**	**Ultimate strength (%)**	**Failure point (%)**
1	**L-2**	0.2904	0.4438	1.1010
2	**R-2**	0.0918	0.1589	0.2441
3	**L-3**	0.3110	0.4606	1.1900
4	**R-6**	0.0160	0.0447	0.3894
5	**L-7**	0.3143	0.7372	1.0520
6	**R-7**	0.3206	0.3282	0.4340
7	**L-11**	0.5166	0.6177	0.7944
8	**L-13**	0.3269	0.3888	0.4919
9	**R-15**	0.6154	0.7822	1.2050
10	**R-16**	0.1541	0.1591	0.2241
Mean		**0.2957**	**0.4121**	**0.7126**
Median		**0.3127**	**0.4160**	**0.6430**
Std. Dev.		**0.1805**	**0.2492**	**0.3989**

L = left; R = right

TABLE 4.6. Strain at yield point, ultimate strength, and failure point for the specimens in group 2. (n = 10)

Strain values: Group 2 (Bone plate and screws)				
Specimen no.	**Specimen ID**	**Yield point (%)**	**Ultimate strength (%)**	**Failure point (%)**
11	**R-5**	0.7833	1.279	2.252
12	**L-6**	0.4610	0.5668	1.0480
13	**L-8**	0.1694	0.1815	0.3134
14	**R-8**	0.2142	0.2272	0.3508
15	**R-11**	0.1890	0.2388	0.3610
16	**L-12**	0.2251	0.3316	1.0680
17	**R-12**	0.4824	0.4818	0.6291
18	**R-13**	0.5100	0.5172	1.2340
19	**L-15**	0.4768	0.7441	0.9111
20	**L-16**	0.1128	0.1541	0.2148
Mean		**0.3624**	**0.4722**	**0.8382**
Median		**0.3431**	**0.4070**	**0.7700**
Std. Dev.		**0.2125**	**0.3425**	**0.6174**

L = left; R = right

TABLE 4.7. Energy absorbed by, and Young's modulus for specimens 1 to 10 in group 1. (n = 10)

Group 1 (IM pin and wires)			
Specimen no.	**Specimen ID**	**Energy absorbed (kJ)**	**Young's Modulus (MPa)**
1	**L-2**	319.133	2.203
2	**R-2**	135.318	4.237
3	**L-3**	194.288	1.247
4	**R-6**	121.828	(15.209)*
5	**L-7**	140.379	0.583
6	**R-7**	35.695	0.677
7	**L-11**	222.865	1.297
8	**L-13**	143.719	1.668
9	**R-15**	106.743	0.242
10	**R-16**	86.915	3.329
Mean		**150.688**	**(2.953)* 1.720**
Median		**137.849**	**1.297**
Std. Dev.		**78.831**	**(4.446)* 1.329**

L = left; R = right
* = Young's modulus for specimen 4 deviated greatly from those of the other specimens and was therefore omitted in final calculations.

TABLE 4.8. Energy absorbed by, and Young's modulus for specimens 11 to 20 in group 2. (n = 10)

Group 2 (Bone plate and screws)			
Specimen no.	**Specimen ID**	**Energy absorbed (kJ)**	**Young's Modulus (MPa)**
11	**R-5**	647.341	0.492
12	**L-6**	305.266	0.809
13	**L-8**	109.682	3.044
14	**R-8**	122.871	2.367
15	**R-11**	114.248	2.248
16	**L-12**	119.277	1.736
17	**R-12**	108.965	0.776
18	**R-13**	180.625	1.204
19	**L-15**	300.112	1.202
20	**L-16**	632.692	3.971
Mean		**207.166**	**1.785**
Median		**121.074**	**1.470**
Std. Dev.		**175.131**	**1.117**

L = left; R = right

4.3. Results of Statistical Analyses

Statistical corrective measures were performed to bring into normality those results that were slightly out of the normal range of distribution. Mean values were therefore used as the basis of all statistical calculations. Median values were not used in any statistical calculations, but were merely included in this text for the sake of comparison.

Results of the descriptive statistics, i.e. mean values, median values, and standard deviation, can be found at the bottom of Tables 4.1 to 4.8. Results of the ANCOVA procedures performed on the raw data are summarized in Table 4.9. The following outcomes were significantly different between the factors, while the co-variates also explained the variation significantly**:** bone diameter ($p = 0.002$) and medullary diameter ($p = 0.001$) by body mass; cortical width ($p = 0.067$), strain at yield point ($p = 0.038$), strain at ultimate strength ($p = 0.029$), stress at failure point ($p = 0.049$), and strain at failure point ($p = 0.093$) by age. Results of Pearson Correlations, correlating the outcome variables with body mass and age of the cadavers, are summarized in Tables F.1 and F.2 in Appendix F.

TABLE 4.9. Results of ANCOVA for comparison of intramedullary pin with full cerclage wires, and bone plate and screws for repair of mid-diaphyseal osteotomies of dachshund tibiae. (n = 20)

Results of ANCOVA for Outcome variables								
Outcome variable	Factor						Co-variate	
	Treatment method					Gender	Age	Body Mass
	IM pin and wires		Bone plate and screws		p			
	Mean	SD	Mean	SD	p	p	p	p
Bone length (mm)	70.300	6.400	68.000	5.700	0.501	0.185	0.117	0.355
Bone diameter (mm)	5.156	0.912	5.202	0.868	0.075*	0.271	0.494	0.002***
Medullary diameter (mm)	3.615	0.972	3.657	0.817	0.090*	0.119	0.178	0.001***
Cortical width (mm)	1.541	0.246	1.545	0.379	0.831	0.209	0.067*	0.554
Yield point (Stress MPa)	0.323	0.137	0.403	0.072	0.299	0.370	0.152	0.256
Yield point (Strain %)	0.296	0.181	0.362	0.213	0.684	0.638	0.038**	0.759
Ultimate strength (Stress MPa)	0.383	0.136	0.431	0.053	0.275	0.469	0.129	0.913
Ultimate strength (Strain %)	0.412	0.249	0.472	0.343	0.778	0.418	0.029**	0.787
Failure point (Stress MPa)	0.345	0.161	0.403	0.082	0.137	0.136	0.049**	0.719
Failure point (Strain %)	0.713	0.399	0.838	0.617	0.505	0.727	0.093*	0.731
Young's Modulus (MPa)	1.720	1.329	1.785	1.117	0.726	0.949	0.122	0.529
Energy absorbed (kJ)	150.688	78.831	207.166	175.131	0.384	0.533	0.317	0.194

Key: * = Significant at 10% level; ** = Significant at 5% level; *** = Significant at 1% level;
SD = Standard deviation; p = Exceedance probability; MPa = Megapascal;
kJ = Kilojoule

4.3.1. Graphic representation

Scatter graphs and bar graphs were drawn to represent the values that were statistically significant. Only values of outcome variables that were significantly correlated to the factors and co-variates (see Table 4.9), were plotted and are indicated in the following scatter graphs. These values are: body mass *vs*. bone diameter ($p < 0.01$), body mass *vs*. medullary diameter ($p < 0.01$), cortical width *vs*. age ($p < 0.1$), strain at yield point *vs.* age ($p < 0.05$), strain at ultimate strength *vs*. age ($p < 0.05$), stress at failure point *vs*. age ($p < 0.05$), and strain at failure point *vs*. age ($p < 0.1$). (See Figures 4.1 to 4.7). Outcome variables with p-values higher than 10% (not statistically significant) were not included in the graphs.

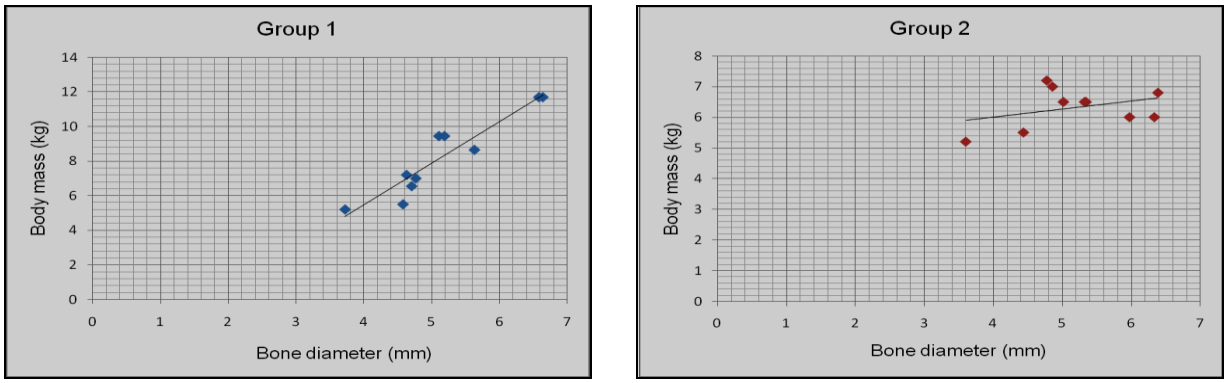

a. **b.**

Figure 4.1 (a and b). Scatter graphs of body mass *vs*. bone diameter for the specimens in groups 1 and 2, with line of best fit (trend line) indicated on the graphs. ($p < 0.01$).

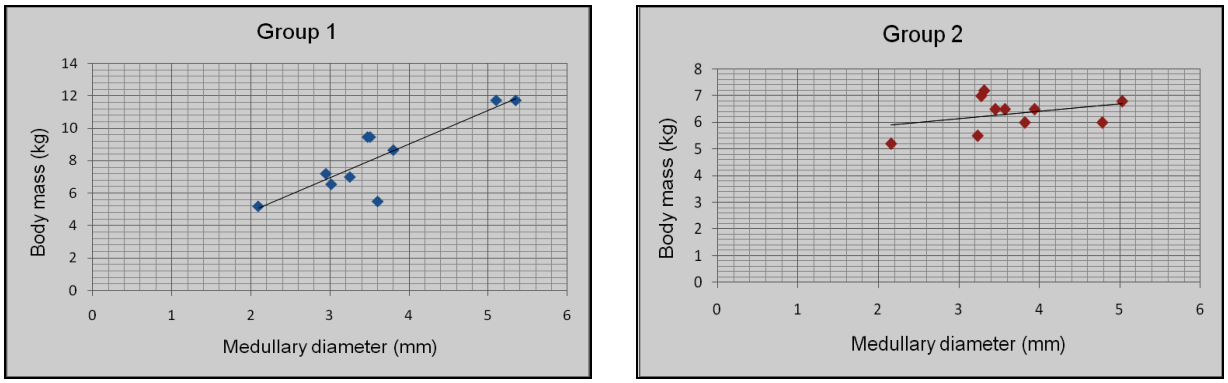

a. **b.**

Figure 4.2 (a and b). Scatter graph of body mass *vs*. medullary diameter for the specimens in groups 1 and 2, with line of best fit (trend line) indicated on the graphs. ($p < 0.01$).

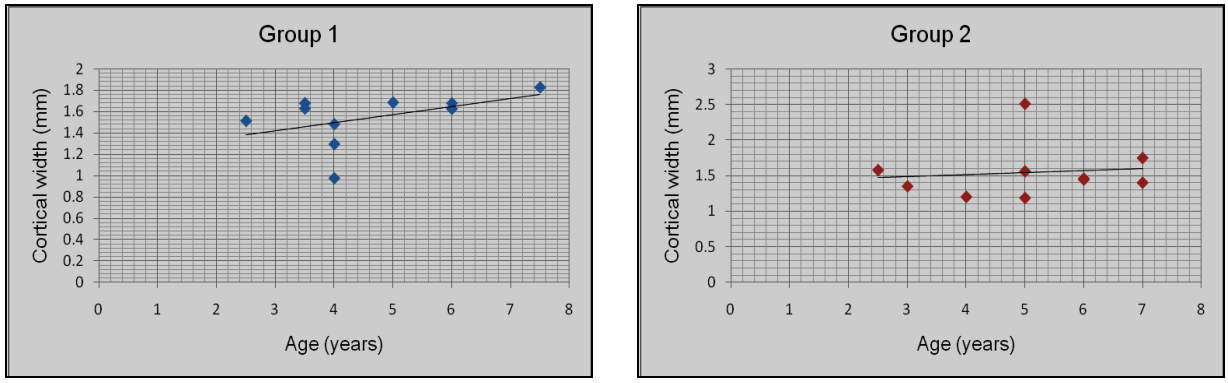

a. **b.**

Figure 4.3 (a and b). Scatter graph of cortical width *vs*. age for the specimens in groups 1 and 2, with line of best fit (trend line) indicated on the graphs. ($p < 0.1$).

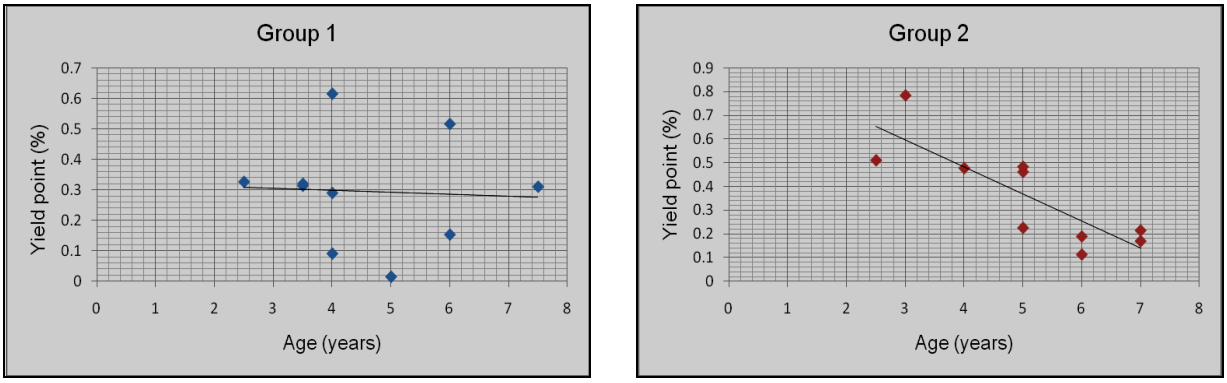

a. **b.**

Figure 4.4 (a and b). Scatter graph of yield point *vs*. age for the specimens in groups 1 and 2, with line of best fit (trend line) indicated on the graphs. ($p < 0.05$).

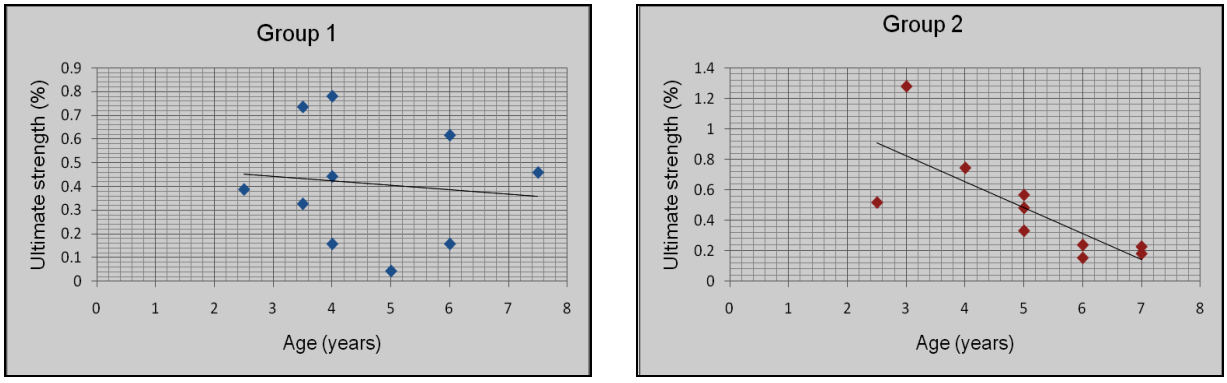

a. **b.**

Figure 4.5 (a and b). Scatter graph of strain at ultimate strength *vs*. age for the specimens in groups 1 and 2, with line of best fit (trend line) indicated on the graphs. ($p < 0.05$).

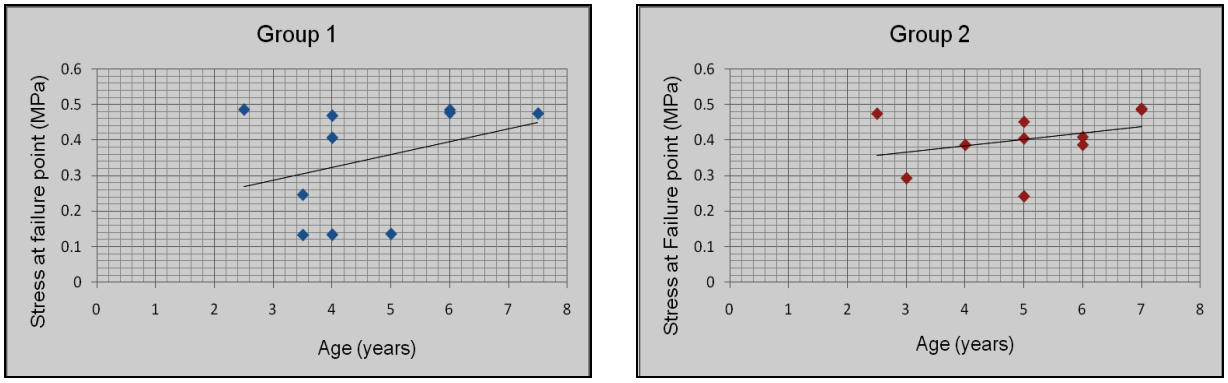

a. **b.**

Figure 4.6 (a and b). Scatter graph of applied stress at the failure point *vs*. age for the specimens in groups 1 and 2, with line of best fit (trend line) indicated on the graphs. (p < 0.05).

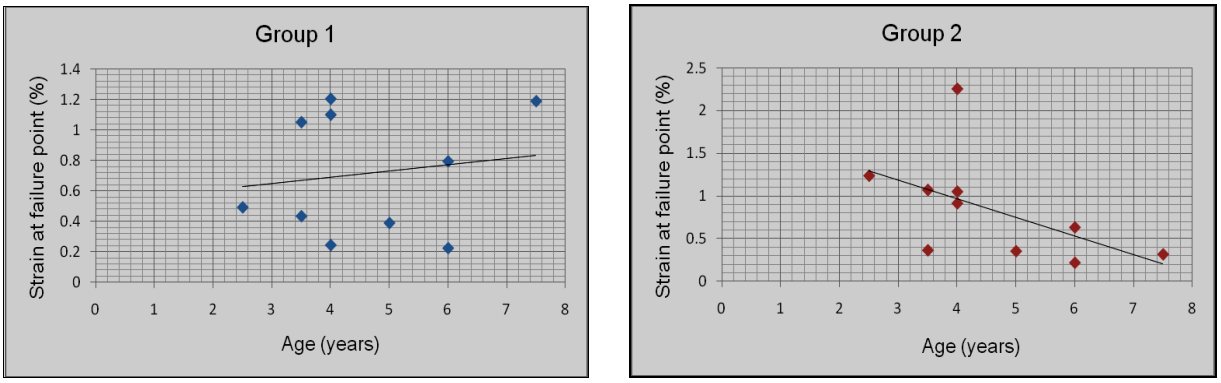

a. **b.**

Figure 4.7 (a and b). Scatter graph of strain at the failure point *vs*. age for the specimens in groups 1 and 2, with line of best fit (trend line) indicated on the graphs. (p < 0.1).

Mean bone diameter ($p < 0.1$) and mean medullary diameter ($p < 0.1$) for the two groups are illustrated in the form of a bar graph. (See Figure 4.8). Mean cortical width, although not statistically significant ($p = 0.831$) was included in this graph for the sake of comparison.

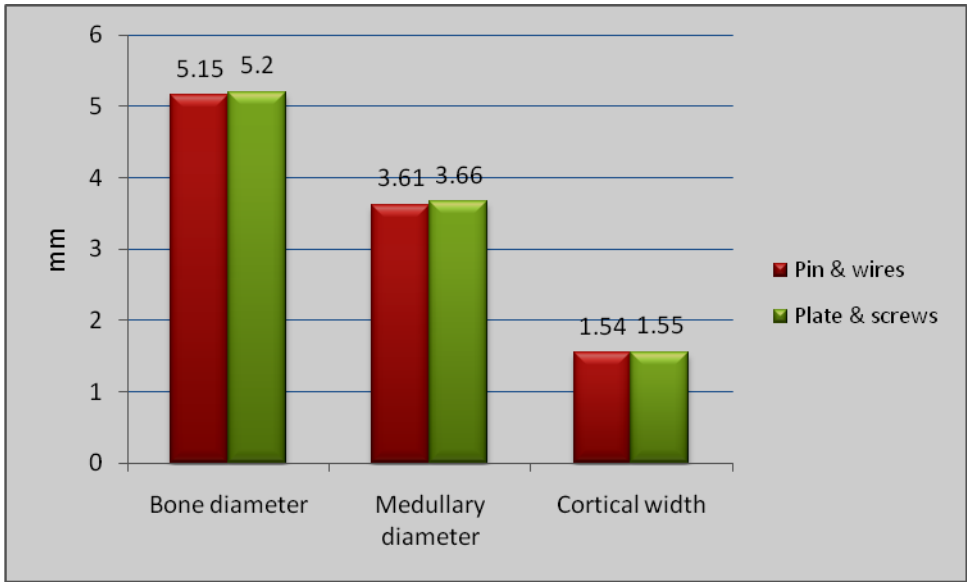

Figure 4.8. Bar graph illustrating mean bone diameter (p < 0.1), mean medullary diameter (p < 0.1), and mean cortical width (p = 0.831) for the two groups.

For groups 1 and 2 respectively, mean stress (applied load) at the yield point were 0.323 MPa (± 0.137) and 0.403 MPa (± 0.072) (p = 0.299), at ultimate strength 0.383 MPa (± 0.136) and 0.431 MPa (± 0.053) (p = 0.275), and at the failure point 0.345 MPa (± 0.161) and 0.403 MPa (± 0.082) (p = 0.137). Mean strain (deformation) at the yield point in the two groups were 0.296% (± 0.181) and 0.362% (± 0.213) respectively (p = 0.684), at ultimate strength 0.412% (± 0.249) and 0.472% (± 0.343) (p = 0.778), and at the failure point 0.713% (± 0.399) and 0.838% (± 0.617) (p = 0.505). (See Table 4.9 and Appendix G).

Mean age of the dachshunds in this study was 4.8 years (± 1.5) and 5.1 years (± 1.5) for the IMPW and BPS groups respectively, while mean age of female cadavers was 5.3 years (± 1.2) and that of male cadavers 3.9 years (± 1.7). Similarly, mean mass was 8.24 kg (± 2.3) and 6.32 kg (± 0.6) for the IMPW and BPS groups respectively, while mean mass of female cadavers was 6.2 kg (± 0.7) and that of male cadavers 9.28 kg (± 1.9).

Bar graphs comparing the mean applied stress at the yield point, ultimate strength, and failure point (see Figure 4.9), and the mean strain at the same points (see Figure 4.10), were drawn for the specimens in groups 1 and 2.

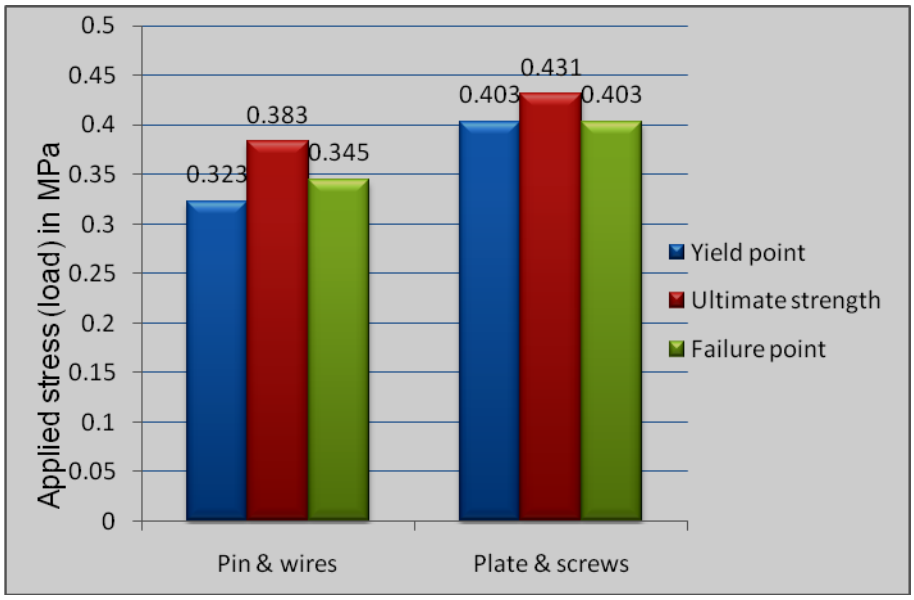

Figure 4.9. Bar graph illustrating the mean applied stress (load) at the Yield point (p = 0.3), Ultimate strength (p = 0.28), and Failure point (p = 0.137) for the specimens in groups 1 (IM pin and wires) and 2 (bone plate and screws).

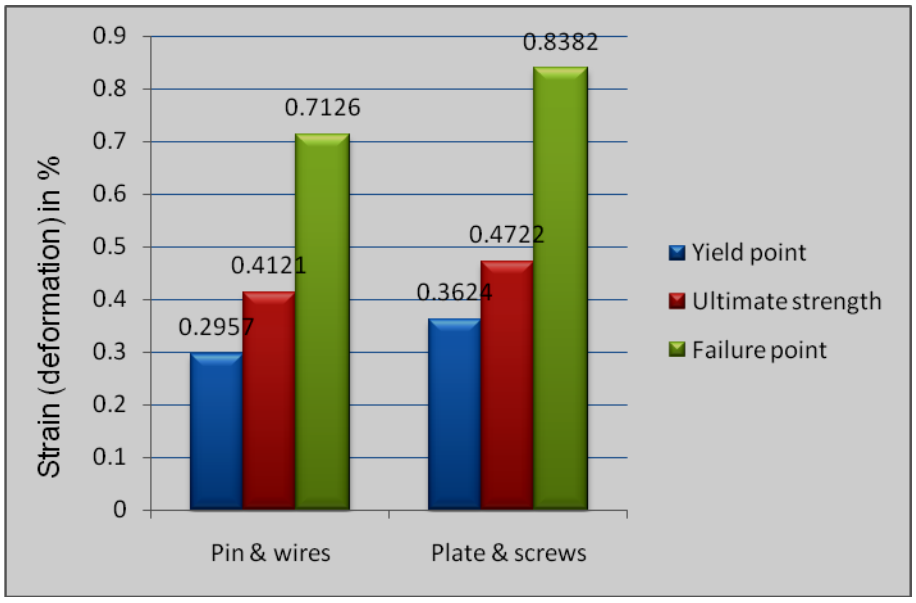

Figure 4.10. Bar graph illustrating the mean strain (deformation) at the Yield point (p = 0.684), Ultimate strength (p = 0.778), and Failure point (p = 0.5) for the specimens in groups 1 (IM pin and wires) and 2 (bone plate and screws).

Mean values for energy absorbed by each specimen until failure, i.e. the area under the stress-strain graph, was determined and the mean value for each group represented as a bar graph. (See Figure 4.11). These mean values were 150.688 kJ (± 78.831) and 207.166 kJ (± 175.131) (p = 0.384) for groups 1 and 2 respectively.

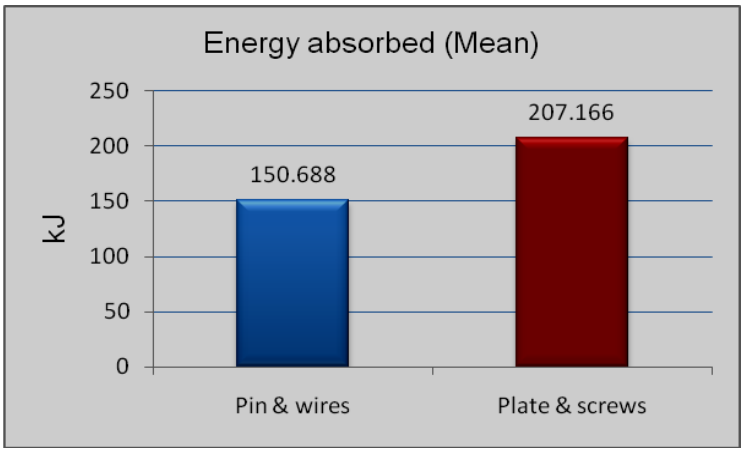

Figure 4.11. Bar graph illustrating mean energy absorbed until failure by the specimens repaired by IM pin and full cerclage wires (group 1), and bone plate and screws (group 2). (p = 0.384).

Mean values for Young's modulus, i.e. the stiffness of the bone-implant unit during the elastic phase, was determined for each specimen and the mean value for each group represented as a bar graph. (See Figure 4.12). These mean values were 1.720 MPa (± 1.329) and 1.785 MPa (± 1.117) (p = 0.726) for groups 1 and 2 respectively.

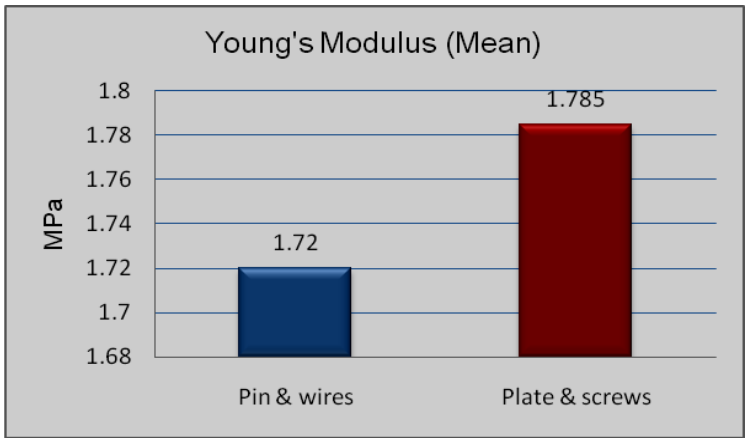

Figure 4.12. Bar graph illustrating Young's modulus (mean) for the specimens repaired by IM pin and full cerclage wires (group 1), and bone plate and screws (group 2). (p = 0.73).

4.4. Modes of Failure

4.4.1. Group 1

During loading to failure, 80% intramedullary pins and 30% cerclage wires underwent plastic (permanent) deformation. Three distinct modes of failure were noted in group 1:

1) Unraveling/slippage with displacement of cerclage wires (50% of specimens in group 1). (See Figure 4.1).

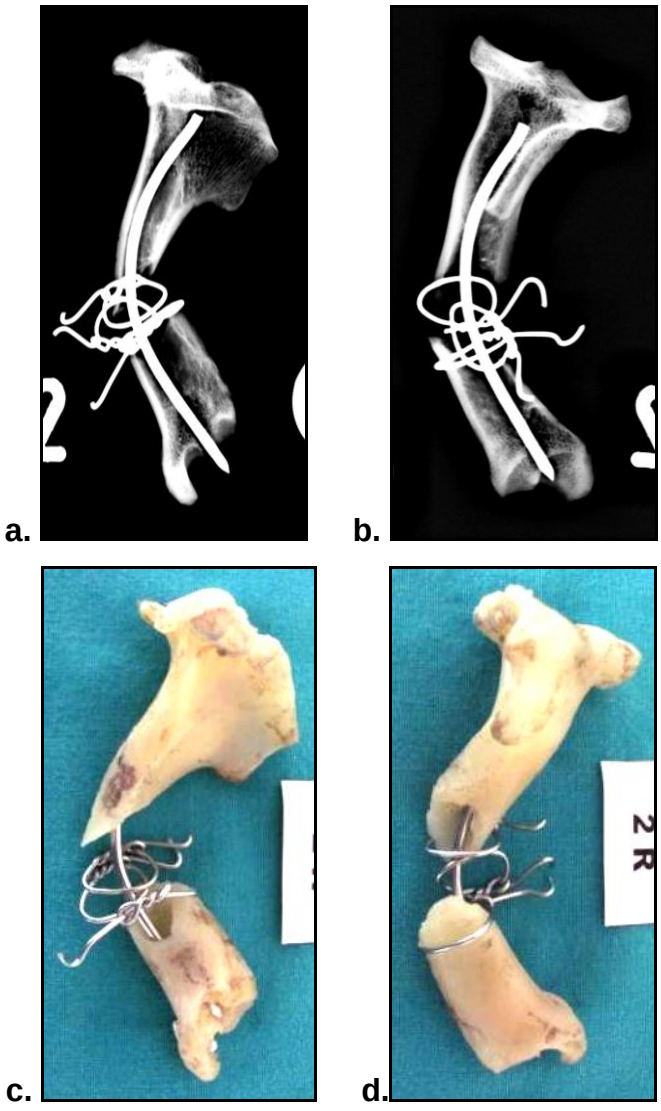

FIGURE 4.13. Unraveling/slippage of cerclage wires. Specimen 2 (R-2): Mediolateral (a) and craniocaudal (b) view radiographs of the left tibia, and its medial (c) and cranial (d) photographic view, taken after completion of the biomechanical tests. Separation of the fragments at the osteotomy site; all 3 cerclage wires were loose and displaced towards the osteotomy site; their free ends were elevated between 40° and 85°; the intramedullary pin underwent plastic deformation.

2) Bone fracture at a cerclage wire (30% of specimens in group 1). (See Figure 4.2).

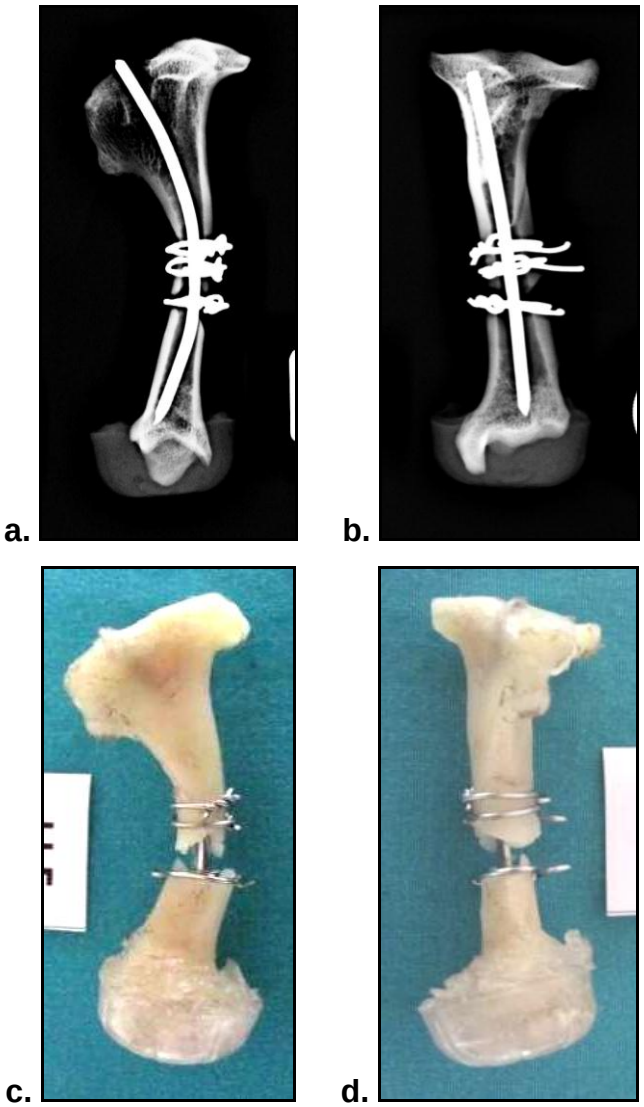

FIGURE 4.14. Bone fracture at a cerclage wire. Specimen 7 (L-11): Mediolateral (a) and craniocaudal (b) view radiographs of the left tibia, and its medial (c) and cranial (d) photographic view, taken after completion of the biomechanical tests. No separation of the fragments at the osteotomy site; complete transverse fracture at the distal wire, involving both fragments; separation took place at this fracture site; the intramedullary pin was intact.

3) Bone fracture not associated with a cerclage wire (20% of specimens in group 1). (See Figure 4.15).

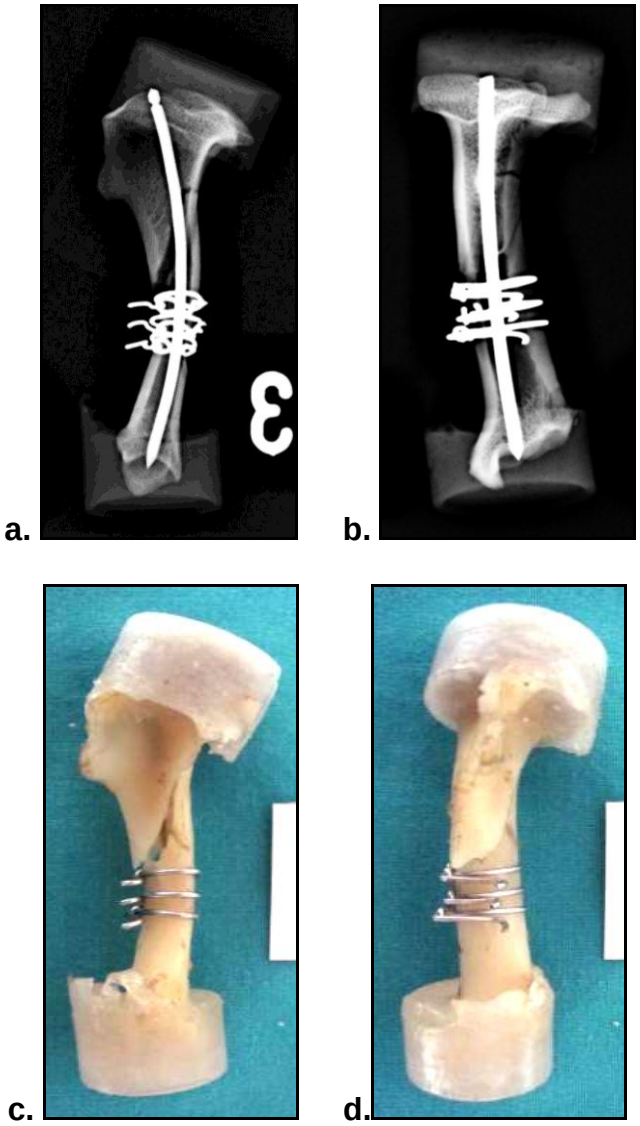

FIGURE 4.15. Bone fracture not associated with a cerclage wire. Specimen 8 (L-13): Mediolateral (a) and craniocaudal (b) view radiographs of the left tibia, and its lateral (c) and cranial (d) photographic views, taken after completion of the biomechanical tests. No separation at the osteotomy site; the cerclage wires were intact; long spiral fracture starting 1mm proximal to the proximal wire on the cranial ridge of the bone, running in a caudo-proximal direction; intramedullary pin underwent a small degree of plastic deformation.

4.4.2. Group 2

None of the bone plates or screws underwent plastic (permanent) deformation. Two distinct modes of failure were noted in group 2:

1) Bone fracture at one or more screw holes (80% of specimens in group 2). (See Figure 4.16).

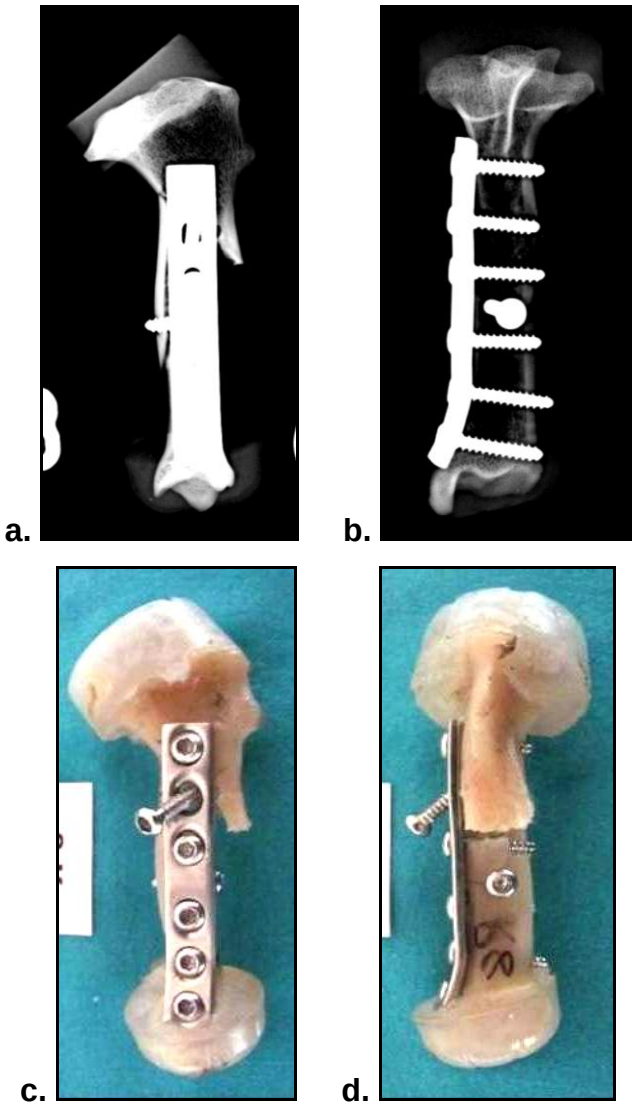

FIGURE 4.16. Bone fracture at one or more screw holes. Specimen 14 (R-8): Mediolateral (a) and craniocaudal (b) view radiographs of the left tibia, and its medial (c) and cranial (d) photographic views, taken after completion of the biomechanical tests. Separation of main bone fragments; complete long oblique fracture involving the cranial aspect of the bone, running in a disto-proximal direction between the length of screw 3 to the length of screw 1; the distal aspect of the fracture line ran transversely on the cranial aspect of the bone along the length of screw 3, just proximal to it; screw 2 was completely loose and displaced, but without any plastic deformation; the bone plate and the rest of the screws were intact, without any plastic deformation. (Screws numbered 1 to 6 proximo-distally).

2) Bone fracture not directly associated with the implants (20% of specimens in group 2). (See Figure 4.17).

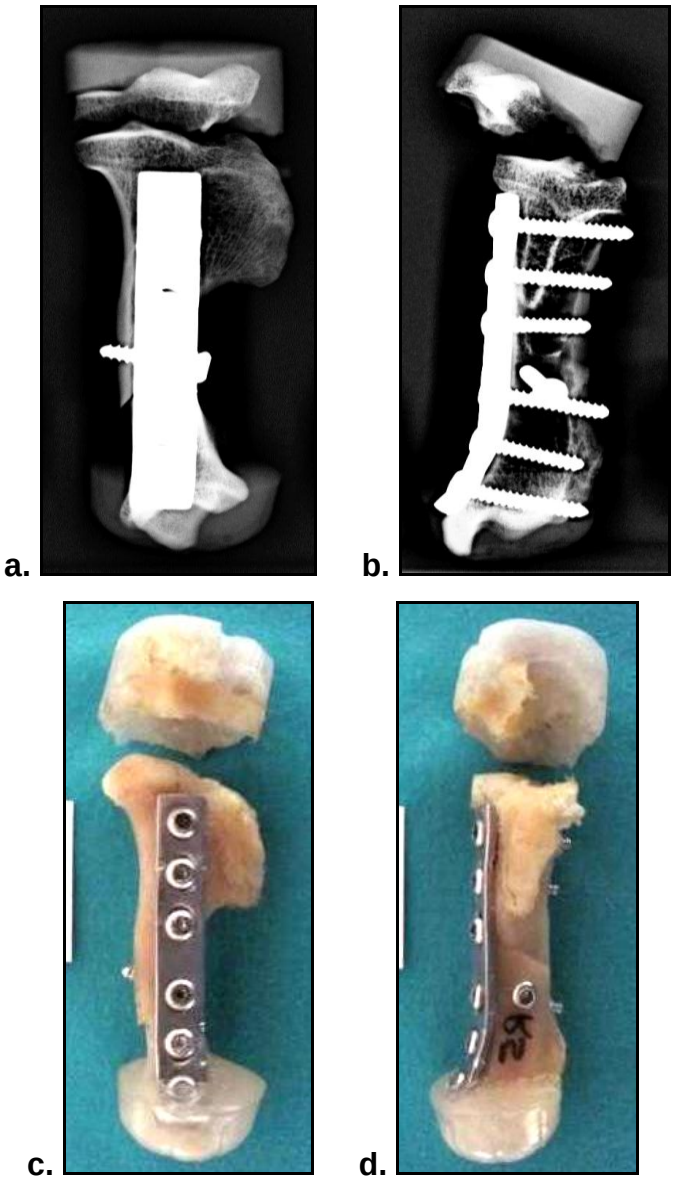

FIGURE 4.17. Bone fracture not associated with the implants. Specimen 11 (R-5): Mediolateral (a) and craniocaudal (b) view radiographs of the left tibia, and its medial (c) and cranial (d) photographic views, taken after completion of the biomechanical tests. No separation of fragments; transverse fracture of the proximal epiphysis of the bone; the bone plate and screws were intact, without any plastic deformation.
(Screws in plate holes numbered 1 to 6 proximo-distally).

Only one screw (3%) loosened and displaced under compression, due to a connecting fissure line that developed along the lengths of the shafts of two adjacent screws. This resulted in separation of the main bone fragments at the osteotomy site in this single specimen.

4.4.3. Summary of individual modes of failure

A summary of the individual modes of failure for each specimen in the two groups can be found in Tables 4.10 and 4.11.

TABLE 4.10. Summary of mode(s) of failure of the specimens in group 1 (specimens 1 to 10). (n = 10)

Group 1 (IM pin and wires)		
Specimen no.	**Specimen ID**	**Mode(s) of failure**
1	**L-2**	Separation of main bone fragments; proximal and distal wire displaced; IM pin plastic deformation.
2	**R-2**	Separation of main bone fragments; all 3 wires displaced; IM pin intact.
3	**L-3**	Separation of main bone fragments; all 3 wires displaced; IM pin plastic deformation.
4	**R-6**	Separation of main bone fragments; wires not displaced; fractures proximal fragment under proximal and middle wires and distal fragment proximal to proximal wire; IM pin intact.
5	**L-7**	Separation of main bone fragments; wires not displaced; fracture proximal fragment under middle wire; IM pin plastic deformation.
6	**R-7**	Separation of main bone fragments; middle and distal wires displaced; fracture under middle wire; IM pin plastic deformation.
7	**L-11**	No separation of fragments; wires not displaced; fracture under distal wire (both fragments); IM pin intact.
8	**L-13**	No separation of fragments; wires not displaced; fracture proximal to proximal wire; IM pin plastic deformation.
9	**R-15**	No separation of fragments; wires not displaced; fracture at proximal tip of bone; IM pin plastic deformation.
10	**R-16**	No separation of fragments; wires not displaced; avulsion fracture caudal head of bone; IM pin plastic deformation.

(Ceclage wires numbered 1 to 3 proximo-distally).
L = left; R = right

TABLE 4.11. Summary of mode(s) of failure of the specimens in group 2 (specimens 11 to 20). (n = 10)

Group 2 (Bone plate and screws)		
Specimen no.	**Specimen ID**	**Mode(s) of failure**
11	**R-5**	No separation of fragments; fracture of proximal epiphysis of the bone; bone plate and screws intact, without plastic deformation.
12	**L-6**	No separation of fragments; fracture at head lag screw; bone plate and screws intact, without plastic deformation.
13	**L-8**	No separation of fragments; fracture at heads screws 1 and 2; bone plate and screws intact, without plastic deformation.
14	**R-8**	Separation of main bone fragments; fracture between body screws 1 and 3; screw 2 loose; bone plate and rest of screws intact, without plastic deformation.
15	**R-11**	No separation of fragments; fracture proximal to proximal end of bone plate; bone plate and screws intact, without plastic deformation.
16	**L-12**	No separation of fragments; fracture between screw tips 1, 2 and 3; bone plate and screws intact, without plastic deformation.
17	**R-12**	No separation of fragments; fracture between heads screw 3, lag screw and screw 4; tibial crest avulsion fracture; bone plate and screws intact, without plastic deformation.
18	**R-13**	No separation of fragments; fracture between screw tips 3 and 4 and from head of lag screw; bone plate and screws intact, without plastic deformation.
19	**L-15**	No separation of fragments; fracture at head lag screw; bone plate and screws intact, without plastic deformation.
20	**L-16**	No separation of fragments; fracture at body of screw 1; bone plate and screws intact, without plastic deformation.

(Screws in plate holes numbered 1 to 6 proximo-distally).
L = left; R = right

4.4.4. Radiographs and photographs

Modes of failure portrayed by radiographs and photographs of each specimen taken after completion of the biomechanical tests are shown in Appendix E. Mediolateral and craniocaudal view radiographs of each specimen taken prior to the biomechanical testing are included for the sake of comparison of the mode(s) of failure.

CHAPTER FIVE: DISCUSSION

5.1 Introduction

The aim of this study was to compare, *in vitro*, the breaking strengths and modes of failure between two methods of repair of oblique diaphyseal tibial fractures of dachshunds. The two treatment methods used were IM pins with full cerclage wires, and bone plates and screws.

This study attempted to define the mechanical behaviour of the two methods of repair by using osteotomized dachshund tibiae, subjected to a two point single cycle compression test under displacement control[74], loaded by increasing compressive forces until these forces reached the levels at which the specimens failed[79]. The test specimens were placed in the test configuration such that simultaneous shear and bending loads also resulted while axial compression was applied. The different modes of failure were determined for each specimen in the two groups. Various parameters were measured and compared, and are discussed in the following sections.

5.2 Specimens

Dachshunds present a unique challenge in the treatment of most appendicular fractures, due to the unusual angular anatomic structure of their long bones[51,52]. This anatomical characteristic is causing implants to be more difficult to apply and implant failure to occur more often than in non-chondrodystrophic dog breeds. Dachshunds were selected as study specimens, because they display the typical characteristics of all chondrodystrophic dog breeds, namely angular deformities of the limbs, and can therefore be considered representative of chondrodystrophic dog breeds in general. The dachshund is a very popular dog breed amongst pet owners all over the world – their high numbers warranted a study such as this. Results of this study could well be applied to similar fractures of other chondrodystrophic dog breeds.

Mean age of dachshunds in groups 1 and 2 was 4.8 years (± 1.5), and 5.05 years (± 1.53) respectively. Age only influenced some results significantly, i.e. strain at yield point (p = 0.038), strain at ultimate strength (p = 0.029), stress at failure point (p = 0.049), strain at failure point (p = 0.093), and mean cortical width (p = 0.067). The higher the age of the dog, the lower the deformation at the yield point ([1]r = −0.174, p = 0.463), and the greater the loads needed to cause failure (r = 0.342, p = 0.140). Mean cortical width also increased with age, causing the bones in the older dogs to be slightly more resistant against external loads than that of younger dogs.

Gender distribution between the two groups was slightly uneven, i.e. six (60%) of the cadavers in group 1 were male, while only one (10%) of the cadavers in group 2 was male. Four (40%) of the cadavers in group 1 were female, while nine (90%) of the cadavers in group 2 were female. Although unevenly distributed, the gender distribution in this study did not significantly influence any biomechanical test results (p ≥ 0.119), suggesting that there was no statistically detectible difference between genders in resistance of their bones to external loads.

In terms of response to different loads, implants used in this study have the following characteristics: single IM pins are able to effectively counteract bending and shearing loads, which are the main forces that normally cause oblique fractures *in vivo*. Intramedullary pins, however, lack the ability to resist axial compression and tension, and torsion loads on their own[44]. Cerclage wires are able to effectively counteract bending, shear, and torsion loads, and also provide interfragmentary compression[10,21,27,45,50,51,52,59,73]. Apart from providing interfragmentary compression when used in lag fashion, bone screws do not provide adequate protection against most of the applied loads. An IM pin, cerclage wires, or bone screws used as single modalities, do not provide rigid fixation or optimum resistance against the relevant loads and should never be used as the only mode of fixation in fracture repair, but rather in combination with another modality. When IM pins combined with full cerclage wires are applied correctly, they provide rigid fixation with resistance against all five loads. Bone similarly provide rigid fixation, leading to primary or direct bone healing.

[1] r = Pearson correlation coefficient

5.3 Experimental technique

The reproduction of similar (due to individual configurations of the bones, not precise) oblique osteotomies of each bone in a consistent fashion *in vitro* was easily achieved, making comparison of specimens meaningful.

In the creation of the osteotomies, the initial intention was to perform standard long oblique osteotomies in the middle third of the diaphysis of between 60° and 70° (to the long axis of each tibia) to accommodate the three full cerclage wires better. However, the variation in bone morphology (bone length, - diameter, and - shape) in some cases resulted in shorter oblique osteotomies than desired. A small, but inevitable amount of bone loss (equal to the thickness of the oscillating saw blade) also caused the osteotomies to incline to a slightly shorter oblique configuration. Although not outspoken, this additional gap in the bone adversely affected the alignment of the bone fragments when attempting to reconstruct the original shape of the bone. To establish proper bone-to-bone contact, the fragments were inevitably forced to slide the width of the gap towards one another. The non-uniform diameter of the tibial diaphyses further affected this alignment negatively, causing some overlap of the cortices, resulting in some degree of step formation. Although still well within acceptable limits, the amount of mutual contact between the fragments was subsequently less than 100%, possibly affecting the strength of the *in vitro* repair adversely. *In vivo*, however, this slight misalignment would not be of importance where bone healing is involved.

The direction of the osteotomy line (proximo-cranial-disto-caudally) in relation to the shape of the tibial bone played a major role in the length of the osteotomy line. By performing an osteotomy in a mirror image direction (proximo-caudal-disto-cranially), a longer osteotomy line would likely have been possible, but this would not have mimicked the naturally occurring configuration of fractures as found in the previous retrospective study conducted by the author that dealt with the configuration of mid-diaphyseal tibial fractures *in vivo*.

These factors contributed to the unavoidable sacrifice of the following surgical principles when some of the cerclage wires were applied[17,50,59,62]**:**

- The guideline requiring the length of the fracture line to be at least twice the diameter of the bone at the fracture site could not be adhered to in every case.
- The principle of placing cerclage wires at 5 mm margins on both ends of the osteotomy line could not be adhered to in every case.
- Spacing between cerclage wires was also affected, causing some to be closer to one another than half the diameter of the bone (which in itself created a challenge due to the non-uniform diameter of dachshund tibial diaphyses).

By measuring the length of the osteotomy lines in group 1, it was concluded that two cerclage wires would have fitted some osteotomy lines better than three, but not without violating yet another important surgical principle for the application of cerclage wires[18,82].

Initial pre-osteotomy radiographs taken of all the bones in this study to determine the diameter of the medullary cavity at its narrowest point, resulted in some interesting findings. The medullary cavity diameter of many of the tibiae was noted to be wider on the craniocaudal view radiographs than those in the same area on their mediolateral view radiographs. This phenomenon implies that the IM pin selected from the mediolateral view radiographs would then fill less of the medullary cavity than estimated. However, because there was no significant difference between the two treatment methods (see later), there was no reason to use a thicker IM pin than was selected from the mediolateral view radiographs. This fact, however, may require further investigation. Mediolateral view radiographs is incidentally the preferred view of radiologists and surgeons for performing calculations in clinical situations, and were consistently found to be more accurate in determining the size of the IM pin. This view was therefore used in this study as the standard of determination of IM pin size.

To allow more accurate comparison between the specimens in the two groups, one standard size IM pin and bone plate respectively, were used throughout. The IM pins had to be thinner than usual to facilitate the pre-bending thereof, but without compromising a proper intramedullary fit. The IM pin was accompanied by three full cerclage wires of a standard size, applied in a standard fashion around each test bone in group 1.

The pre-bending of IM pins was performed to conform to the curve of the medullary cavity of each dachshund's tibia on mediolateral view radiographs. The curve in the pins was then confirmed by comparing them to the curve in the diaphysis on the medial aspect of each bone specimen. The pre-bending was performed in the transverse plane only, which is adequate to accomplish proper pin seating in the clinical situation. Further contouring of the IM pin in any other plane would complicate the placing of the pin and could potentially weaken the structure of the metal to such an extent that premature implant failure could result.

No power tools were used for repair of the osteotomized tibiae in group 1, because the shape of the medullary cavity, in addition to the shape of the pre-bent IM pin, would not allow 360° turns of the pins, as with the use of power tools. The pin was aimed in a disto-caudo-medial direction[17,21,50,51,52,70], turning the chuck manually not more than an eighth to a quarter turn clockwise or anti-clockwise each time[17].

Three evenly spaced, 1.0 mm diameter full cerclage wires, selected on the basis of the mean weight of all the dachshund cadavers used in this study[8,59,62], were applied throughout the group 1 tibiae, making use of pre-prepared cortical grooves on the three prominent angles (cranial, caudomedial and caudolateral) of their diaphyses[24,50,56,57,82]. To minimize its influence on bone strength, the groove depth was standardized to be no deeper than one quarter to one third of the diameter of the cortex of the tibial diaphysis (i.e. less than 0.5 mm deep). The purpose of these grooves was to anchor the wires more effectively, especially in areas where the diaphysis had a funnel shape and/or a non-uniform diameter. A possible disadvantage of this method is the risk of the cortical grooves acting as stress risers with applied load. Due to the actual contact area with the underlying bone being less than the diameter of the wire, cortical grooves minimally interfere with cortical blood flow[24,26] in clinical cases. The key in preserving cortical blood supply is that all cerclage wires must be tight around the bone, since a moving wire disrupts the periosteal capillary network, devascularizing the underlying bone and disrupting some of the periosteal callus formation[50,56,57].

The bent eyelet wire method, in which a single wire loop encircles the bone, was used to apply the cerclage wires in the group 1 specimens, using a wire loop tightener. This

method is widely used in veterinary orthopaedics and is considered stronger than the conventional twisting method[8,14,60,68]. The wires were spaced not more than half a bone's diameter apart[62], starting and ending not more than 0.5 cm from the tips of the fragments and perpendicular to the long axis of the bone[18].

It was evident from the test results that the combination of an IM pin with full cerclage wires, as used in this study, provided adequate protection against all the applied loads.

All osteotomized bones for plating were repaired by stabilizing the bone fragments with a cortical screw in lag fashion first, to provide static interfragmental compression. Maximal interfragmental compression was achieved by inserting the screw in a cranio-proximo-caudal direction through the middle of the osteotomy line, directed more or less at right angles to the osteotomy plane. When a screw in lag fashion is inserted in any other direction, shearing loads will be introduced and the fragments may shift[12,59,67].

Due to the limited protection provided by bone screws against most of the applied loads when used alone, the group 2 fixations in this study were protected during weight-bearing by a DCP, contoured and attached to the medial aspect of the tibia with cortical screws in a neutralization mode[12].

The test method used in this study was a two point single cycle axial compression test loaded under displacement control[74], where the test specimens were inserted into custom made testing cups so that the two opposite ends were firmly fixed in the direction of the linear axis. The specimens were loaded by sequential increasing compressive forces until these forces reached the values at which the specimens failed[79].

Compressive tests are performed to determine the strength (a measure of how well a material withstands axially directed "pushing" forces) and to characterize how a material behaves under various conditions of loading[28]. Axial compression testing is a useful procedure for measuring the plastic flow behaviour and ductile fracture limits of a material[3,28,32].

An alternative test method, the cyclic fatigue method[28,74], which can be considered more physiological in terms of the magnitude of forces exerted on a dachshund tibia during normal walking or running, was used in a pilot study. Fatigue testing can be defined as simply applying cyclic loading to a test specimen to understand how it will perform under similar conditions in actual use[28]. A fixed[3,74] cyclical load was repeatedly applied to each bone-implant composite for one million cycles. The ASTM specifies the cycle limit for a fatigue test on orthopaedic implants to be approximately one million cycles, even if skeletal healing time is normally much shorter *in vivo* (only approximately 150 000 to 250 000 cycles over a period of 2 to 3 months)[3]. Four specimens (two from each group) were tested in the pilot study, using the two-point cyclic fatigue method, but all resulted in similar stress-strain graphs, i.e. a horizontal line in a single plane, from which none of the study parameters could be determined. In none of these cases the fatigue limit was exceeded, which means that only non-physiological loads, i.e. loads much higher than those used in the pilot study, would be able to cause plastic deformation and or failure (fracture) of the implant[41,42]. It was concluded that no measurable effect was going to be obtained using the predetermined cyclic loads on any of the specimens over the specified one million cycles[3,74]. The author subsequently decided to abandon the use of the cyclic fatigue method for the purposes of this study and rather replace it with the two point single cycle compression test[74]. This test method provided an excellent and simple way of determining the breaking strengths of the test specimens in this study[28].

The *Schenck® 100 kN* testing machine that was used in this study, is capable of simulating only compressive loads. In order for the test specimens to undergo as many different loads as possible, they were fixed at an incline of 20° craniocaudally. This resulted in a simulation of a combination of three of the five loads acting on long bones, (i.e. axial compression, bending, and shearing), and the possibility of tension as well. The *Schenck® 100 kN* testing machine was not able to simulate torsion.

Additional specimens were biomechanically tested for the author's own interest (not reported here), using two full cerclage wires in combination with an IM pin, instead of the usual minimum of three full cerclage wires in oblique to long oblique osteotomies. The question that had to be answered was whether two full cerclage wires would offer

sufficient resistance to the appropriate applied loads. Only two specimens were tested, resulting in no significant difference between the use of two and three full cerclage wires in their yield points, ultimate strengths, failure points, and median values. To determine the clinical significance of these results, more specimens should be studied *in vivo*.

A large number of the stress-strain graphs from both groups (see Appendix D) had a flat plateau at the top of the curve for various strain ranges. The reason for this is that the length of the curve (usually the plateau seen) after completion of each test (at the point of failure), was dependent on the time the test equipment was switched off, which was manually performed by the operator. This resulted in different lengths of this part of the curve in each case, but because the relevant values (yield, ultimate strength and failure) were recorded prior to the start of the plateau, the length of the plateau is irrelevant.

5.4 Findings

Three distinct modes of failure were determined in group 1 (IM pins and cerclage wires), i.e. unravelling/slippage with displacement of cerclage wires (50% of specimens), bone fracture at the site of a cerclage wire (30% of specimens), and bone fracture not associated with a cerclage wire (20% of specimens). Separation of the bone fragments at the osteotomy line subsequently occurred in six of the ten specimens in this group. In group 1, eight of the ten IM pins and nine of the thirty cerclage wires that were used, underwent plastic (permanent) deformation under compression.

Two distinct modes of failure were determined in group 2 (bone plate and screws), i.e. bone fracture at one or more screw holes (80% of specimens), and bone fracture not associated with the implants (20% of specimens). Only one screw (3%) became loose and displaced under compression. This occurred due to a connecting fissure line that had developed along the lengths of the shafts of two adjacent screws, resulting in separation of the main bone fragments at the osteotomy site in this single specimen. In this specimen, these screws acted as stress risers. In group 2, none of the bone plates or screws underwent plastic (permanent) deformation under compression, indicating a

higher AMI and Young's modulus of elasticity compared to the IM pins and cerclage wires used in this study.

Possible reasons for failure of the IM pins and cerclage wires can be attributed to a number of factors. The growing compressive load applied to each test specimen under displacement control[74] increased every 0.17 seconds until these loads eventually reached the levels at which either the bone or the implants, or both, inevitably had to fail[79]. The angle of the osteotomy line as well as the relative smoothness of the cut edges created by the oscillating saw blade, were instrumental in the process of failure of the cerclage wires. Being oblique in nature and possessing little traction between the bone fragments, shearing inevitably occurred due to the applied load. Although the *Schenck® 100 kN* testing machine is only able to produce axial compression loads, the 20° angle in which the test specimens were fixed in the fixation cups, contributed greatly to the additional loads that were created in this manner, i.e. bending and shearing, further leading to implant failure. The so-called "human factor" in combination with the natural non-uniform shape of dachshund tibiae, was probably also important in the failure of the specimens. No two bones, (not even those from the same animal), will ever exactly be uniform in shape, length, diameter, and strength, while the repair of osteotomized bone specimens will always leave room for error. The pre-prepared cortical grooves on the cranial, caudomedial and caudolateral aspects of the diaphysis of the bones, used to anchor the cerclage wires, were in all probability instrumental in the failure of some of the test specimens by acting as stress risers, causing the bone to easier fracture at the site of a cerclage wire. Bone fractures not associated with a cerclage wire could have occurred due to possible structural and/or material bone deficiencies. All these factors warrant further investigation *in vivo*.

As soon as the rigid fixation supplied by the cerclage wires failed, load sharing between the implants ceased. The IM pin then had to bear most of, or the entire load, causing the pin to fail soon after the cerclage wires. An important fact to keep in mind was that the IM pins were pre-bent when they were inserted into the bone. A degree of metal fatigue, although probably minor, was an important possible sequel to the pre-bending process, lowering the AMI and therefore weakening the pin's resistance against axial compression, bending and shearing loads.

Bone screws acting as stress risers played an important role in bone fractures that occurred at one or more screw holes. Bone was removed by drilling the screw holes, thereby weakening the bone structure in these areas. Load sharing between the bone plate, bone screws and the bone itself occurred, but the absence of bone healing *in vitro* prevented any increase in bone strength over time, leading to a more pronounced stress rising effect originating from the screw holes.

Bone fractures not directly associated with a bone plate or a bone screw could have occurred due to possible structural and/or material bone deficiencies. In addition, the proximal end of the bone plate acted as a fulcrum under the applied compressive load. This caused failure in some of the specimens in the area proximal to the bone plate.

Statistically, there were no significant differences in the mean applied stress (load) at yield ($p = 0.299$), ultimate strength ($p = 0.275$), or failure ($p = 0.137$) between the two groups. Similarly, there were no significant differences in the mean strain (deformation) at yield ($p = 0.684$), ultimate strength ($p = 0.778$), or failure ($p = 0.505$) between the two groups. This could indicate either that there was practically no difference between the treatment methods, or that the study was not statistically powerful enough in terms of sample numbers. *In vivo* studies will be necessary to determine the clinical significance thereof.

In this study, the co-variates (mass and age) contributed more (having smaller p-values) in explaining the variance of the parameters than the factors (treatment methods and gender). In other words, heavier and older animals had slightly stronger bones, which were more prone to significantly influence the outcome of the test results than the bones of younger and lighter animals. Likewise, using either IM pins and cerclage wires, or bone plates and screws in repairing the osteotomies, did not significantly influence the outcome of the test results.

It is clear from the scatter graphs (see Figures 4.1 to 4.7) that the following parameters had a strong positive correlation in group 1**:** body mass *vs*. bone diameter (i.e. increasing body mass with increasing bone diameter), and body mass *vs*. medullary diameter (i.e. increasing body mass with increasing medullary diameter), while they had

a weaker positive correlation in group 2. Cortical width *vs*. age had a weak positive correlation in both groups (i.e. mild increase in cortical width with increasing age), strain at the yield point *vs*. age, and strain at the ultimate strength *vs*. age had a weak to strong negative correlation in both groups (i.e. mild to large decrease in strain at the yield point with increasing age, and mild to large decrease in strain at the ultimate strength with increasing age). Both stress and strain at the failure points *vs*. age had a weak positive correlation in both groups (i.e. mild increase in stress and strain at the failure points with increasing age), but with the exception of strain at the failure point *vs*. age in group 2, which was weakly negatively correlated (i.e. mild decrease in strain at the failure point with increasing age).

In both groups, mean body mass did not significantly influence any biomechanical test results ($p > 0.1$). Mean body mass of cadavers in group 1 was 8.24 kg (± 2.34), while those of cadavers in group 2 was 6.32 kg (± 0.64). Heavier animals had significantly greater total bone diameters ($p < 0.01$), accompanied by significantly greater medullary diameters ($p < 0.01$), but mean body mass had no significant influence on cortical width ($p = 0.831$) or bone length ($p = 0.5$). Bone diameter and medullary diameters, both at the narrowest point of the medullary cavity, had a significant influence on the test results ($p > 0.1$), i.e. the greater the bone diameter and the medullary width, the greater the yield point, ultimate strength and failure point.

Statistically between the two methods of repair, mean bone diameter ($p < 0.1$) and mean medullary diameter ($p < 0.1$) were significantly different, while mean cortical width ($p = 0.831$) and mean bone length ($p = 0.501$) were not significantly different between the groups.

Young's modulus of elasticity, i.e. the stiffness of the test specimen during the elastic phase, was determined from the stress-strain graph for each specimen. Modulus for specimens repaired by bone plates and screws was generally higher (mean value 1.720 MPa) than those repaired with IM pins and cerclage wires (mean value 1.785 MPa). However, there was no statistically significant difference between the two values ($p > 0.1$), which indicates that the difference in Young's modulus between the groups was not clinically meaningful.

Energy absorbed by each specimen until failure was determined. Specimens repaired by bone plates and screws in general required more energy to reach the point of failure (mean value 207.166 kJ) than those repaired with IM pins and cerclage wires (mean value 150.688 kJ). However, no statistically significant difference between the two groups was found ($p \geq 0.384$ for both outcome variables), indicating that these differences may not be clinically meaningful.

More test specimens may have resulted in the detection of a statistically significant difference between the groups, both for Young's modulus of elasticity, and energy absorbed by each specimen until failure. In contrast, however, it would be possible to have a highly statistically significant difference, but the magnitude of the difference so small that it would still not be clinically relevant, irrespective of test specimen numbers.

5.5 Limitations of study

A few limitations were retrospectively identified for this study. Although the sample size was sufficient to perform a satisfactory analysis, larger sample sizes are always desirable. The larger the sample size, the more effective error is likely to be eliminated.

Because this study was performed *in vitro*, no other factors involved could be tested. Bone healing played no role in the structural and material strength of the test specimens, while the inherent properties of intact parts of the bones contributed minimally to the strength of the test specimens, due to the weakening effect of the osteotomies on the bones. This resulted in a net load directed towards the implants, rather than the bones *per se*. The degree to which bone-on-bone contact contributed to construct stability is unknown. Furthermore, there were no surrounding soft tissues present to aid in stabilizing the fracture area and protecting the bone and its implants against external loads. The so called *in vivo* "race" between bone healing and implant failure did therefore not apply here.

Although the bone fragments had nearly perfect contact at the osteotomy site, the smooth cuts made by the oscillating saw blade excluded any possible stability achieved through interdigitation of the fragments. Due to the nature of the osteotomies, the

applied loads caused the bone to tend to collapse due to slight shearing of the fragments.

Although cyclic fatigue testing can probably be considered more physiological in terms of the magnitude of the specific loads exerted *in vivo* during normal walking or running, it was concluded after the pilot study (using this method), that no measurable effect was going to be obtained for any of the specimens over the specified one million cycles[3,74]. Therefore, the two point single cycle compression until failure test was used in stead[74], which, however, could be considered less physiological in terms of the loads applied, with failure in this manner being unlikely to occur *in vivo*.

The *Schenck® 100 kN* testing machine that was used in this study was only able to perform compression testing, and even after placing the test specimen at a 20° angle cranio-caudally (that indirectly resulted in additional bending and shearing loads), torsion and distraction loads could still not be simulated.

Apart from the implants and the applied loads that were successfully standardized, as well as variables such as age, gender, and radiological normality, standardizing the majority of other factors was difficult to obtain, mainly due to intrabreed differences in size and shape of the tibiae, together with inherent differences in structural and material properties of the bones. In addition, the so-called “human factor” cannot be totally ruled out, e.g. the ability or not to precisely duplicate the osteotomies in terms of length and angle, the tightness and spacing of the cerclage wires, and cortical groove depths. However, although potentially important, these factors are unlikely to have affected the outcome of this study.

5.6 Future studies

The following recommendations for possible future studies on the subject were made by the author**:**

- In similar studies in future, larger sample sizes may be necessary to more effectively eliminate possible error.

- Although in terms of the parameters tested, the loads used in this study were proven sufficient, the additional use of torsion and tension loads will make such a study even more meaningful.
- Standardizing test specimens by the use of test bones manufactured from a material with similar structural and material properties as normal bone, but with the added advantage of being absolutely uniform in shape and size, could make testing in general much simpler and the results more accurate.
- Another method of creating fractures in a consistent fashion, having interdigitation with a perfect fit between the fragments should be devised to rule out some inconsistencies arising from the use of an oscillating saw blade.
- A similar, expanded study could be considered, comparing the strength and effectiveness of IM pins and cerclage wires with additional internal fixators, which have different characteristics than DCPs, such as more recently developed products, e.g. limited contact dynamic compression plates (LC-DCPs), or locking plates such as limited contact locking auto compression plates (LCPs) and the String of Pearls™ (SOP™) universal interlocking plate system.
- *In vivo* studies may be necessary to determine the clinical significance of the results. *In vivo* studies at various stages of bone healing have the potential to render more meaningful results regarding both the strength of the bone and the implants, although less practical (or ethical) to perform.
- Cyclic fatigue testing can be considered as alternative test method *in vivo*, hereby utilizing more intrinsic factors originating from the live patient.

.

CHAPTER SIX: CONCLUSION

Clinically, there appeared to be a slight indication for bone plates and screws to be more resistant to deformation by the loads applied on them than intramedullary pins and cerclage wires. Applied stress (load) and strain (deformation), appeared to be higher in the bone plate and screws fixated specimens than in those of intramedullary pin and cerclage wires fixated specimens at the yield point, ultimate strength and failure point respectively.

However, statistically, this study did not show enough evidence to prove a significant difference between the overall performance and strength of the two methods of repair. This could mean that there either truly was no difference between the treatment methods, or that the study was not powerful enough in terms of sample numbers.

Co-variates such as body mass and age contributed more in explaining the variance of the parameters than factors such as treatment methods and gender.

CHAPTER SEVEN: RECOMMENDATIONS

Many small animal practitioners do not have access to the specialized and costly equipment necessary to apply bone plates, or lack the essential skills to perform such operations. However, most practitioners have access to, and are skilled in using the simpler, more affordable equipment necessary to place an intramedullary pin and cerclage wires. For those practitioners in particular, the recommendations arising from this study will be of value.

The use of bone plates and screws are still considered the gold standard in internal fixation, but with results of this study in mind, it is suggested that intramedullary pins and cerclage wires could be used as an acceptable alternative to bone plates and screws in the treatment of oblique mid-diaphyseal tibial fractures in chondrodystrophic dog breeds.

REFERENCES

1. Adams DF 2007 Testing tech: the modified D 695 compression test method. *Advanced Composites:* 3-4

2. Alexander JW 1982 Tibial fractures and their management. *Compendium on Continuing Education for the Practicing Veterinarian.* 4: 78-87

3. American Standards of Test Materials (ASTM) F1264-03 2007 Standard specification and test methods for intramedullary fixation devices. *Annual Book of ASTM Standards, Volume 13 (03).* 100 Barr Harbor Drive, West Conshohocken, PA: 1-18

4. Aron DN, Foutz TL, Keller WG, Brown J 1991 Experimental and clinical experience with an IM pin external skeletal fixator tie-in configuration. *Veterinary Comparative Orthopedics and Traumatology* 4: 86-94

5. Audekercke RV, Martens M 1984 Mechanical properties of cancellous bone. In Hastings GW, Ducheyne P (ed) *Natural and Living Biomaterials.* CRC Press, Florida: 7-18

6. Blood DC, Studdert VP 1999 *Saunders Comprehensive Veterinary Dictionary, 2nd ed.* WB Saunders Co, London: 10, 230

7. Blood DC, Studdert VP 1995 *Bailliere's Comprehensive Veterinary Dictionary.* Bailliere Tindall, London: 8, 245, 252

8. Blass CE, Piermattei DL 1986 Static and dynamic cerclage wire analysis. *Veterinary Surgery* 15: 181-184

9. Boone EG, Johnson AL, Montovan P, Hohn RB 1986 Fractures of the tibial diaphysis in dogs and cats. *Journal of the American Veterinary Medical Association* 188(1): 41-45

10. Boudrieau RJ 2003 Fractures of the tibia and fibula. In Slatter DH (ed) *Textbook of Small Animal Surgery (3rd ed).* Saunders, Philadelphia: 2144-2157

11. Bouvy BM, Markel MD, Chelikani S, Egger EL, Piermattei D, Vanderby R 1993 *Ex vivo* biomechanics of Kirschner-Ehmer external skeletal fixation applied to canine tibiae. *Veterinary Surgery* 22: 194-207

12. Brinker WO, Hohn RB, Prieur WD 1984 *Manual of internal fixation in small animals.* Springer-Verlag, Heidelberg: 29-79 & 104-107

13. Brinker WO, Verstraete ME, Soutas-Little RW 1985 Stiffness studies on various configurations and types of external fixators. *Journal of American Animal Hospital Association* 21: 280-288

14. Brooks RL, Tarvin GB 1982 *In vitro* cerclage wiring analysis *Veterinary Surgery* 11: 39-43

15. Carter DR, Spengler DM 1982 Biomechanics of Fracture. In Sumner-Smith G (ed) *Bone in Clinical Orthopedics.* WB Saunders, Philadelphia: 586-595

16. Coetzee G.L. 2002 Basic principles for the application of bone plates and screws in small animal patients. *CPD course for veterinary surgeons, Pretoria, September 7, 2002.* Roth Medical Components (Pty) Ltd, Pinelands, South Africa: 1-23

17. Coetzee GL 1999 Long bone fracture fixation with an intramedullary pin and C-clamp-on plate in dogs. *Veterinary Comparative Orthopedics and Traumatology* 12: 26-32

18. Dixon BC, Tomlinson JL, Wagner-Mann CC 1994 Effects of three intramedullary pinning techniques on proximal pin location and articular damage in the canine tibia. *Veterinary Surgery* 23: 448-455

19. Durall I, Diaz-Bertrana MC, Puchol JL, Franch J 2003 Radiographic findings related to interlocking nailing: windshield wiper effect, and locking screw failure. *Veterinary Comparative Orthopedics and Traumatology* 16: 217-222

20. Durall I, Falcon C, Diaz-Bertrana MC, Franch J 2004 Effects of static fixation and dynamization after interlocking femoral nailing locked with an external fixator: an experimental study in dogs. *Veterinary Surgery* 33: 323-332

21. Eaton-Wells RD, Matis U, Robins GM, Whittick WG 1990 The pelvis and the pelvic limb. In Whittick WG *Canine Orthopedics (2nd ed).* Lea & Febiger, Philadelphia: 449-465

22. Finley JB, Moroz TK, Rorabeck CH, Davey JR 1987 Stability of ten configurations of the Hoffmann external fixation frame. *The Journal of Bone and Joint Surgery* 69-A: 734-743

23. Florin M, Arzdorf M, Linke B, Auer JA 2005 Assesment of stiffness and strength of 4 different implants available for equine fracture treatment: A study on a 20° oblique long-bone fracture model using a bone substitute. *Veterinary Surgery* 34: 231-238

24. Gothman L 1962 Local arterial changes associated with experimental fractures of the rabbit's tibia treated with encircling wires (cerclage) – a microangiographic study. *Acta Chirurgica Scandinavica* 123: 1-8

25. Harari J 2004 *Small Animal Surgery Secrets.* Hanley & Belfus Inc., Philadelphia: 290

26. Hinko PJ, Rhinelander W 1975 Effective use of cerclage in the treatment of long-bone fractures in dogs. *Journal of American Veterinary Medical Association* 166: 520-524

27. Hulse D, Hyman B 2003 Fracture biology and biomechanics. In Slatter DH (ed) *Textbook of Small Animal Surgery (3rd ed).* Saunders, Philadelphia: 1785-1792

28. Instron® 2011 *Compression test.* Instron Worldwide Headquarters, 825 University Avenue, Norwood, MA 02062-2643, USA: 1-2

29. Johnson AL, Boone EG 2003 Fractures of the tibia and fibula. In Slatter DH (ed) *Textbook of Small Animal Surgery (2nd ed).* WB Saunders Company, Philadelphia: 1866-1876

30. Johnson K 2009 Locking plates – the ultimate implant? *Veterinary Comparative Orthopedics and Traumatology* 22: I-II

31. Kraus KH 1993 Healing of bone fractures. In Harari J (ed) *Surgical complications and wound healing in the small animal practice.* WB Saunders Company, Philadelphia: 203-221

32. Kuhn H 2000 Mechanical behavior under tensile and compressive loads. In Kuhn H, Medlin D (ed) *ASM Handbook® Volume 8 Mechanical testing and evaluation.* ASM International, Materials Park, OH 44073-0002, USA: 99-108

33. Kuhn H 2000 Stress-strain behavior in bending. In Kuhn H, Medlin D (ed) *ASM Handbook® Volume 8 Mechanical testing and evaluation.* ASM International, Materials Park, OH 44073-0002, USA: 109-114

34. Kuhn H 2000 Uni-axial compression testing. In Kuhn H, Medlin D (ed) *ASM Handbook® Volume 8 Mechanical testing and evaluation.* ASM International, Materials Park, OH 44073-0002, USA: 143-151

35. Lambrechts NE, Verstraete FJM, Sumner-Smith G, Raath AD, Van der Linde MJ, Groeneveld HT 1993 Internal fixation of femoral neck fractures in the dog – an *in vitro* study. *Veterinary Comparative Orthopedics and Traumatology* 6: 188-193

36. Little F.M. 2001 Bending properties of stainless steel dynamic compression plates and limited contact dynamic compression plates. *Veterinary Comparative Orthopedics and Traumatology.* 14: 64-68

37. Lipowitz AJ, Newton CD, Caywood DD, Schwartz A 1996 *Complications in Small Animal Surgery.* Williams & Wilkins, Baltimore: 592-593

38. McCartney WT, Garvan CB, Kiss K 2009 Repair of thirty-six fractures in dogs using the Mennen clamp-on plate: preliminary results. *Veterinary Comparative Orthopedics and Traumatology* 22: 406-411

39. Meade JB 1989 The adaptation of bone to mechanical stress: Experimentation and current concepts. In Cowin SC (ed) *Bone Mechanics.* CRC Press, Florida: 141-145

40. Mears DC, Rothwell GP 1982 The mechanical behavior of real materials. In Mears DC (ed) *Materials and orthopaedic surgery (1st ed).* Williams & Wilkins Company, Baltimore: 75-89

41. Muir P. 1995 Area moment of inertia for comparison of implant cross-sectional geometry and bending stiffness. *Veterinary Comparative Orthopedics and Traumatology.* 8: 146-152

42. Ness MG 2006 Implant failure. In Coughlan AR, Miller A (ed) *BSAVA Manual of Small Animal Fracture Repair and Management.* Replika Press Pvt. Ltd, India: 291-295

43. Ness MG 2009 repair of Y-T humeral fractures in the dog using paired “String of Pearls” locking plates. *Veterinary Comparative Orthopedics and Traumatology* 22: 492-497

44. Nordin M, Frankel VH 1980 Biomechanics of whole bones and bone tissue. In Frankel VH, Nordin M (ed) *Basic Biomechanics of the Skeletal System*. Lea & Febiger, Philadelphia: 132-137

45. Nunamaker DM 1985 Fractures of the tibia and fibula. In Newton CD, Nunamaker DM (ed) *Textbook of Small Animal Orthopaedics.* JB Lippincott Company, Philadelphia: 439-444

46. Pardo AD 1994 Relationship of tibial intramedullary pins to canine stifle joint structures: a comparison of normograde and retrograde insertion. *Journal of the American Animal Hospital Association* 30: 369-374

47. Pelker RR, Friedlander GE, Markham TC 1984 Effects of freezing and freeze-drying on the biomechanical properties of rat bone. *Journal of Orthopaedic Research* 1: 405-411

48. Perren SM 1989 The biomechanics and biology of internal fixation using plates and nails. *Orthopedics* 12: 21-26

49. Piekarski K 1984 Fractography of bone. In Hastings GW, Ducheyne P (ed) *Natural and Living Biomaterials.* CRC Press, Florida: 36-40

50. Piermattei DL, Flo GL, De Camp, CE 2006 *Brinker, Piermattei and Flo's handbook of small animal orthopedics and fracture repair (4th ed).* WB Saunders Company, Philadelphia: 25-159, 633-660

51. Pope ER 1990 Fixation of tibial fractures. In Bojrab MJ (ed) *Current techniques in Small Animal Surgery (3rd ed).* Lea & Febiger, Philadelphia: 722-728

52. Pope ER 2003 Fixation of tibial fractures. In Bojrab MJ (ed) *Current techniques in small animal surgery (4th ed).* Williams & Wilkins, Baltimore: 1050-1055

53. Pratley® 2003 *Instruction Leaflet for Pratley Quickset Putty*. Pratley (Pty) Ltd, P.O. Box 3055, Kenmare, 1745, Gauteng, South Africa: 1

54. Radcliffe RM, Lopez MJ, Turner TA., Watkins JP, Radcliffe CH, Markel MD 2001 An *in vitro* biomechanical comparison of interlocking nail constructs and double plating for fixation of diaphyseal femur fractures in immature horses. *Veterinary Surgery* 30*:* 179-190

55. Reems MR, Beale BS, Hulse DA 2003 Use of a plate-rod construct and principles of biological osteosynthesis for repair of diaphyseal fractures in dogs and cats: 47 cases (1994-2001). *Journal of American Veterinary Medical Association* 223(3): 330-335

56. Rhinelander FW 1974 Tibial blood supply in relation to fracture healing. *Clinical Orthopedics* 105: 34-39

57. Rhinelander FW, Wilson JW 1982 Blood supply to developing, mature, and healing bone. In Sumner-Smith G (ed) *Sumner-Smith's Bone in clinical orthopedics: a study in comparative osteology.* WB Saunders Company, Philadelphia: 7-28

58. Roe S 2006 Biomechanical basis of bone fracture and fracture repair. In Coughlan AR, Miller A (ed) *BSAVA Manual of Small Animal Fracture Repair and Management.* British Small Animal Veterinary Association, Gloucester: 14-24

59. Roe S 2003 Internal fracture fixation. In Slatter DH (ed) *Textbook of Small Animal Surgery (3rd ed).* Saunders, Philadelphia: 1798-1818

60. Roe SC 1997 Mechanical characteristics and comparisons of cerclage wires: introduction of the double wrap and loop/twist tying methods. *Veterinary Surgery* 26: 310-316

61. Roe SJ, Pijanovsky GJ, Johnson AL 1988 Biomechanical properties of canine cortical allografts: Effects of preparation and storage. *American Journal of Veterinary Research* 49: 873-877

62. Rooks RL, Tarvin GB 1982 In vitro cerclage wire analysis. *Veterinary Surgery* 11: 39-43

63. Rose BW, Pluhar GE, Novo RE, Lunos S 2009 Biomechanical analysis of stacked plating techniques to stabilize distal radial fractures in small dogs. *Veterinary Surgery* 38: 954-960

64. Roylance D 2001 Stress-strain curves. *Massachusetts Institute of Technology, Cambridge, MA 02139:* 1-14

65. Rudy RL 1975 Principles of intramedullary pinning. *Veterinary Clinics of North America* 5(2): 209-228

66. Saikku-Bäckström A, Räihä JE, Välimaa T, Tulamo R-M 2005 Repair of radial fractures in toy breed dogs with self-reinforced biodegradable bone plates, metal screws, and light-weight external coaptation. *Veterinary Surgery* 34: 11-17

67. Schatzker J 1991 Screws and plates and their application. In Allgöwer M (ed) *Manual of internal fixation: techniques recommended by the AO-ASIF group (3rd ed).* Springer-Verlag, Berlin: 179-199

68. Schulz RS 1985 Strength of stainless steel surgical wire in various fixation modes. *Clinical Orthopedics* 198: 304-308

69. Schwarz PD 1993 Fracture biomechanics of the appendicular skeleton: causes and assessment. In Bojrab MJ (ed) *Disease mechanisms in small animal surgery (2nd ed).* Lea & Febiger, Philadelphia: 1009-1026

70. Seaman JA, Simpson AM 2004 Tibial fractures. *Clinical Techniques in Small Animal Practice* 19(3): 151-167

71. Securos Catalog of Products 2008. Securos (Pty) LtdCompany, 443 Main Street, Fiskdale, MA 01518: 98-99

72. Shaw JA, Daubert HB 1988 Compression capability of cerclage fixation systems – a biomechanical study. *Othopaedics* 11: 169-174

73. Sinibaldi KR 1983 Fractures of the tibia. In Bojrab MJ (ed) *Current techniques in small animal surgery (2nd ed).* Lea & Febiger, Philadelphia: 630- 636

74. Sod GA, Hubert JD, Martin GS, Gill MS 2005 An in vitro biomechanical comparison of a limited-contact dynamic compression plate fixation with a dynamic compression plate fixation of osteotomized equine third metacarpal bones. *Veterinary Surgery* 34: 579-586

75. Ting D, Cabassu JB, Guillou RP, Sinnott MT, Meyer EG, Haut RC, Dejardin LM 2009 In vitro evaluation of the effect of fracture configuration on the mechanical properties of standard and novel interlocking nail systems in bending. *Veterinary Surgery* 38: 881-887

76. Tomlinson JL, Payne JT 1993 Effects of cerclage wire on bone. In Bojrab MJ (ed) *Disease mechanisms in small animal surgery (2nd ed).* Lea & Febiger, Philadelphia: 1102-1104

77. Turner CH, Burr DB 1993 Basic biomechanical measurements of bone: A Tutorial. *Bone* 14: 595-608

78. Vasseur PB, Paul HA, Crumley L 1984 Evaluation of fixation devices for prevention of rotation in transverse fractures of the canine femoral shaft: an in vitro study. *American Journal of Veterinary Research* 45: 1504-1507

79. Wendlova J 2008 Bone quality, elasticity and strength. *Bratislavske Lekarske Listy* 109 (9): 383-386

80. Wilson JW 1987 Effect of cerclage wires on periosteal bone in growing dogs. *Veterinary Surgery* 16: 299-302

81. Wilson JW 1985 Microvascular and histological effect of circumferential wire on appositional bone growth in immature dogs. *Journal of Orthopedic Research* 3: 412-415

82. Wilson JW 1991 Vascular supply to normal bone and healing fractures. *Seminars in Veterinary Medicine and Surgery* 6: 26-38

83. Wolfe AR, Weiner M 1989 Compression test results – a tough nut to crack. *Composites 2004 Convention and Trade show, October 6-8, 2004.* American Composites Manufacturers Association, Tampa, Florida, USA: 57-63

84. Wolfe AR, Weiner M 2004 Compression testing – comparison of various test methods. *Composites 2004 Convention and Trade show, October 6-8, 2004.* American Composites Manufacturers Association, Tampa, Florida, USA: 35-45

85. Zahn K, Matis U 2004 The clamp rod internal fixator – application and results in 120 small animal fracture patients. *Veterinary Comparative Orthopedics and Traumatology* 17: 110-120

APPENDICES

APPENDIX A

Fracture study consent form

Dear Client

We would like to express our deepest sympathy with the death of your dog. We know your dog had a very special place in your life. To commemorate his/her life, we would like to invite you to allow him/her to assist us even now to help other dogs of the same breed to have a better quality of life.

The Small Animal Surgery section at the Faculty of Veterinary Science of the University of Pretoria is currently conducting a study on the best techniques in the treatment of fractures in dogs, specifically dachshunds. We hope to gain valuable additional insights into this topic to enable us to treat future patients even better than before.

We would be very grateful if you would allow us to include your late pet in this study. All procedures will be performed after death under strict ethical standards and with sincere respect, using only two bones in the hind limbs.

There will be no additional costs for you.

Pet's name:_____

Breed:_____

Age:_____ Gender:_____

I hereby give consent to the inclusion of my late pet to the study as described above.

Client signature:_____ Date:_____

Client name:_____

Client no.:_____ Telephone:_____

Thank you for allowing us to include your late pet in this study. Your participation is greatly appreciated.

DR. FREDDIE MALAN (Cell phone: 082 5547 312)

APPENDIX B

Implants and instruments used in bone fixation

FIGURE B.1. Synthes® number 1 orthopaedic wire (a), and 2 mm Steinmann pins (K-wires) (b) that were used during the procedures in group 1.

FIGURE B.2. An example of a 6 hole, 2.7 mm DCP with a collection of 2.7 mm cortical screws of various lengths, similar to those used in repairing the osteotomized Dachshund tibiae in group 2.

FIGURE B.3. Instruments used to apply the intramedullary pins and cerclage wires in group 1. (a.) Small fragment forceps. (b.) Jacobs chuck and key with T-handle. (c.) Bone file, flat. (d.) Eyelet cerclage wire loop tightener. (e.) Wire twister/cutter. (f.) Pin cutter.

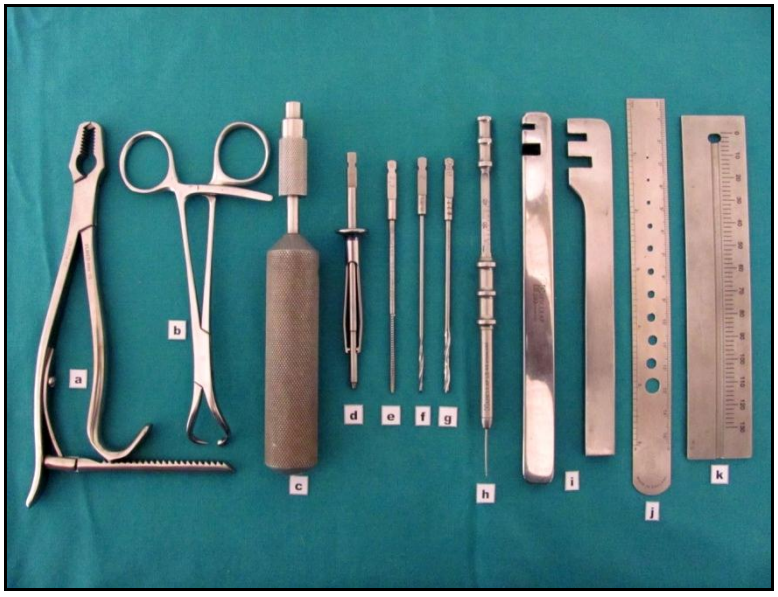

FIGURE B.4. Instruments used in applying the bone plates and screws in group 2. a. Small fragment bone holding forceps. b. Plate holder. c. Universal handle for screw drivers, taps and drill bits. d. Screw driver tip for 2.7 and 3.5 mm screws. e. 2 mm tap. f. 2 mm drill bit. g. 2.7 mm drill bit. h. Depth gauge. i. Plate benders. j. Ruler, to measure screw (and/or intramedullary pin) diameter. k. Ruler, to measure screw length.

FIGURE B.5. ***Makita®*** ***60180*** **orthopaedic power drill and key, used for drilling of holes for the bone screws.**

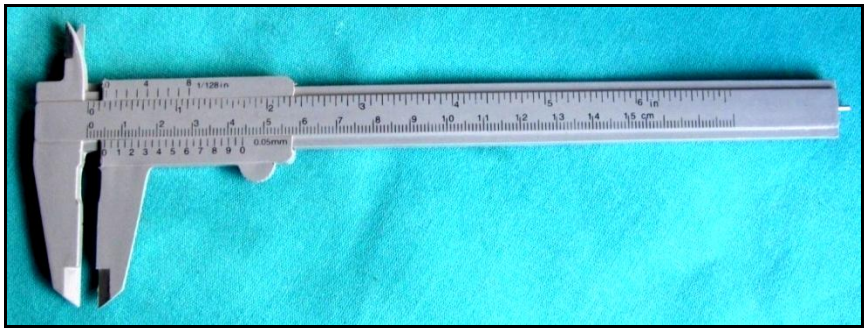

FIGURE B.6. Vernier™ caliper used in the bone measurements.

APPENDIX C

Basic steps in applying tibial implants in group 2

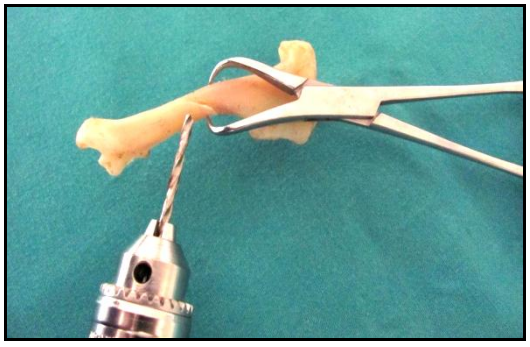

Figure C.1. The gliding hole in the *cis* cortex is drilled, using a 2.7 mm drill bit.

FIGURE C.2. After drilling through the trans cortex with a 2 mm drill bit, the depth of the hole is measured, using a depth gauge.

FIGURE C.3. The hole is tapped, using a 2.7 mm tap.

FIGURE C.4. A 12 mm long 2.7 mm cortical screw is inserted as a lag screw to achieve compression at the osteotomy site.

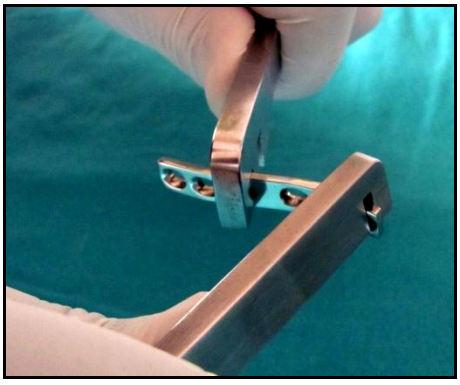

FIGURE C.5. Bending irons used to contour the plate to fit the bone on its medial aspect.

FIGURE C.6. A screw hole is drilled in the bone using a 2 mm drill bit, while the plate is kept in position by a plate holder.

FIGURE C.7. A depth gauge is used to measure the depth of the screw hole.

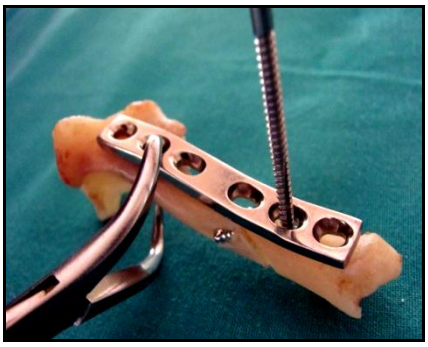

FIGURE C.8. The screw hole is tapped using a 2.7 mm tap.

FIGURE 3.9. A 10 mm long 2.7 mm screw is inserted using a screw driver.

APPENDIX D

Stress-strain graphs: Group 1

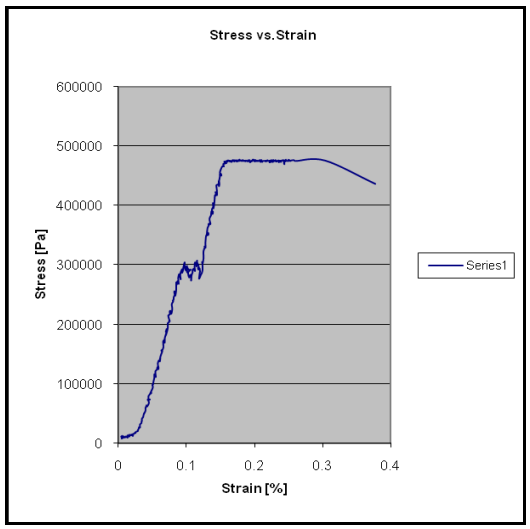

FIGURE D.1. Stress-strain graph for specimen 1 (R-2) repaired by intramedullary pin and cerclage wires. (R = right)

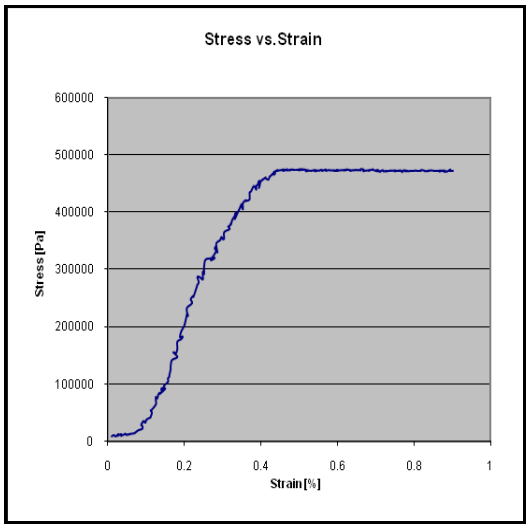

FIGURE D.2. Stress-strain graph for specimen 2 (L-2) repaired by intramedullary pin and cerclage wires. (L = left)

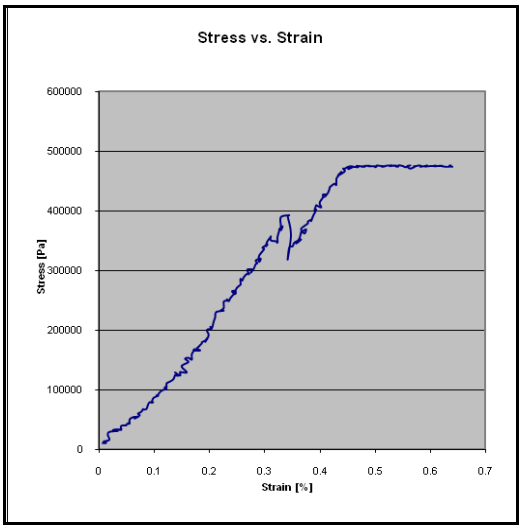

FIGURE D.3. Stress-strain graph for specimen 3 (L-3) repaired by intramedullary pin and cerclage wires. (L = left)

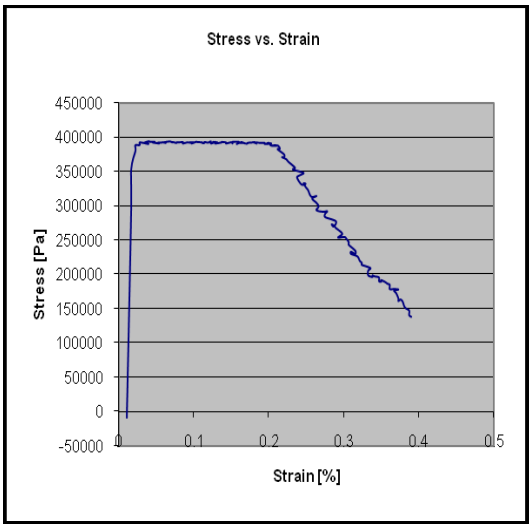

FIGURE D.4. Stress-strain graph for specimen 4 (R-6) repaired by intramedullary pin and cerclage wires. (R = right)

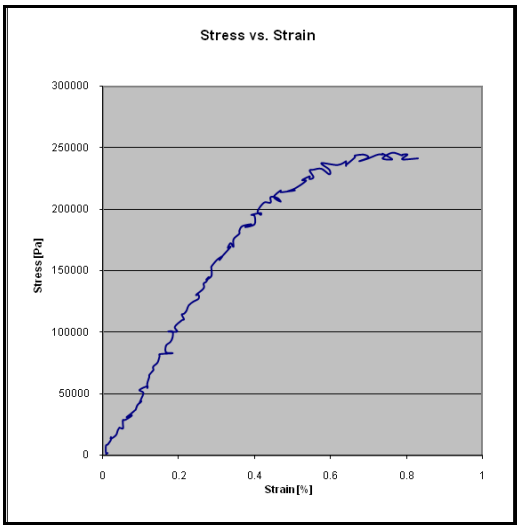

FIGURE D.5. Stress-strain graph for specimen 5 (L-7) repaired by intramedullary pin and cerclage wires. (L = left)

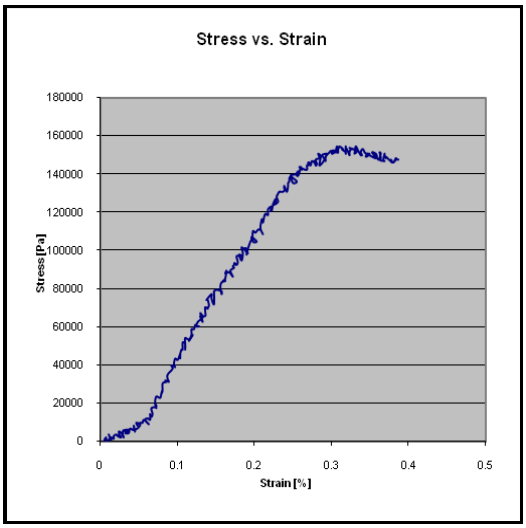

FIGURE D.6. Stress-strain graph for specimen 6 (R-7) repaired by intramedullary pin and cerclage wires. (R = right)

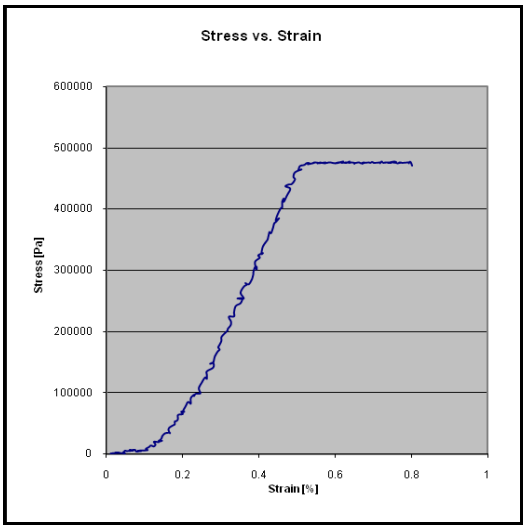

FIGURE D.7. Stress-strain graph for specimen 7 (L-11) repaired by intramedullary pin and cerclage wires. (L = left)

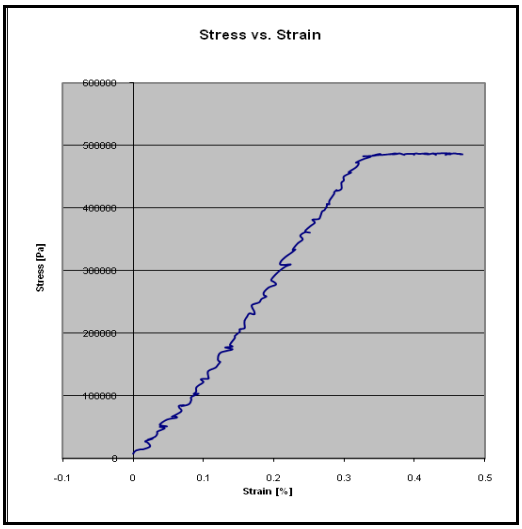

FIGURE D.8. Stress-strain graph for specimen 8 (L-13) repaired by intramedullary pin and cerclage wires. (L = left)

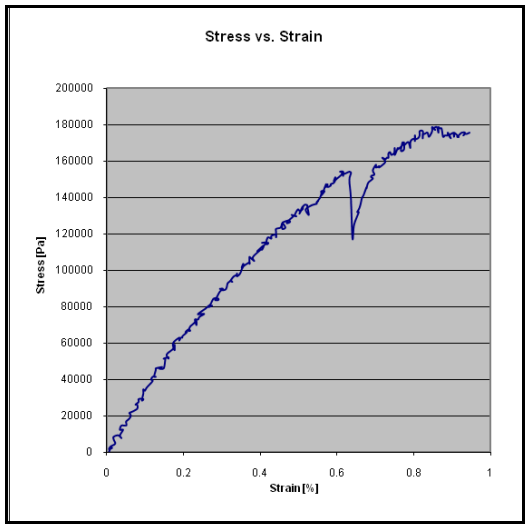

FIGURE D.9. Stress-strain graph for specimen 9 (R-15) repaired by intramedullary pin and cerclage wires. (R = right)

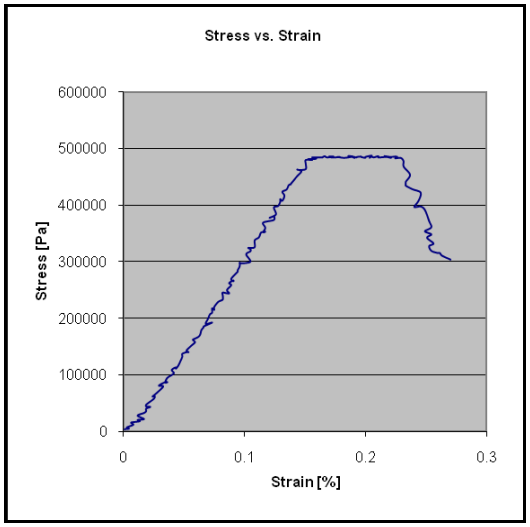

FIGURE D.10. Stress-strain graph for specimen 10 (R-16) repaired by intramedullary pin and cerclage wires. (R = right)

Stress-strain graphs: Group 2

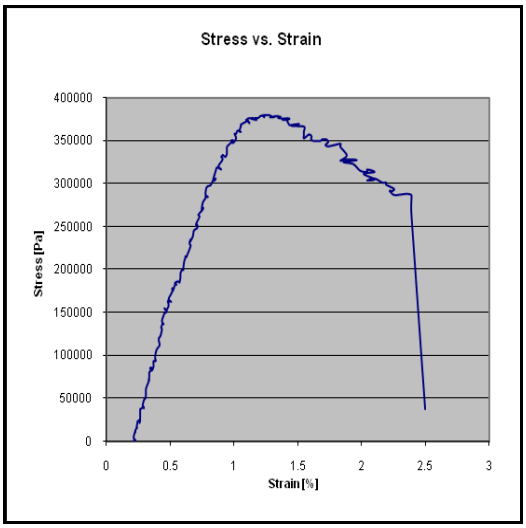

FIGURE D.11. Stress-strain graph for specimen 11 (R-5) repaired by bone plate and screws. (R = right)

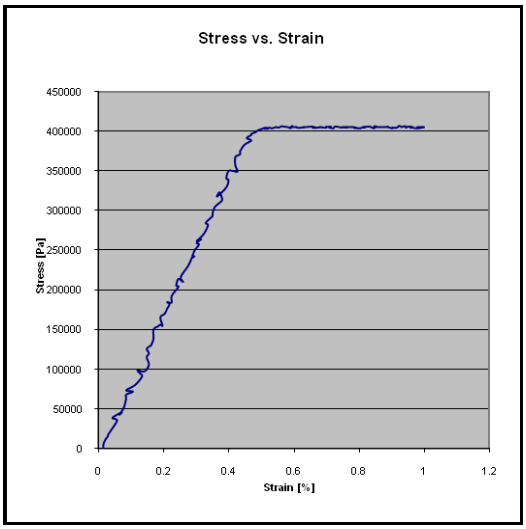

FIGURE D.12. Stress-strain graph for specimen 12 (L-6) repaired by bone plate and screws. (L = left)

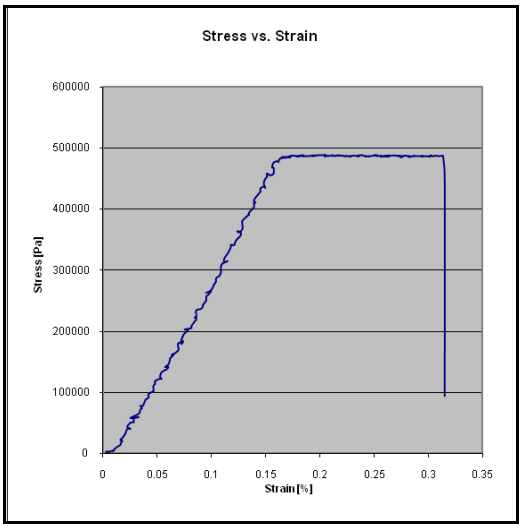

FIGURE D.13. Stress-strain graph for specimen 13 (L-8) repaired by bone plate and screws. (L = left)

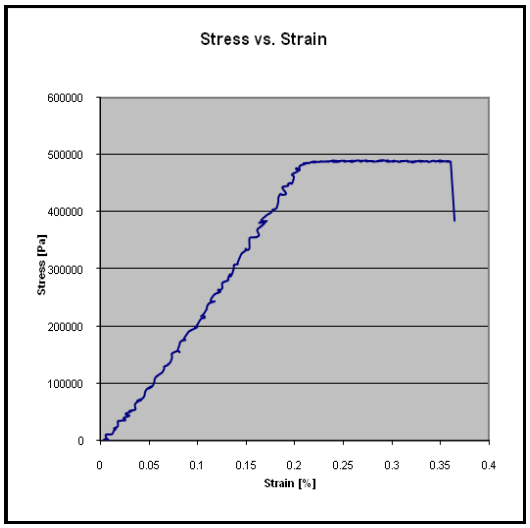

FIGURE D.14. Stress-strain graph for specimen 14 (R-8) repaired by bone plate and screws. (R = right)

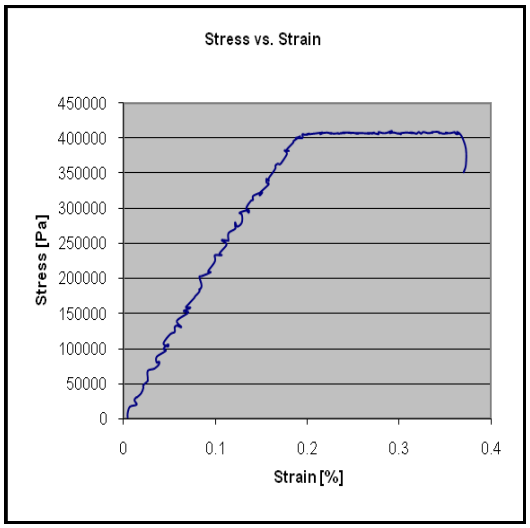

FIGURE D.15. Stress-strain graph for specimen 15 (R-11) repaired by bone plate and screws. (R = right)

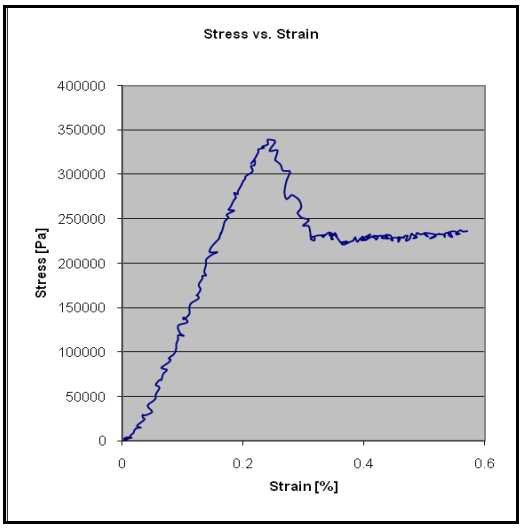

FIGURE D.16. Stress-strain graph for specimen 16 (L-12) repaired by bone plate and screws. (L = left)

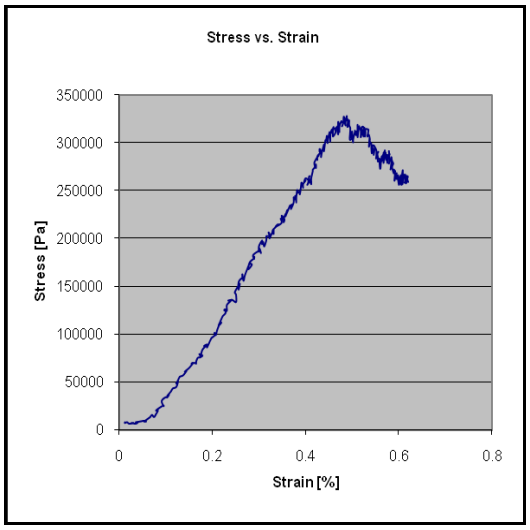

FIGURE D.17. Stress-strain graph for specimen 17 (R-12) repaired by bone plate and screws. (R = right)

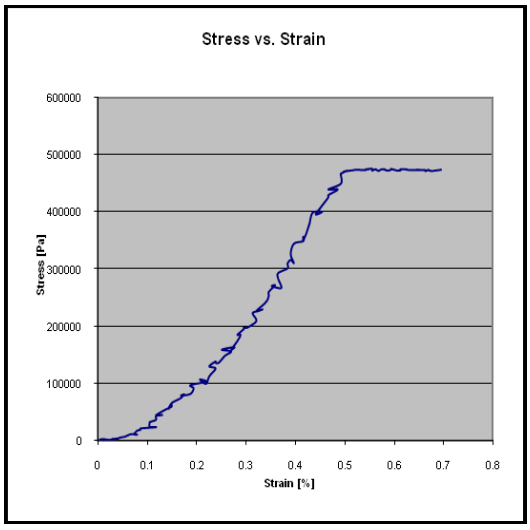

FIGURE D.18. Stress-strain graph for specimen 18 (R-13) repaired by bone plate and screws. (R = right)

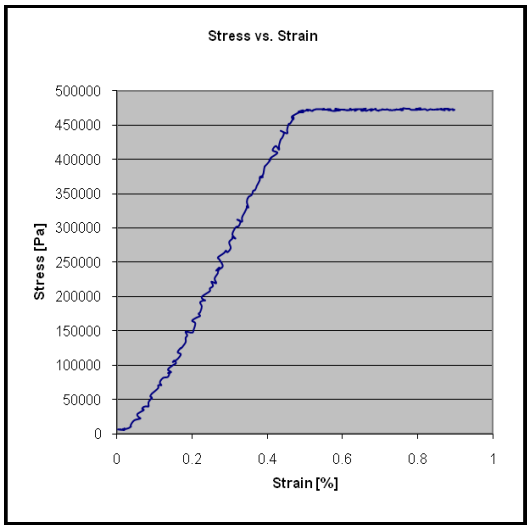

FIGURE D.19. Stress-strain graph for specimen 19 (L-15) repaired by bone plate and screws. (L = left)

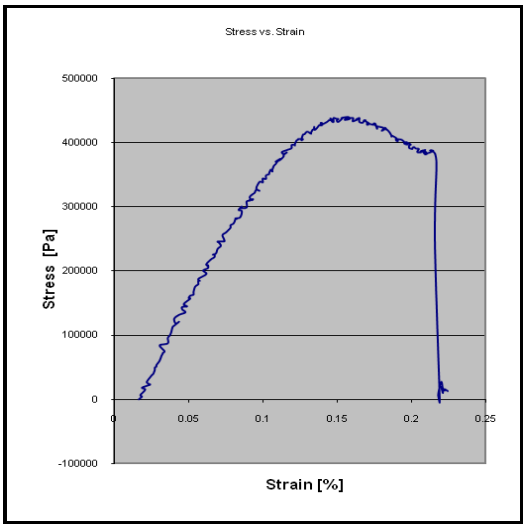

FIGURE D.20. Stress-strain graph for specimen 20 (L-16) repaired by bone plate and screws. (L = left)

APPENDIX E

Modes of failure: Group 1

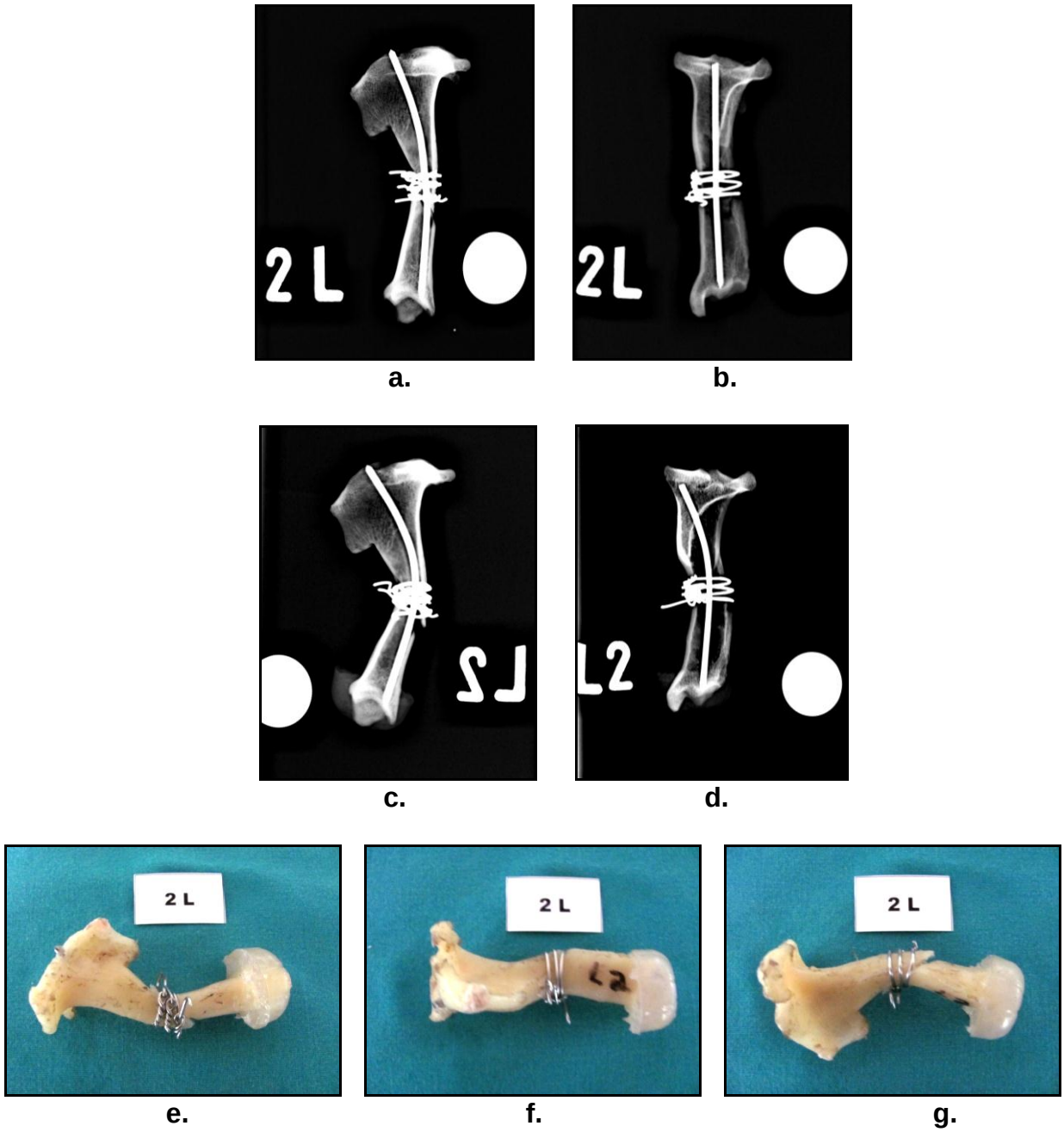

a. b. c. d. e. f. g.

FIGURE E.1. Specimen 1 (L-2): Mediolateral (a) and craniocaudal (b) view radiographs of the left tibia taken prior to the biomechanical testing, compared to the mediolateral (c) and craniocaudal (d) radiographs of the same specimen, and its medial (e), cranial (f) and lateral (g) photographic view, taken after completion of the biomechanical tests. Separation of the fragments at the osteotomy site; wire 1 was displaced distally on the caudomedial ridge of the bone; wire 3 was displaced proximally on the cranial ridge of the bone, with the free end of the distal wire elevated 45°; the intramedullary pin underwent plastic deformation.

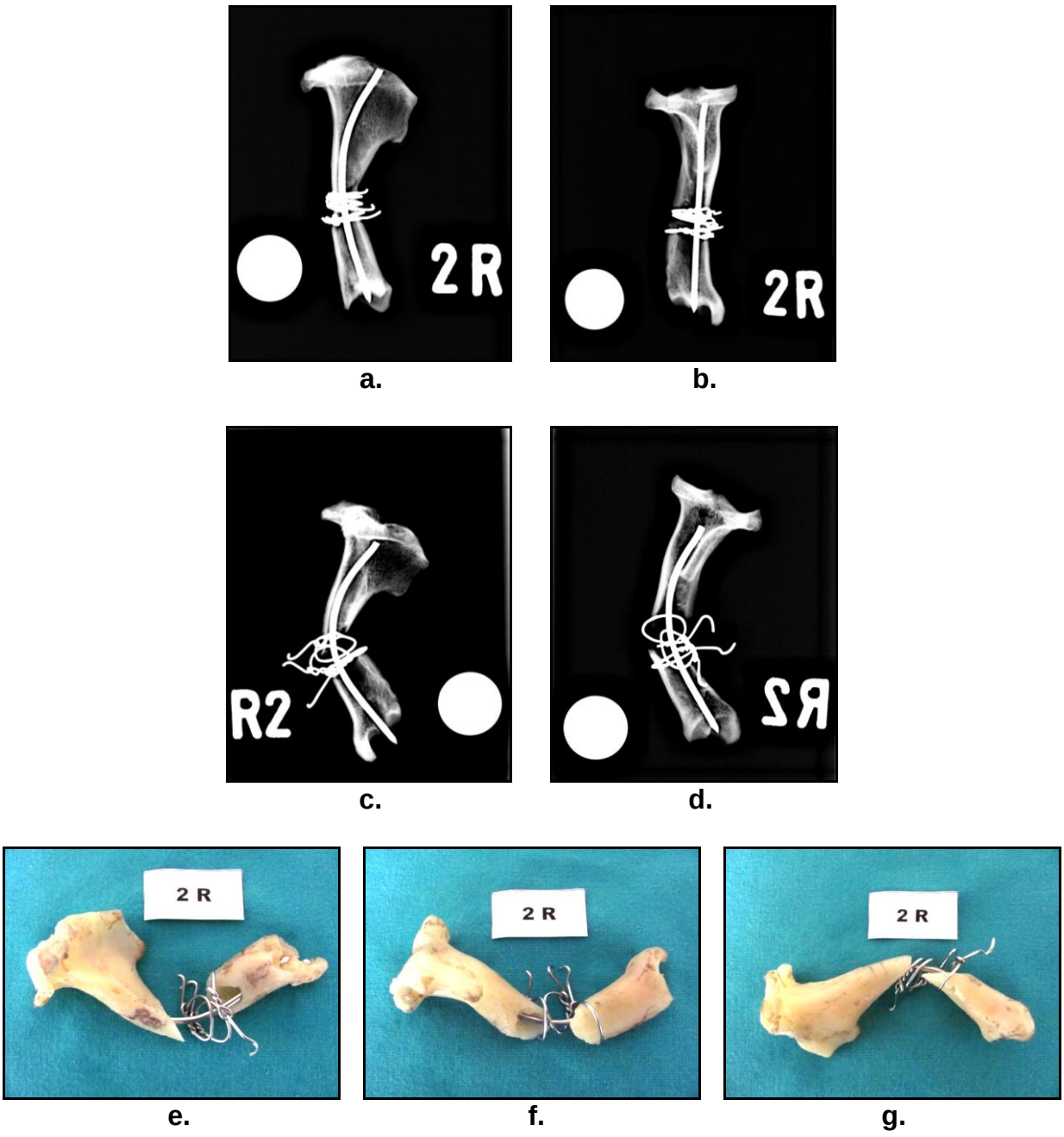

a. b. c. d. e. f. g.

FIGURE E.2. Specimen 2 (R-2): Mediolateral (a) and craniocaudal (b) view radiographs of the left tibia taken prior to the biomechanical testing, compared to the mediolateral (c) and craniocaudal (d) radiographs of the same specimen, and its medial (e), cranial (f) and lateral (g) photographic view, taken after completion of the biomechanical tests. Separation of the fragments at the osteotomy site; all 3 wires were unraveled and displaced towards the osteotomy site; their free ends were elevated between 40° and 85°; the intramedullary pin underwent plastic deformation.

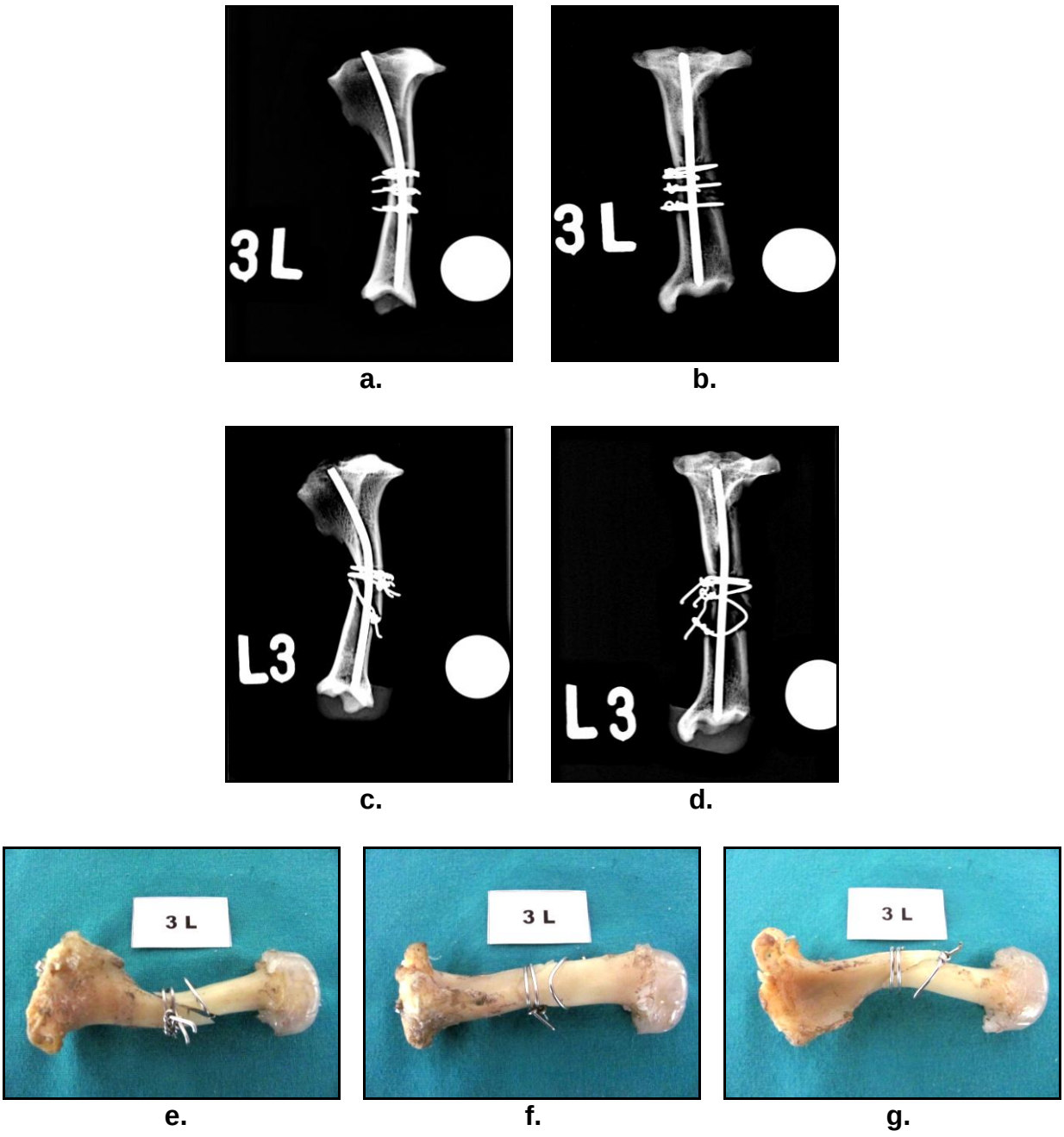

a. b. c. d. e. f. g.

FIGURE E.3. Specimen 3 (L-3): Mediolateral (a) and craniocaudal (b) view radiographs of the left tibia taken prior to the biomechanical testing, compared to the mediolateral (c) and craniocaudal (d) radiographs of the same specimen, and its medial (e), cranial (f) and lateral (g) photographic view, taken after completion of the biomechanical tests. Separation of the fragments at the osteotomy site; all 3 wires were unraveled, the distal wire was distally displaced; their free ends were elevated between 90° and 180°; the intramedullary pin underwent plastic deformation.

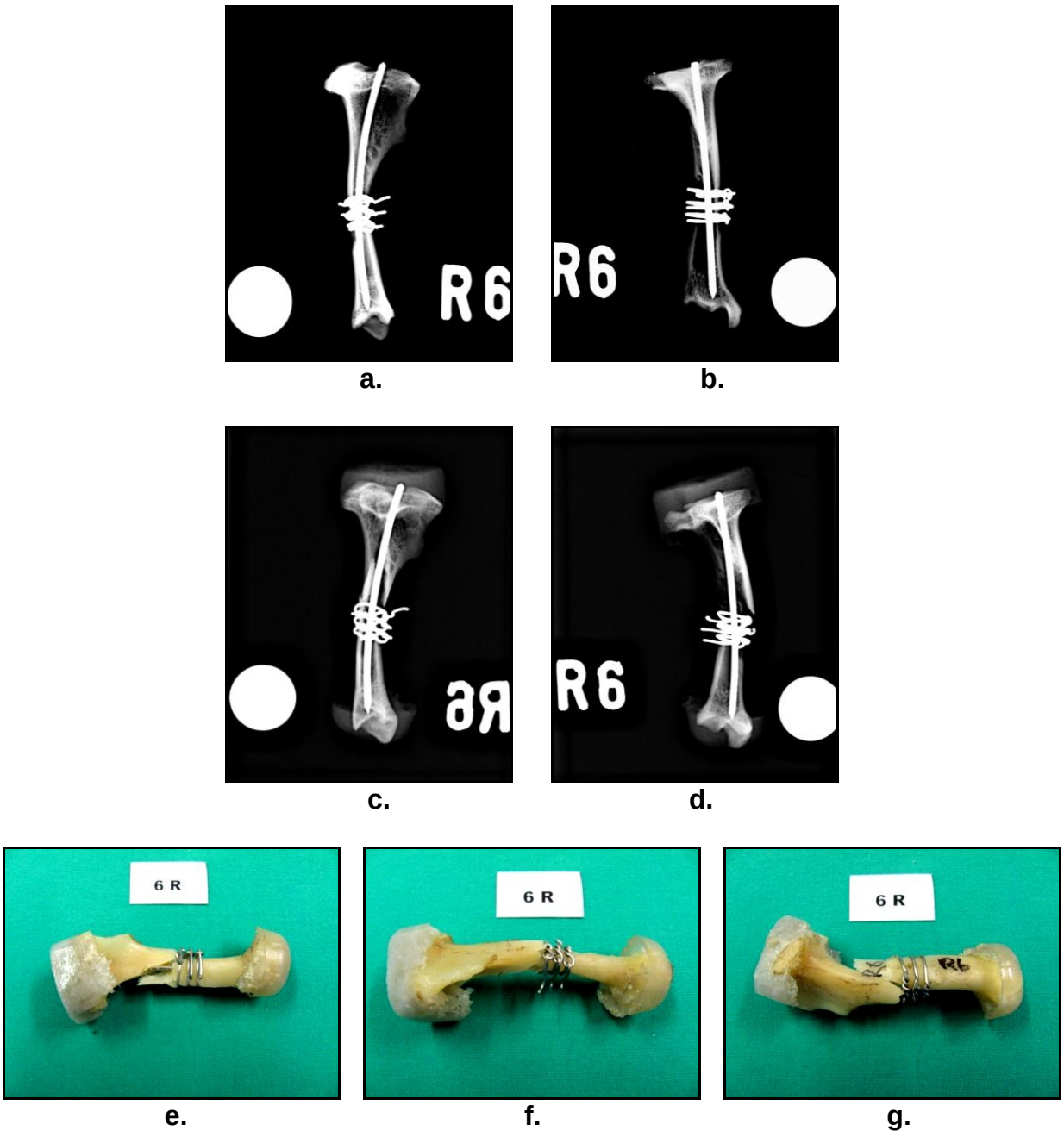

FIGURE E.4. Specimen 4 (R-6): Mediolateral (a) and craniocaudal (b) view radiographs of the left tibia taken prior to the biomechanical testing, compared to the mediolateral (c) and craniocaudal (d) radiographs of the same specimen, and its medial (e), cranial (f) and lateral (g) photographic view, taken after completion of the biomechanical tests. Separation of the fragments at the osteotomy site; cerclage wires were not displaced, but the free end of the proximal wire was elevated 25°; a transverse incomplete fracture at the distal end of the proximal fragment under the proximal and middle wires on the medial aspect of the bone; a transverse fracture of the distal fragment 2 mm proximal to the proximal wire on the caudal aspect of the bone; the intramedullary pin was intact.

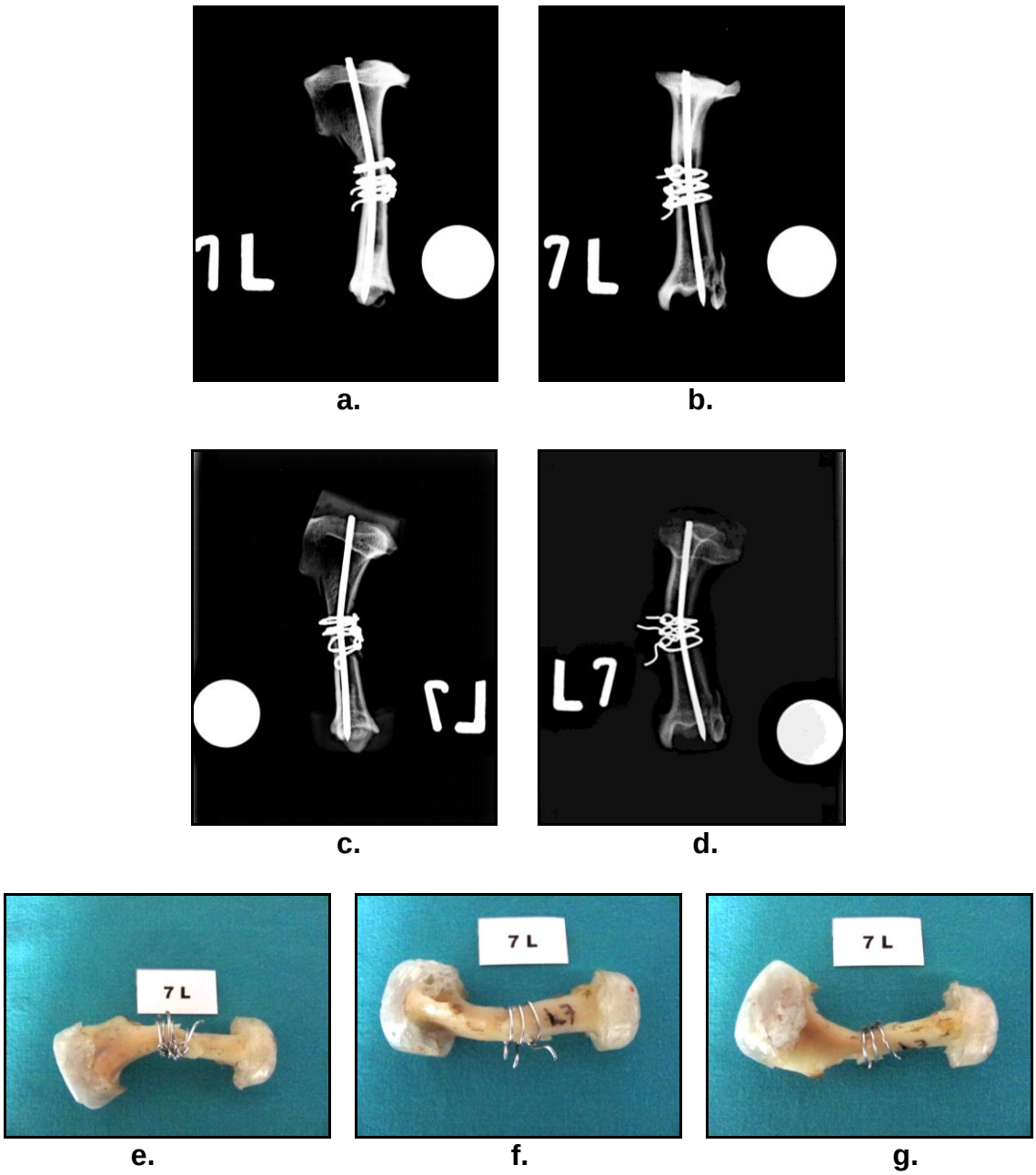

FIGURE E.5. Specimen 5 (L-7): Mediolateral (a) and craniocaudal (b) view radiographs of the left tibia taken prior to the biomechanical testing, compared to the mediolateral (c) and craniocaudal (d) radiographs of the same specimen, and its medial (e), cranial (f) and lateral (g) photographic view, taken after completion of the biomechanical tests. Separation of the fragments at the osteotomy site; cerclage wires were not displaced, but the free ends of the middle and distal wires were elevated between 15° and 30°; a transverse fracture of the proximal fragment under the middle wire on the caudal aspect of the bone; the intramedullary pin underwent plastic deformation.

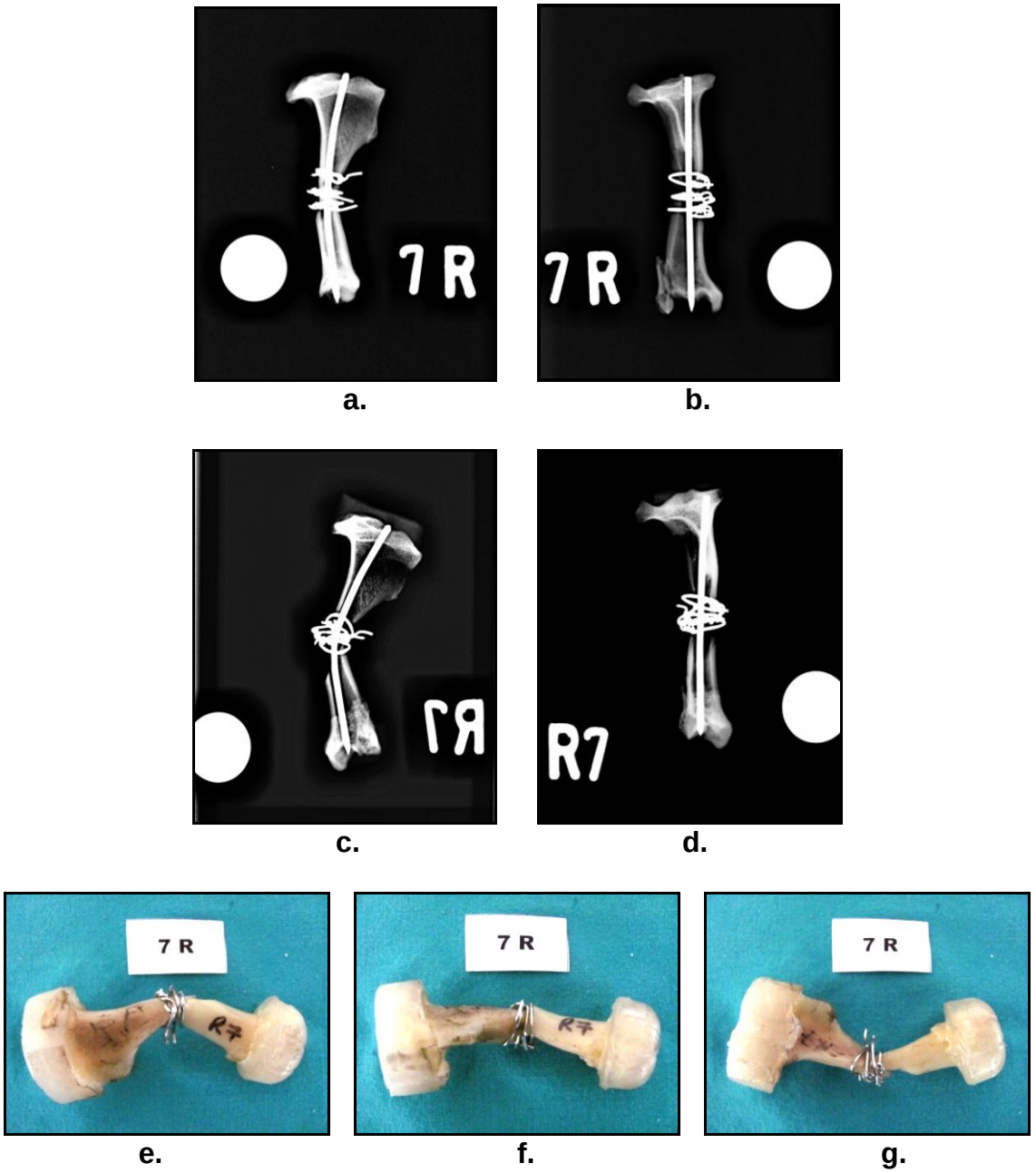

FIGURE E.6. Specimen 6 (R-7): Mediolateral (a) and craniocaudal (b) view radiographs of the left tibia taken prior to the biomechanical testing, compared to the mediolateral (c) and craniocaudal (d) radiographs of the same specimen, and its medial (e), cranial (f) and lateral (g) photographic view, taken after completion of the biomechanical tests. Separation of the fragments at the osteotomy site; the middle and distal wires were unraveled and displaced towards the osteotomy site; oblique fracture at the middle wire; the intramedullary pin underwent plastic deformation.

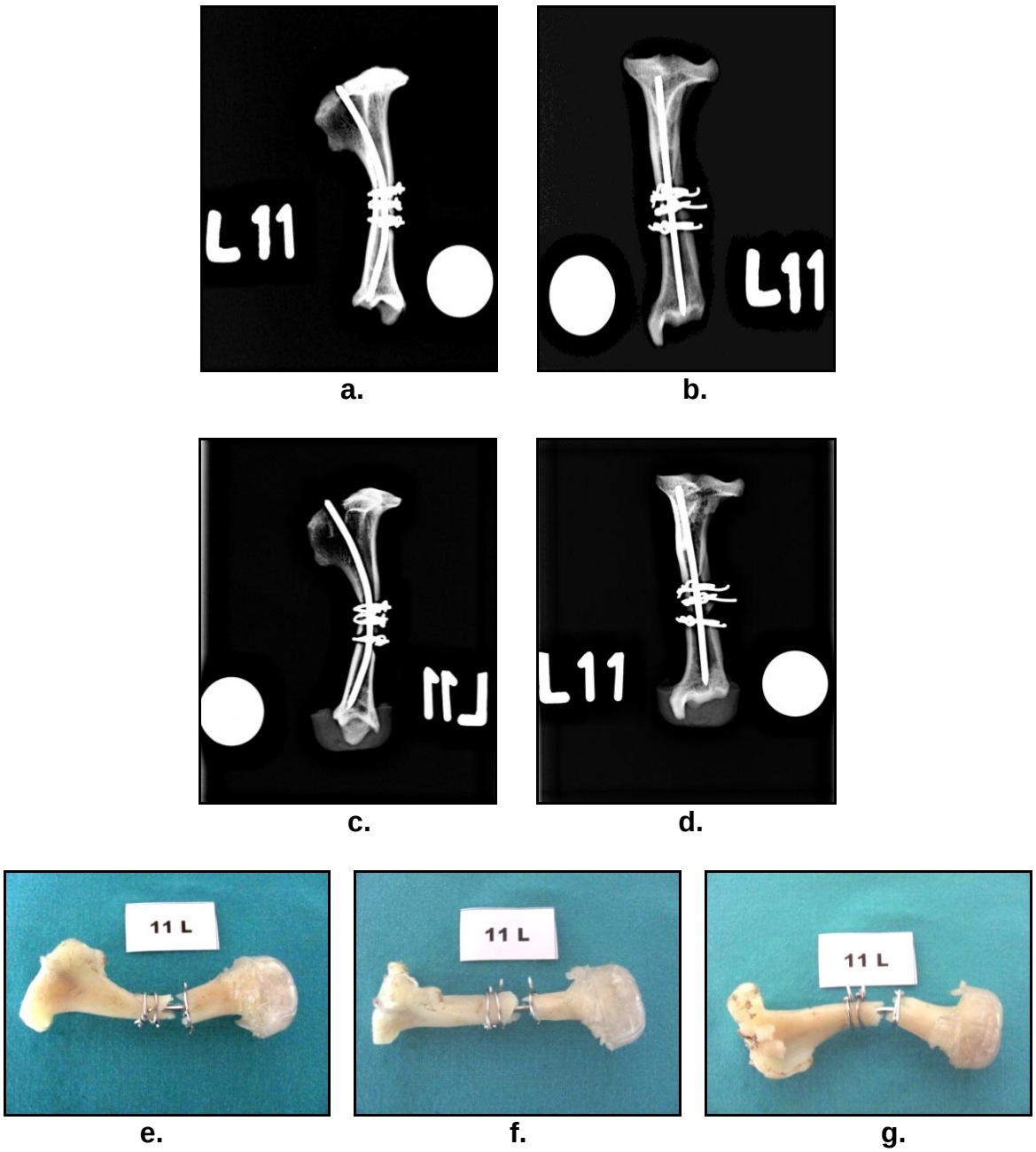

a. b. c. d. e. f. g.

FIGURE E.7. Specimen 7 (L-11): Mediolateral (a) and craniocaudal (b) view radiographs of the left tibia taken prior to the biomechanical testing, compared to the mediolateral (c) and craniocaudal (d) radiographs of the same specimen, and its medial (e), cranial (f) and lateral (g) photographic view, taken after completion of the biomechanical tests. No separation of the fragments at the osteotomy site; complete transverse fracture at distal wire, involving both fragments; separation took place at this fracture site; the intramedullary pin was intact.

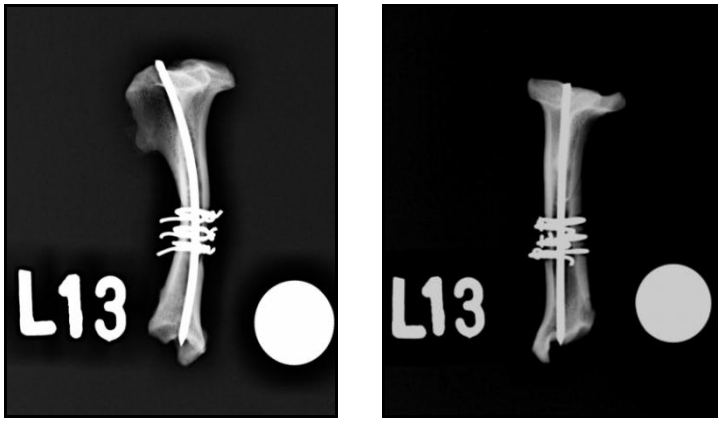

a. b.

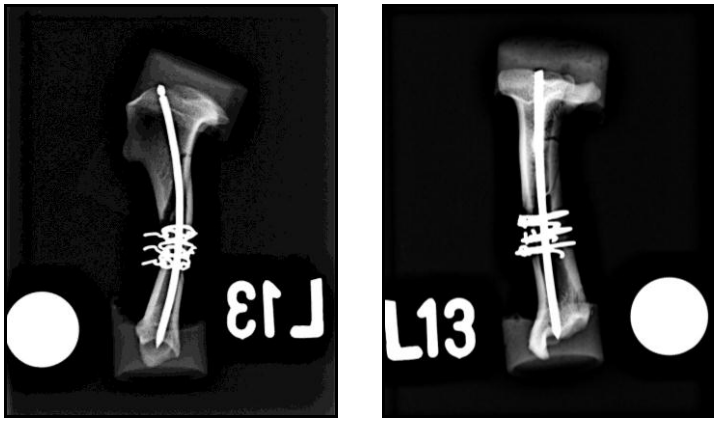

c. d.

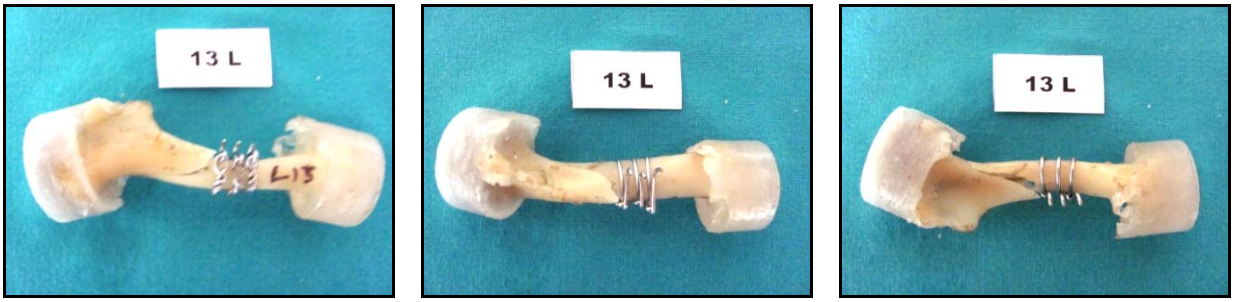

e. f. g.

FIGURE E.8. Specimen 8 (L-13): Mediolateral (a) and craniocaudal (b) view radiographs of the left tibia taken prior to the biomechanical testing, compared to the mediolateral (c) and craniocaudal (d) radiographs of the same specimen, and its medial (e), cranial (f) and lateral (g) photographic view, taken after completion of the biomechanical tests. No separation at the osteotomy site; the cerclage wires were intact; long spiral fracture starting 1 mm proximal to the proximal wire on the cranial ridge of the bone, running in a caudoproximal direction; intramedullary pin underwent a small degree of plastic deformation.

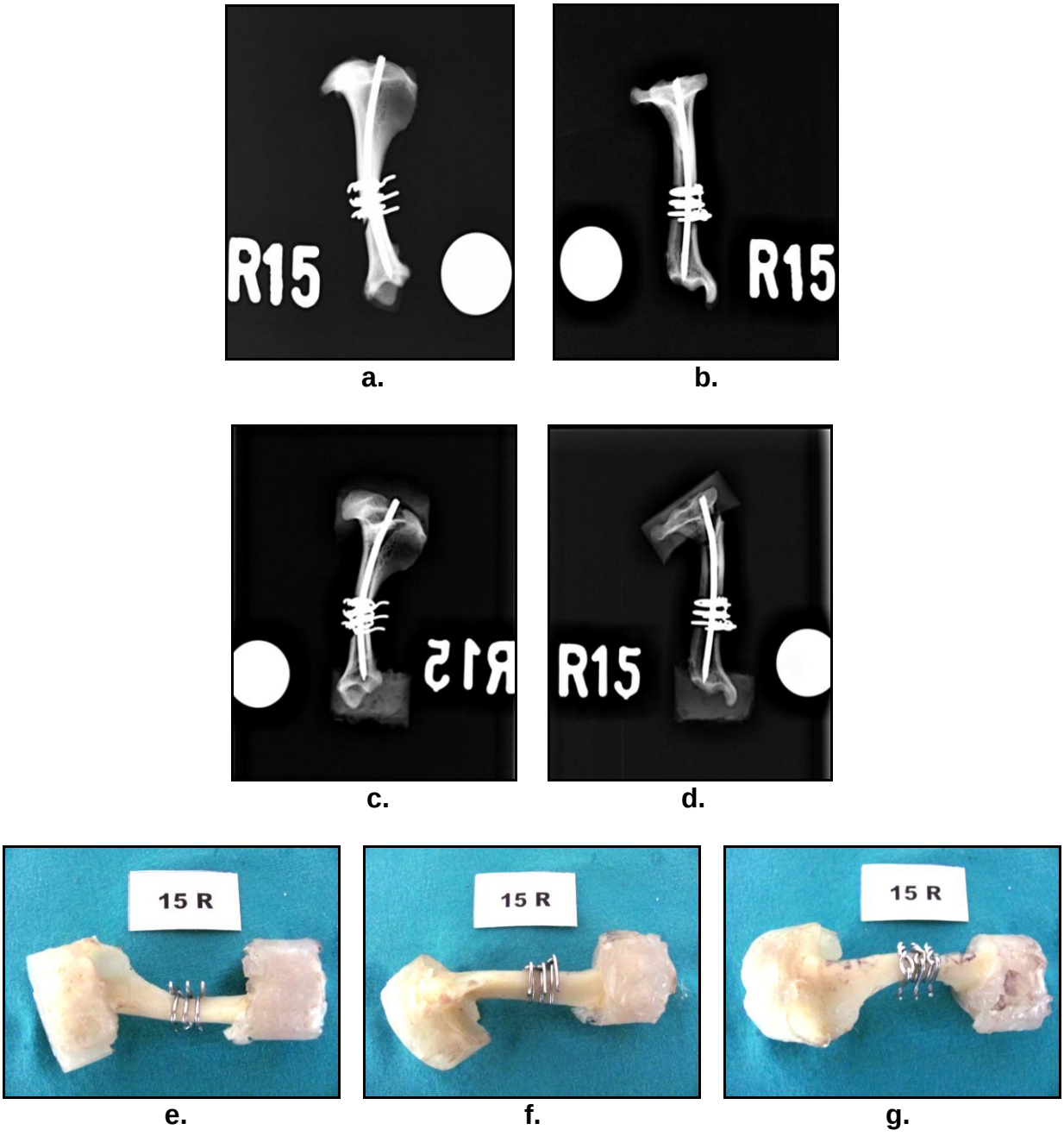

FIGURE E.9. Specimen 9 (R-15): Mediolateral (a) and craniocaudal (b) view radiographs of the left tibia taken prior to the biomechanical testing, compared to the mediolateral (c) and craniocaudal (d) radiographs of the same specimen, and its medial (e), cranial (f) and lateral (g) photographic view, taken after completion of the biomechanical tests. No separation at the osteotomy site; the cerclage wires were intact; short oblique fracture of proximal aspect of the bone, running caudodistally; the intramedullay pin underwent plastic deformation.

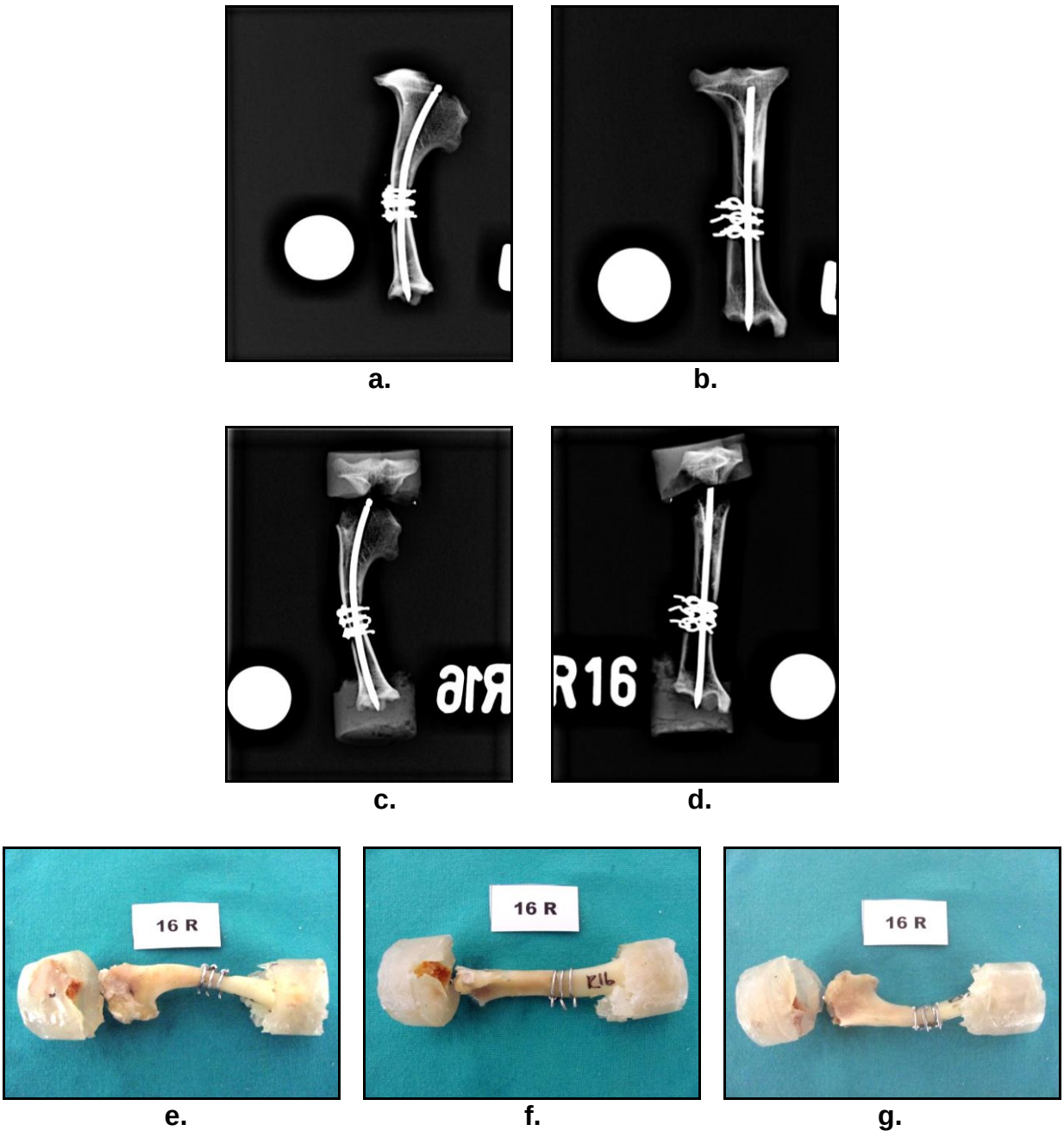

FIGURE E.10. Specimen 10 (R-16): Mediolateral (a) and craniocaudal (b) view radiographs of the left tibia taken prior to the biomechanical testing, compared to the mediolateral (c) and craniocaudal (d) radiographs of the same specimen, and its medial (e), cranial (f) and lateral (g) photographic view, taken after completion of the biomechanical tests. No separation at the osteotomy site; the cerclage wires were intact; avulsion fracture of the caudal aspect of the head of the bone; the intramedullay pin underwent slight plastic deformation.

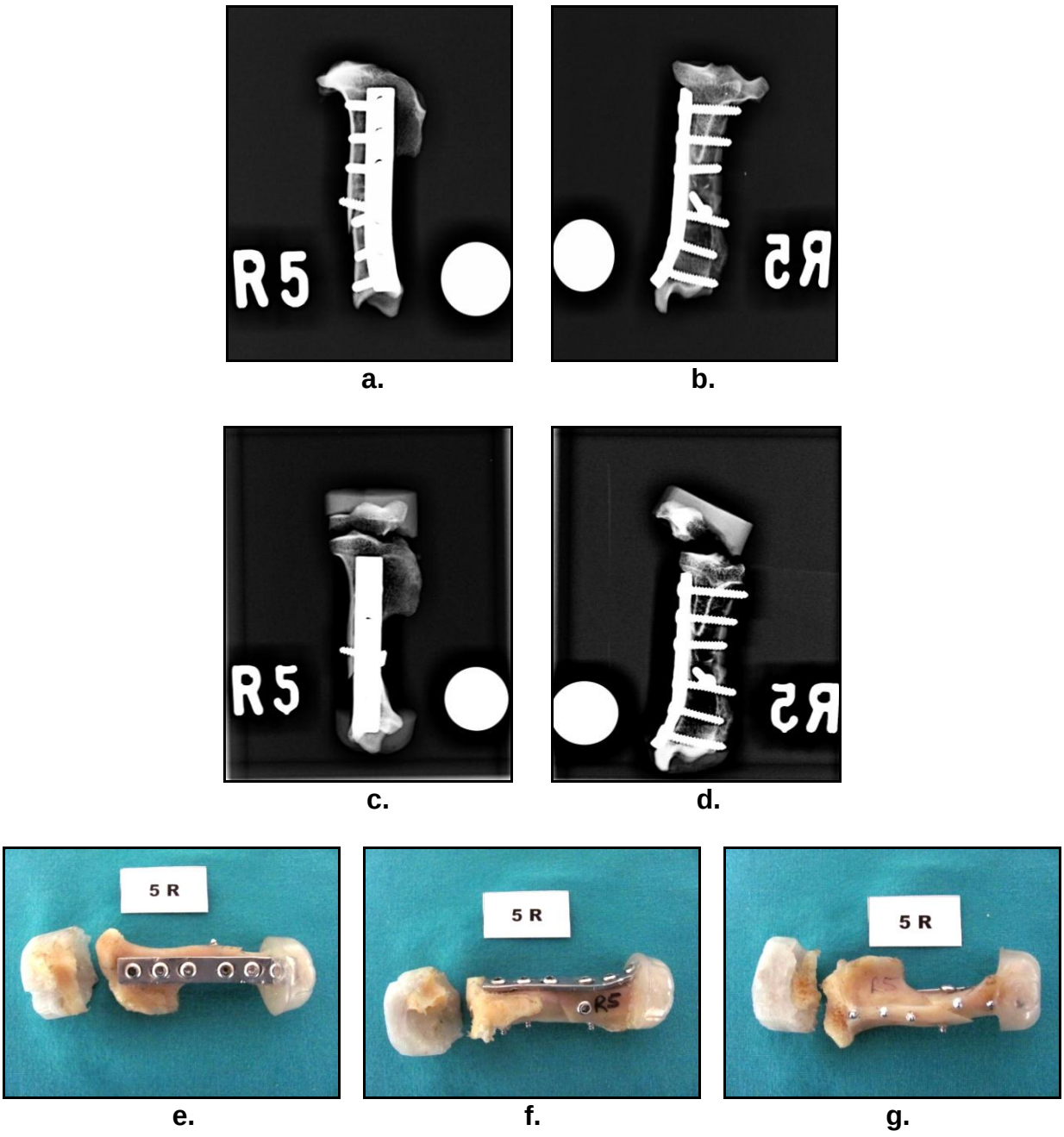

FIGURE E.11. Specimen 11 (R-5): Mediolateral (a) and craniocaudal (b) view radiographs of the left tibia taken prior to the biomechanical testing, compared to the mediolateral (c) and craniocaudal (d) radiographs of the same specimen, and its medial (e), cranial (f) and lateral (g) photographic view, taken after completion of the biomechanical tests. No separation of fragments; transverse fracture of the proximal epiphysis of the bone; the bone plate and screws were intact, without any plastic deformation. (Screws in plate holes numbered 1 to 6 proximo-distally).

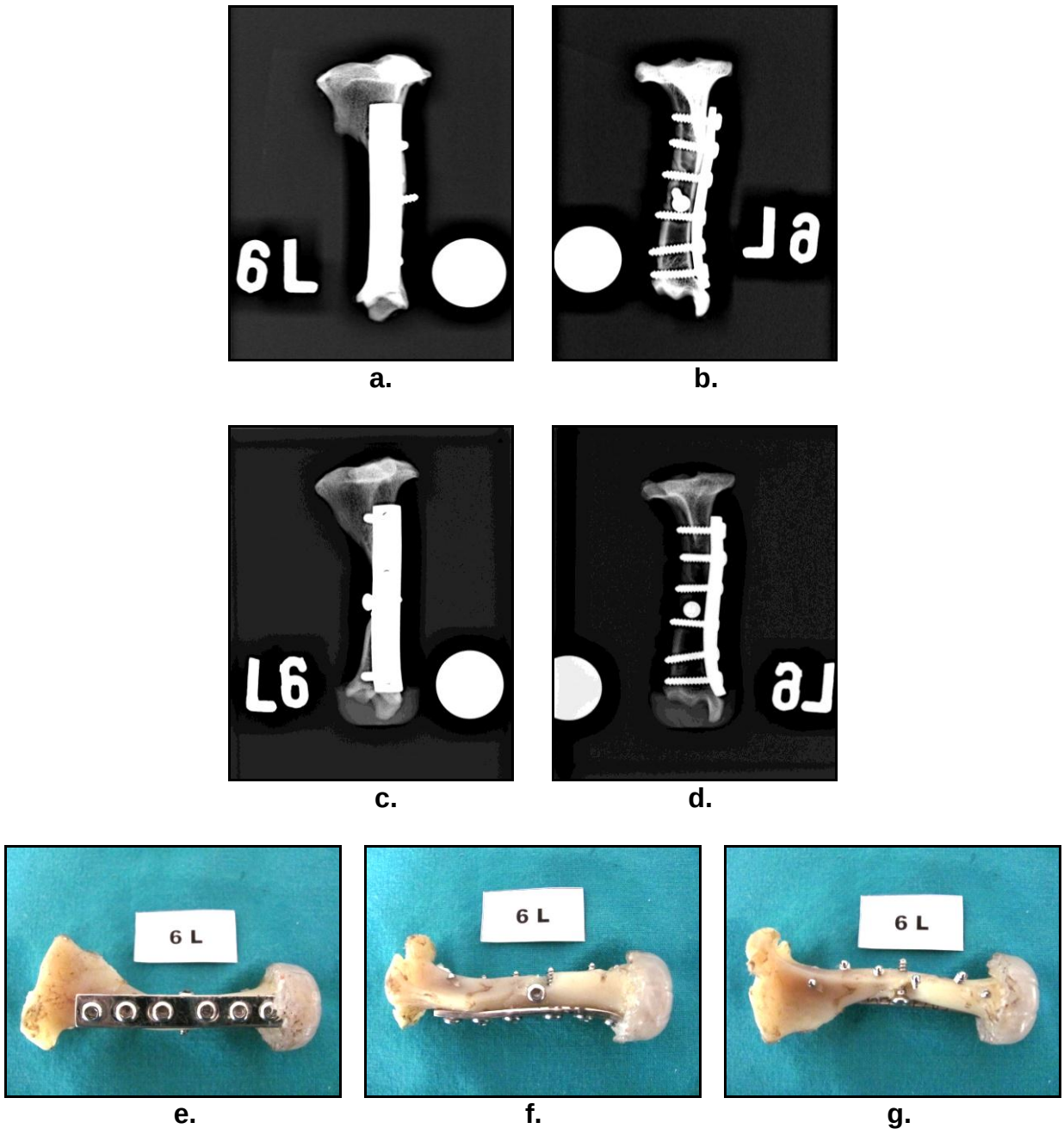

FIGURE E.12. Specimen 12 (L-6): Mediolateral (a) and craniocaudal (b) view radiographs of the left tibia taken prior to the biomechanical testing, compared to the mediolateral (c) and craniocaudal (d) radiographs of the same specimen, and its medial (e), cranial (f) and lateral (g) photographic view, taken after completion of the biomechanical tests. No separation of fragments; short oblique fracture between the head of the lag screw and the tip of screw 4 on the craniolateral aspect of the bone, running in a dorsoventral oblique direction; the bone plate and screws were intact, without any plastic deformation. (Screws in plate holes numbered 1 to 6 proximo-distally).

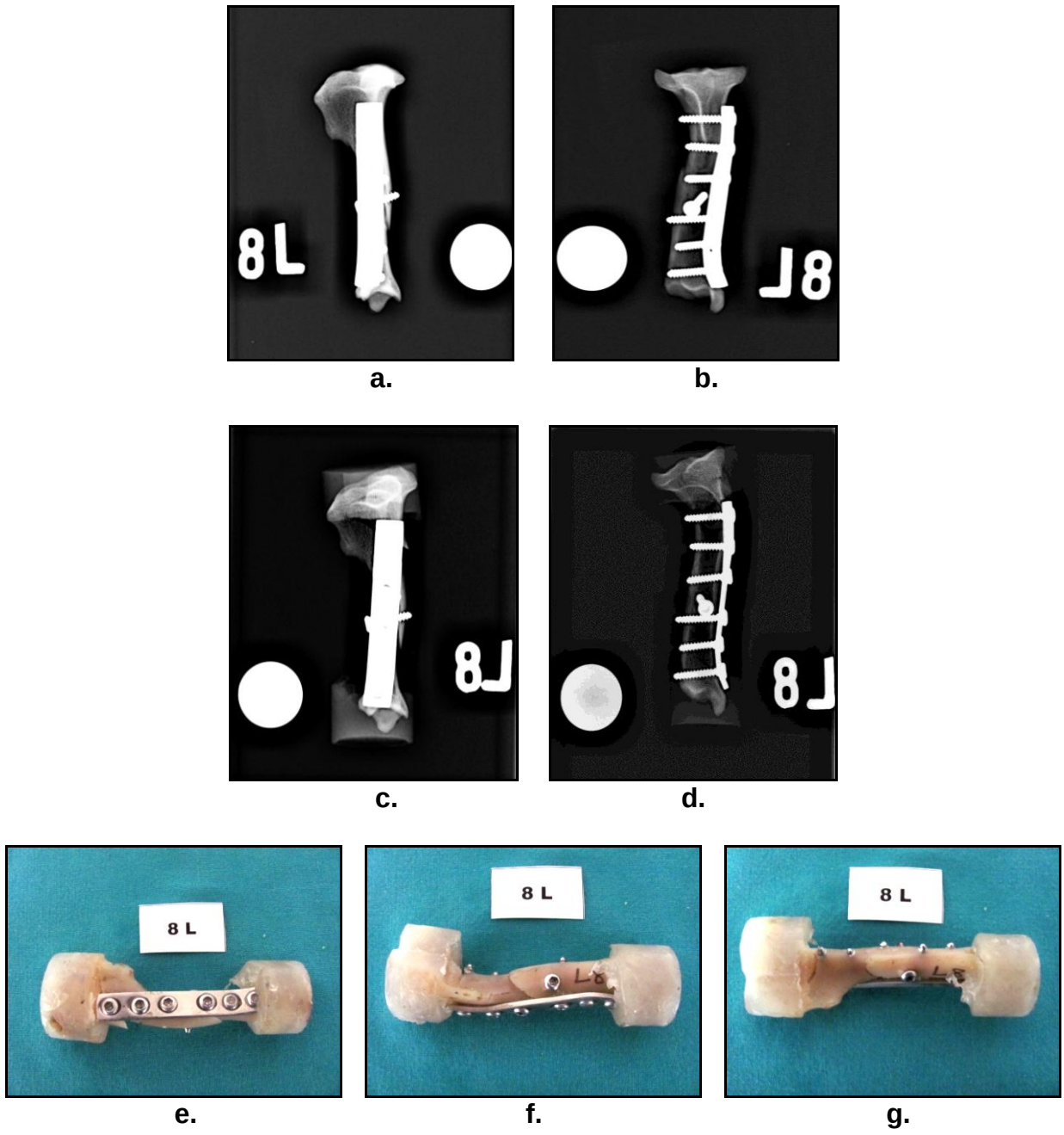

a. b. c. d. e. f. g.

FIGURE E.13. Specimen 13 (L-8): Mediolateral (a) and craniocaudal (b) view radiographs of the left tibia taken prior to the biomechanical testing, compared to the mediolateral (c) and craniocaudal (d) radiographs of the same specimen, and its medial (e), cranial (f) and lateral (g) photographic view, taken after completion of the biomechanical tests. No separation of fragments; spiral fracture between heads of screws 1 and 2, running in a craniodorsal direction on the lateral aspect of the bone; the bone plate and screws were intact, without any plastic deformation. (Screws in plate holes numbered 1 to 6 proximo-distally).

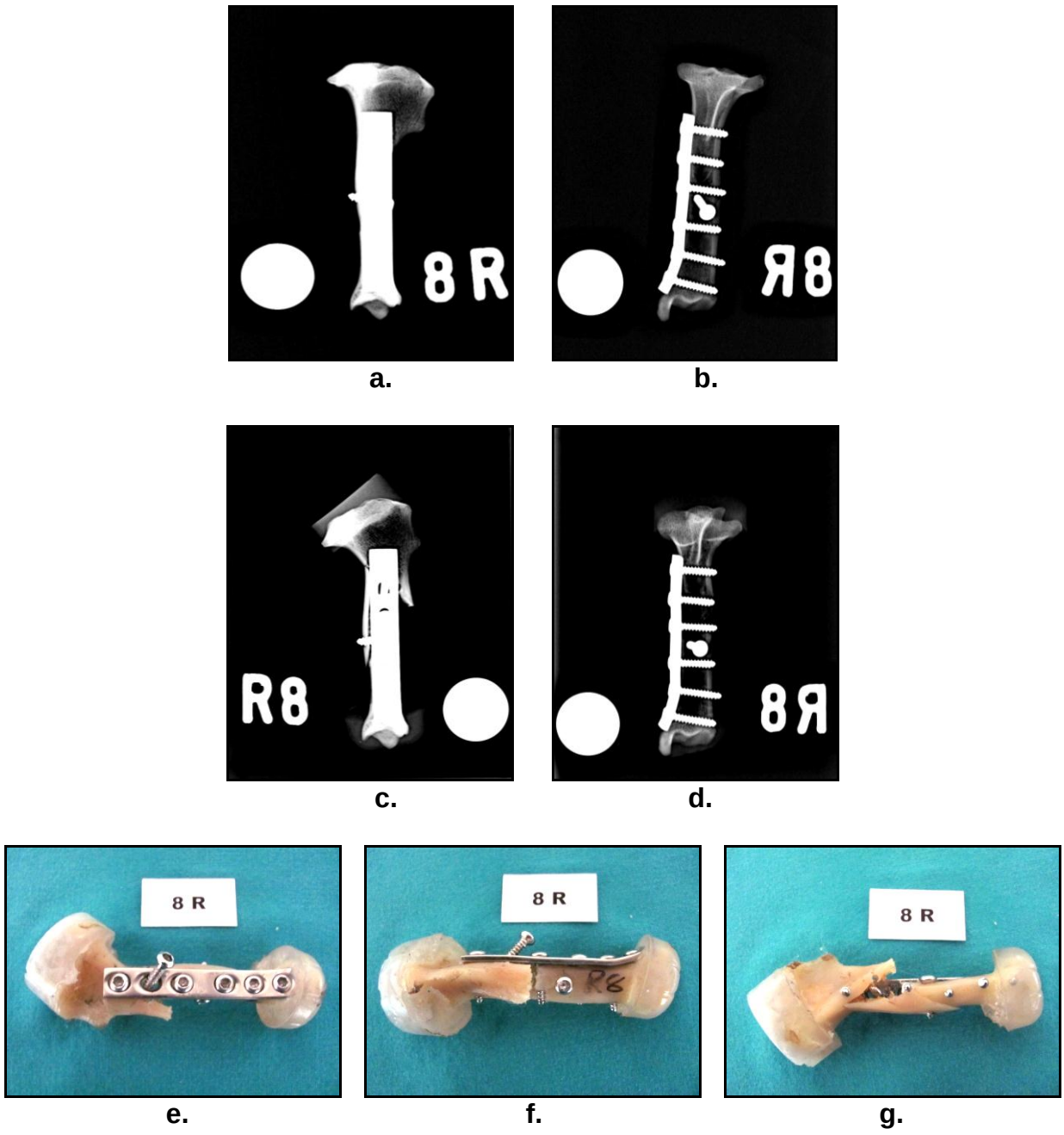

a. b. c. d. e. f. g.

FIGURE E.14. Specimen 14 (R-8): Mediolateral (a) and craniocaudal (b) view radiographs of the left tibia taken prior to the biomechanical testing, compared to the mediolateral (c) and craniocaudal (d) radiographs of the same specimen, and its medial (e), cranial (f) and lateral (g) photographic view, taken after completion of the biomechanical tests. Separation of main bone fragments; complete long oblique fracture involving the cranial aspect of the bone, running in a ventrodorsal direction between the length of screw 3 to the length of screw 1; the distal aspect of the fracture line ran transversely on the cranial aspect of the bone along the length of screw 3, just proximal to it; screw 2 was completely loose and displaced, but without any plastic deformation; the bone plate and the rest of the screws were intact, without any plastic deformation. (Screws in plate holes numbered 1 to 6 proximo-distally).

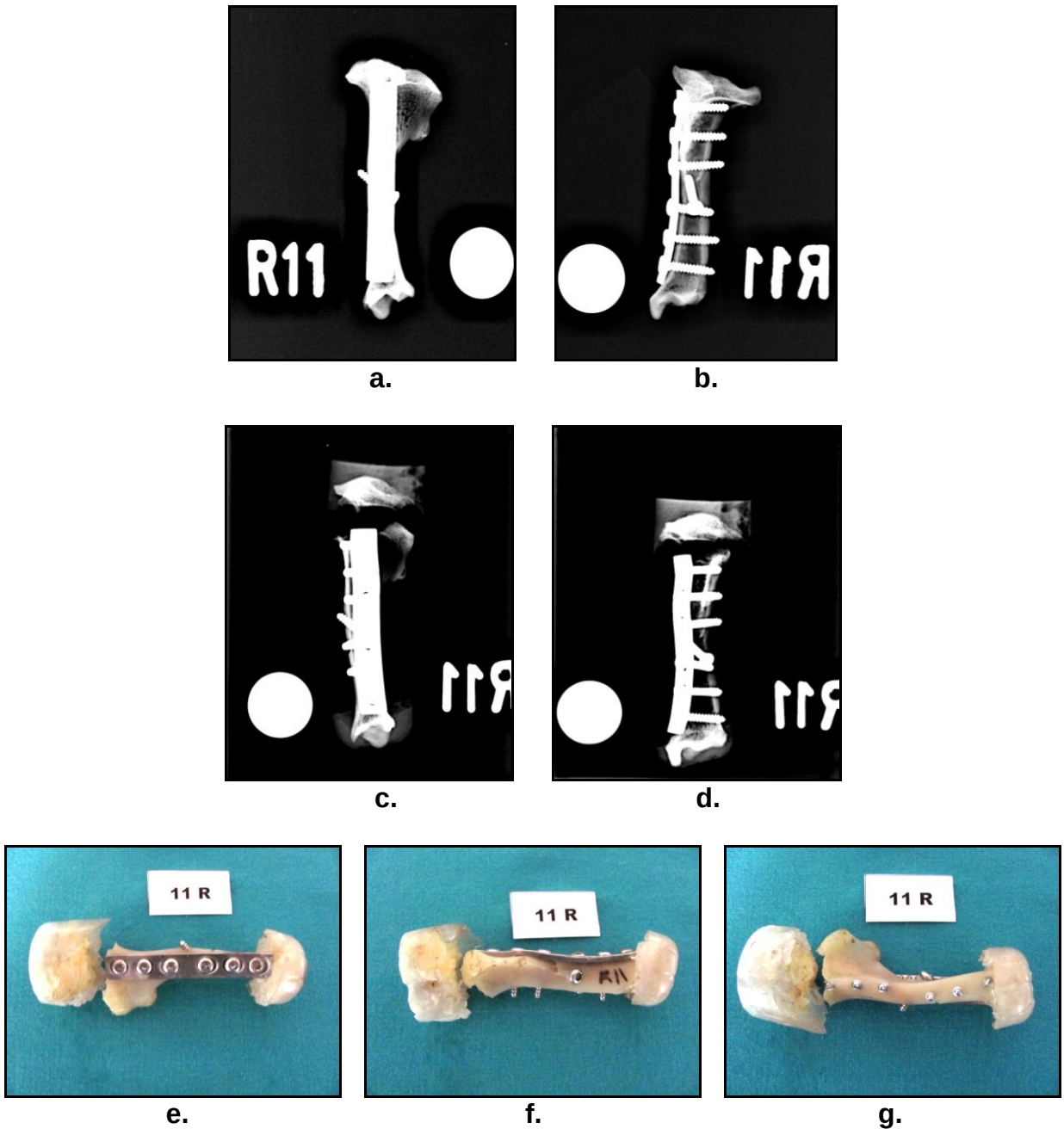

FIGURE E.15. Specimen 15 (R-11): Mediolateral (a) and craniocaudal (b) view radiographs of the left tibia taken prior to the biomechanical testing, compared to the mediolateral (c) and craniocaudal (d) radiographs of the same specimen, and its medial (e), cranial (f) and lateral (g) photographic view, taken after completion of the biomechanical tests. No separation of fragments; transverse fracture through the entire bone, just proximal to the proximal end of the bone plate; the bone plate and screws were intact, without any plastic deformation. (Screws in plate holes numbered 1 to 6 proximo-distally).

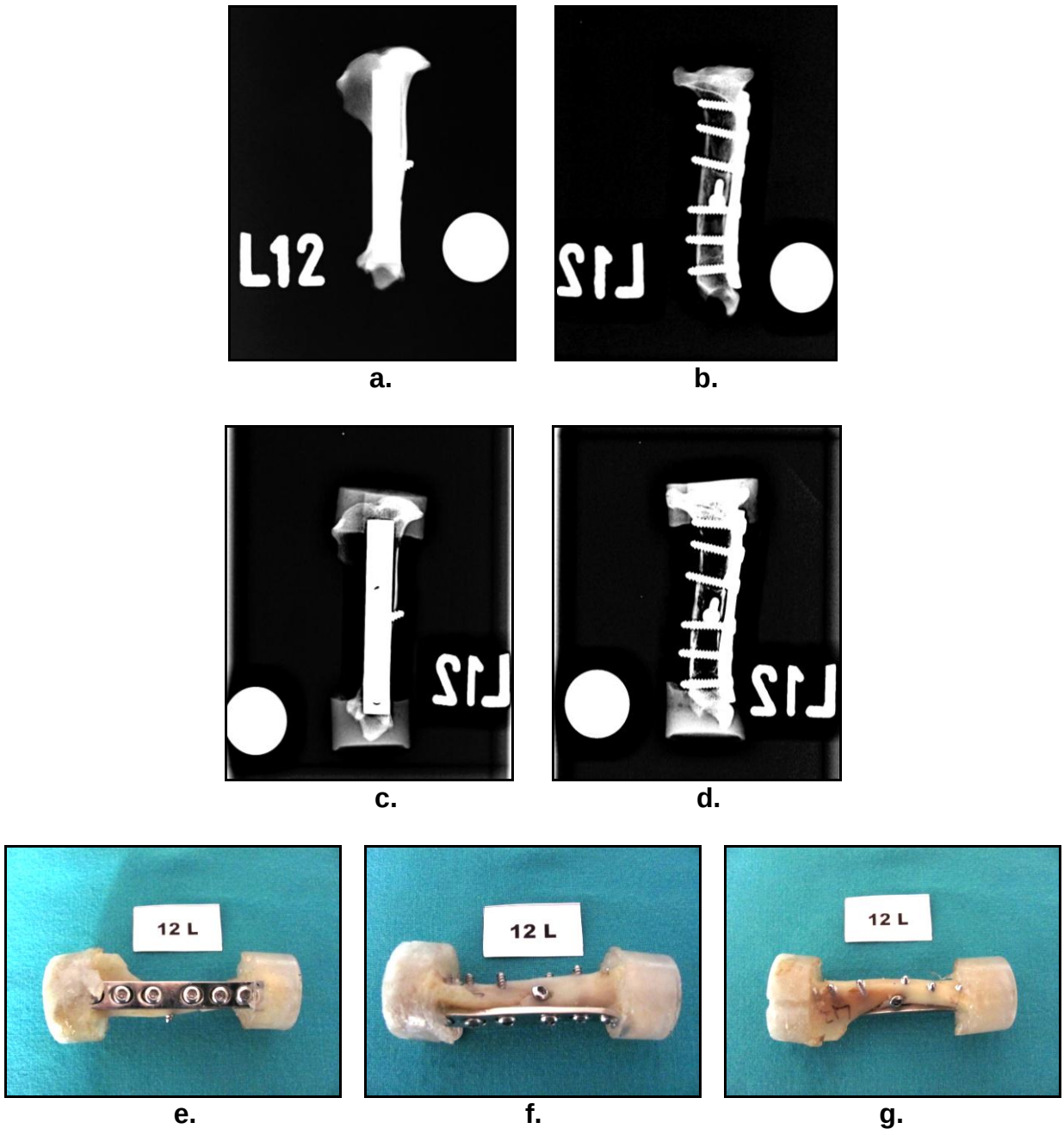

FIGURE E.16. Specimen 16 (L-12): Mediolateral (a) and craniocaudal (b) view radiographs of the left tibia taken prior to the biomechanical testing, compared to the mediolateral (c) and craniocaudal (d) radiographs of the same specimen, and its medial (e), cranial (f) and lateral (g) photographic view, taken after completion of the biomechanical tests. No separation of fragments; fracture running between the tips of screws 1, 2 and 3 on the caudolateral ridge of the bone, running in a ventrodorsal direction; incomplete oblique fracture from screw 2 caudodorsally in the caudal cortex of the bone; the bone plate and screws were intact, without any plastic deformation. (Screws in plate holes numbered 1 to 6 proximo-distally).

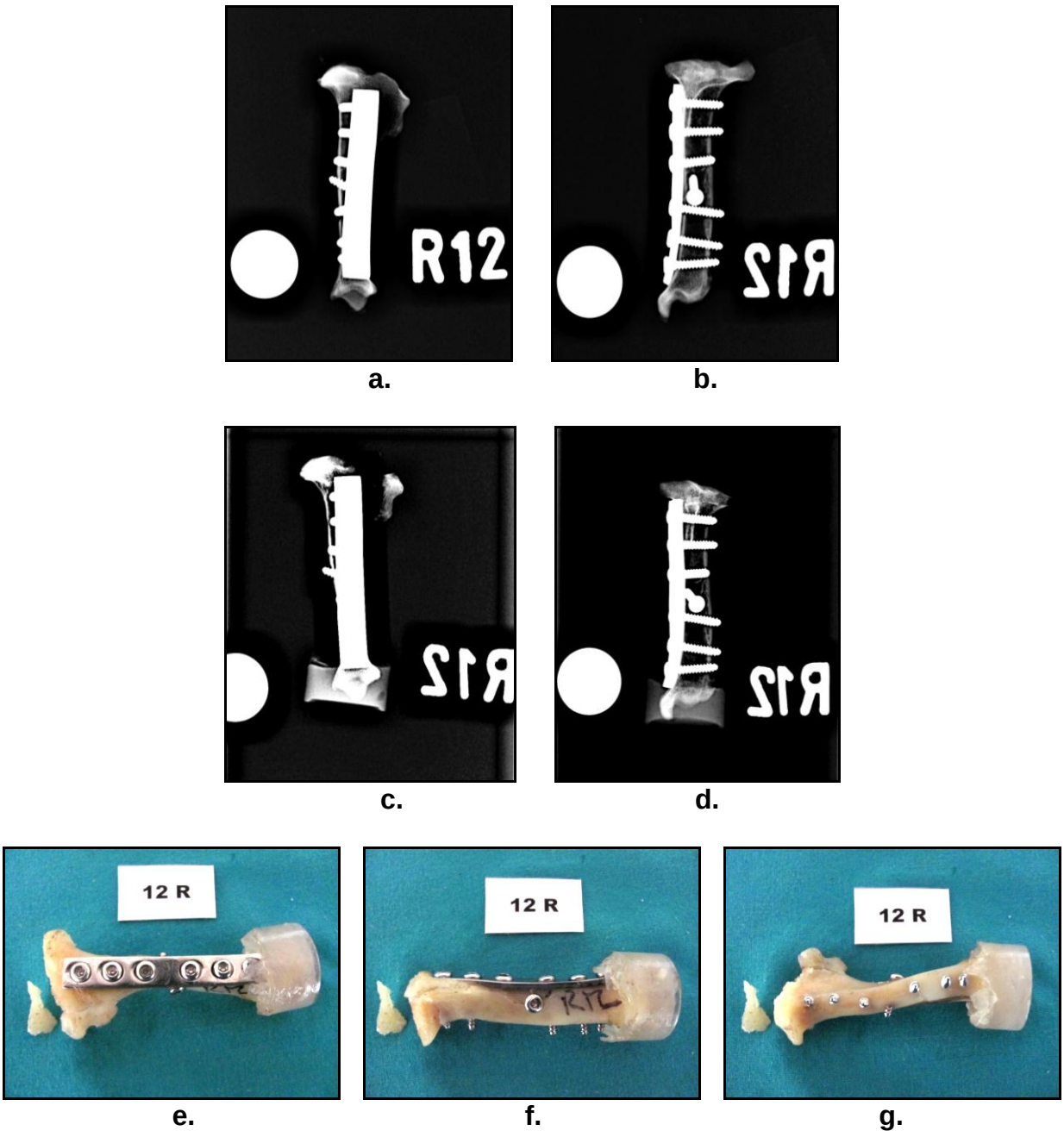

FIGURE E.17. Specimen 17 (R-12): Mediolateral (a) and craniocaudal (b) view radiographs of the left tibia taken prior to the biomechanical testing, compared to the mediolateral (c) and craniocaudal (d) radiographs of the same specimen, and its medial (e), cranial (f) and lateral (g) photographic view, taken after completion of the biomechanical tests. No separation of fragments; fracture line connecting the heads of screw 3, the lag screw and screw 4 on the cranial aspect of the bone; the tibial crest had a less important (does not bear weight) avulsion fracture in a dorsoventral direction; the bone plate and screws were intact, without any plastic deformation. (Screws in plate holes numbered 1 to 6 proximo-distally).

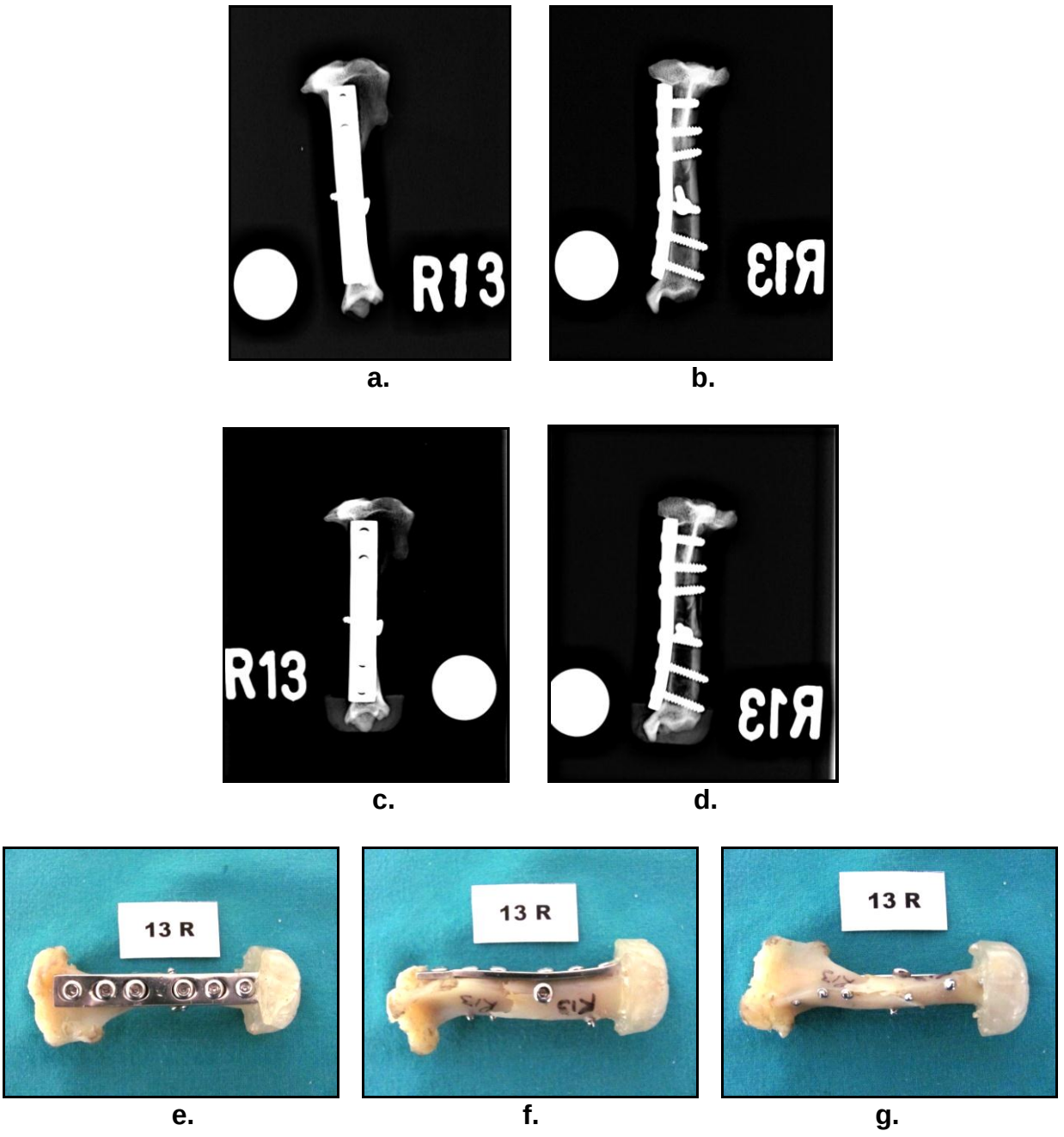

FIGURE E.18. Specimen 18 (R-13): Mediolateral (a) and craniocaudal (b) view radiographs of the left tibia taken prior to the biomechanical testing, compared to the mediolateral (c) and craniocaudal (d) radiographs of the same specimen, and its medial (e), cranial (f) and lateral (g) photographic view, taken after completion of the biomechanical tests. No separation of fragments; fracture between tips of screws 3 and 4 on the caudolateral ridge, running in a dorsoventral direction; another fracture of the proximal tip of the distal fragment, running from the head of the lag screw ventrodorsally; the bone plate and screws were intact, without any plastic deformation. (Screws in plate holes numbered 1 to 6 proximo-distally).

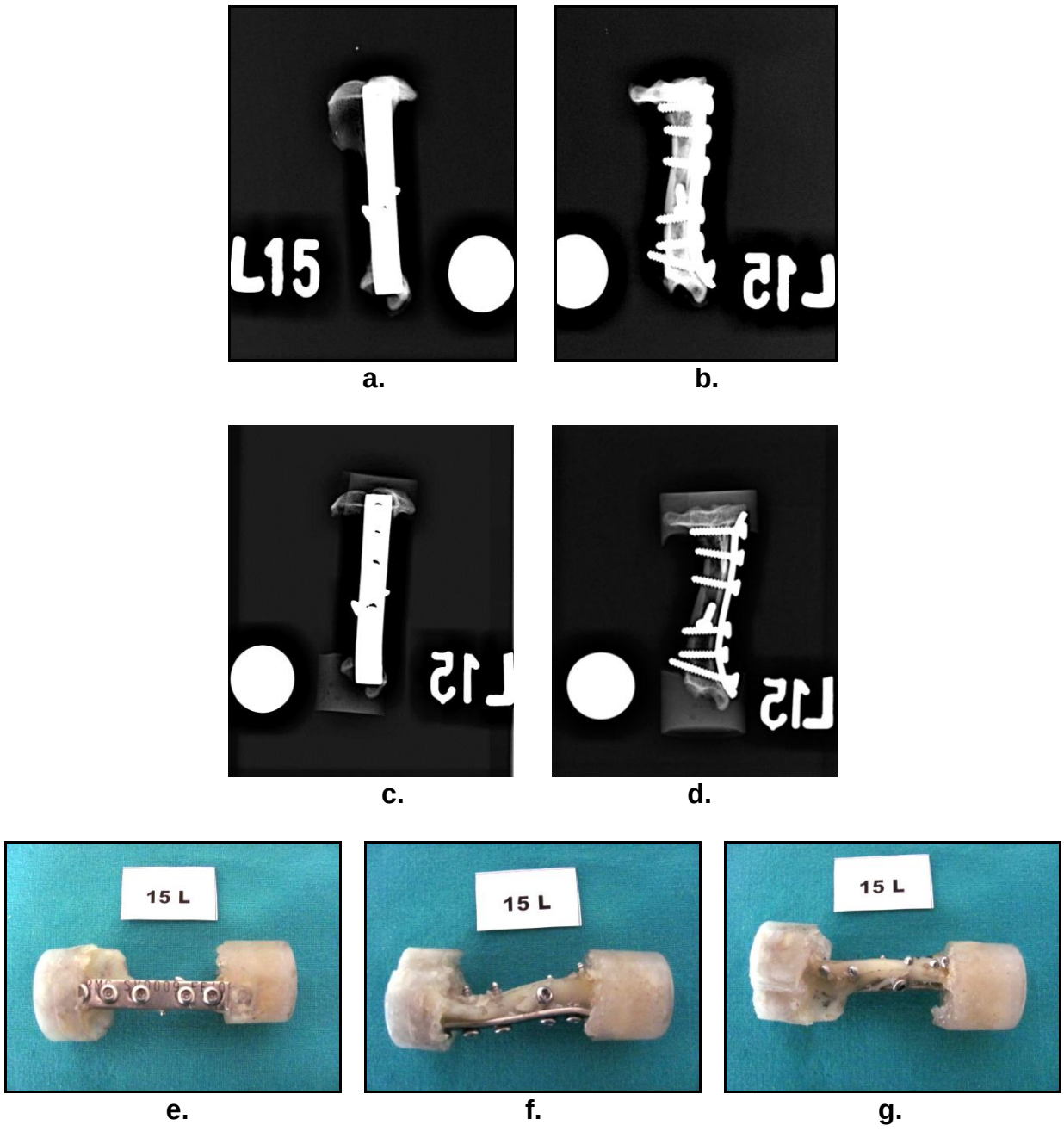

a. b. c. d. e. f. g.

FIGURE E.19. Specimen 19 (L-15): Mediolateral (a) and craniocaudal (b) view radiographs of the left tibia taken prior to the biomechanical testing, compared to the mediolateral (c) and craniocaudal (d) radiographs of the same specimen, and its medial (e), cranial (f) and lateral (g) photographic view, taken after completion of the biomechanical tests. No separation of fragments; transverse fracture at the head of the lag screw on the cranial aspect of the bone, involving the proximal tip of the distal fragment; the bone plate and screws were intact, without any plastic deformation. (Screws in plate holes numbered 1 to 6 proximo-distally).

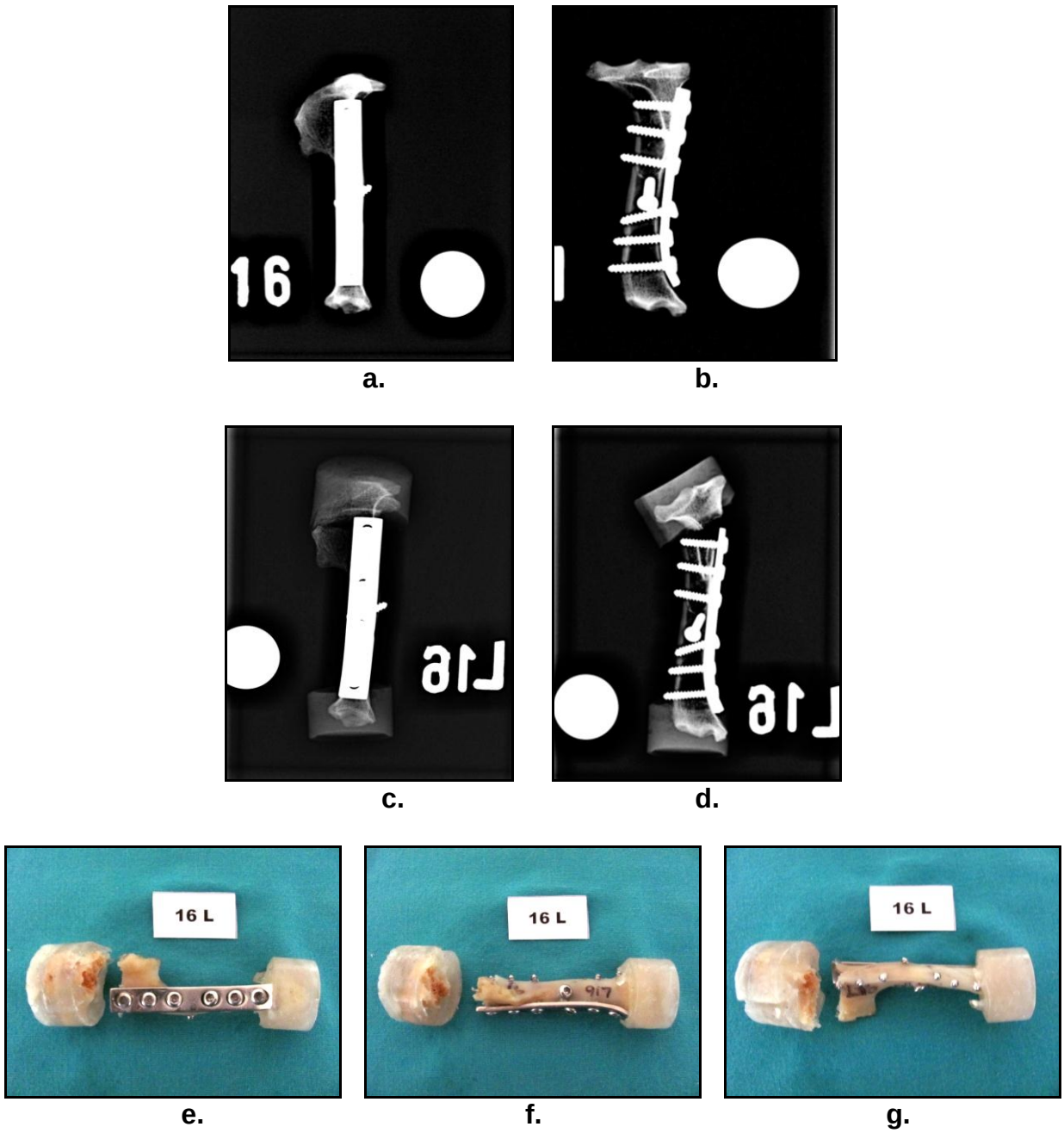

a. b. c. d. e. f. g.

FIGURE E.20. Specimen 20 (L-16): Mediolateral (a) and craniocaudal (b) view radiographs of the left tibia taken prior to the biomechanical testing, compared to the mediolateral (c) and craniocaudal (d) radiographs of the same specimen, and its medial (e), cranial (f) and lateral (g) photographic view, taken after completion of the biomechanical tests. No separation of fragments; transverse fracture through the entire bone, just proximal to the 1st screw; the bone plate and screws were intact, without any plastic deformation. (Screws in plate holes numbered 1 to 6 proximo-distally).

APPENDIX F

Pearson Correlation Coefficients

TABLE F.1. Pearson Correlation Coefficients of the outcome variables with body mass and age for the cadavers in group 1 (IM pin and cerclage wires). (n = 10)

Group 1: Pearson Correlation Coefficients				
Outcome variable	**Body mass**	**p-value**	**Age**	**p-value**
Bone length (mm)	0.578	0.080	-0.038	0.917
Bone diameter (mm)	0.936	<0.0001	-0.170	0.638
Medullary diameter (mm)	0.865	0.001	-0.277	0.439
Cortical width (mm)	0.053	0.860	0.462	0.180
Yield point (%)	-0.238	0.510	-0.056	0.880
Yield point (MPa)	-0.290	0.417	0.378	0.281
Ultimate strength (%)	-0.050	0.890	-0.112	0.758
Ultimate strength (MPa)	0.081	0.825	0.401	0.251
Failure point (%)	0.103	0.778	0.154	0.670
Failure point (MPa)	0.151	0.678	0.335	0.344
Young's Modulus (MPa)	0.283	0.461	0.111	0.775
Energy absorbed (kJ)	0.417	0.230	0.200	0.560

TABLE F.2. Pearson Correlation Coefficients of the outcome variables with body mass and age for the cadavers in group 2 (bone plates and screws). (n = 10)

Group 2: Pearson Correlation Coefficients				
Outcome variable	**Body mass**	**p-value**	**Age**	**p-value**
Bone length (mm)	0.473	0.167	0.331	0.350
Bone diameter (mm)	0.356	0.313	-0.187	0.605
Medullary diameter (mm)	0.364	0.301	-0.250	0.486
Cortical width (mm)	0.030	0.934	0.111	0.761
Yield point (%)	0.242	0.499	-0.827	0.003
Yield point (MPa)	0.100	0.784	0.280	0.435
Ultimate strength (%)	0.156	0.667	-0.765	0.010
Ultimate strength (MPa)	-0.042	0.907	0.222	0.537
Failure point (%)	0.285	0.425	-0.822	0.004
Failure point (MPa)	0.209	0.561	0.339	0.338
Young's Modulus (MPa)	-0.323	0.362	0.709	0.022
Energy absorbed (kJ)	0.239	0.507	-0.623	0.055

APPENDIX G

Mean stress (load) and strain (deformation) values

TABLE G.1. Mean stress (load) for group 1 (IM pin and full cerclage wires) and group 2 (bone plate and screws). (n = 10)

Mean stress (load) for groups 1 and 2					
Outcome variable	Group 1		Group 2		p
	Stress (MPa)	SD	Stress (MPa)	SD	
Yield point	0.323	0.137	0.403	0.072	0.299
Ultimate strength	0.383	0.136	0.431	0.053	0.275
Failure point	0.345	0.161	0.403	0.082	0.137

TABLE G.2. Mean strain (deformation) for group 1 (IM pin and full cerclage wires) and group 2 (bone plate and screws). (n = 10)

Mean strain (deformation) for groups 1 and 2					
Outcome variable	Group 1		Group 2		p
	Strain (%)	SD	Strain (%)	SD	
Yield point	0.296	0.181	0.362	0.213	0.684
Ultimate strength	0.412	0.249	0.472	0.343	0.778
Failure point	0.713	0.399	0.838	0.617	0.505